EXPERIMENTAL STUDY FOR DETECTION OF THERMAL RUNAWAY, EXPLOSION, AND FIRE IN LI-ION BATTERIES INITIATED BY HOT PLATE METHOD

by

Corbin Scott Coe

A dissertation submitted to the faculty of
The University of North Carolina at Charlotte
in partial fulfillment of the requirements
for the degree of Master of Science in
Civil Engineering

Charlotte

2022

Approved by:

_____
Dr. Nicole Braxtan

_____
Dr. Shen-En Chen

_____
Dr. Tiefu Zhao

ABSTRACT

CORBIN COE. Experimental Study for Detection of Thermal Runaway, Explosion, and Fire in Li-Ion Batteries Initiated by Hot Plate Method

(Under the direction of DR. NICOLE BRAXTAN)

In 2006, Tesla announced the first fully electric lithium-ion battery (LIB) powered car, and shortly after in 2010, the Chevy Volt and Nissan Leaf began production [1]. Through the Recovery Act, the United States Department of Energy has since invested $115 million to install 18,000 residential and commercial electric vehicle (EV) charging stations across the country [1]. Industry manufacturers have also added thousands more charging locations and there will only be more in the years to come [1]. It's clear that LIB powered vehicles are the future of human travel, with predictions from UBS Bank that 20 percent of new car sales in 2025 will be electric, and virtually 100 percent will be by 2040 [2]. Electric cars are not the only industry with emerging LIB technology, as both passenger and freight, rail manufacturers and operators are preparing to integrate the technology as well. One of the main challenges presented by this mass influx of LIB usage is their safety. Reports of LIB battery fires in vehicles started occurring shortly after they were introduced, such as the May 2011 Chevy Volt that caught fire a week after crash testing in a National Highway and Traffic Safety Administration (NHTSA) parking lot, burning multiple cars [3]. There have since been dozens of LIB fire incident reports and their numbers increase with growing production. Manufacturing defects and battery abuse are the leading causes of fire incidents [4]. Being able to predict and prevent unsafe LIB scenarios is key to their societal acceptance, economic growth, and ease of integration into everyday human life. The goal of this research was to provide insight on the effectual capacity of certain LIB characteristics on the likelihood and severity of explosions and fires when manual abuse of the cells was performed.

As the common cause of LIB fire hazards, thermal runaway in the tested cells was catalyzed using hot plate-applied, thermal abuse. To measure key parameters in the LIB cells before, during, and after hot plate exposure, a unique, wireless, multi-instrument data monitoring and recording system was developed. The

Fire Early Detection System (FEDS) was used to collect infrared (IR) thermal images and thermocouple (TC) temperature readings of the heated cells and their surroundings. Both single-cell, and multi-cell tests were performed to investigate the LIBs at the individual and modular level. The two most common LIB shape classifications, prismatic and cylindrical, were researched, along with three different cathode chemistries namely lithium cobalt oxide (LCO, ICR), lithium manganese oxide (LM, IMR), and lithium manganese nickel (NMC, INR). For all cells tested individually, the state of charge (SOC) of the cells was noted, to determine the effect of stored electrical energy on thermal runaway and fire. Multiple tests were performed for incrementally different SOC levels across the cells.

Through analysis of the collected cell test data, key findings on the behavior of LIBs during thermal runaway were made. Selected notable findings include:

- The SOC and physical structure of the cells was seen to correlate with the probability and magnitude of explosions/fires during simulated thermal abuse.
- The progression of thermal runaway identifiers is consistent within all cell types, though more so in the cylindrical cells. These markers can be used to predict impending safety hazards in LIBs and could possibly be used in the prevention of some fire events.
- Cylindrical cells always failed at their designed safety vents first; and any fire events successive to vent failure initiated from these vents. This information can be used to optimize safety in cylindrical module designs for both general and train-specific use.
- Overall, the hot plate heating method was a reliable and controllable experiment design component.
- The FEDS system was effective in conducting safe fire-data acquisition and provides a prototypical infrastructure that can continue to be improved.

The contributions delivered from these findings, and the research as a whole, are as follows:

- By conducting real, fire tests, independent verification of the fire initiation and propagation for LIBs was achieved, which can be used to determine the early warning stages for the FEDS.
- This research has helped design a hot plate initiated, fire test setup at UNC Charlotte. This experiment design has shown that hot plate fire initiation can provide a consistent and repeatable fire start.
- These tests demonstrated that, despite the different age of the batteries, they exhibit a consistent correlation between their thermal stability and fire behavior, and their SOC.
- Based on this study, a fire detection and prevention strategy has been proposed.

ACKNOWLEDGMENTS

I would like to personally thank Dr Nicole Braxtan, Dr. Shen-En Chen and Dr. Tiefu Zhao for their guidance as advisors and committee members for this thesis, along with my fellow students Karl Lin, Xiwen Xu, Kamal Paul, Mason Sun, and Seth Cathey for all their help both technically and during the battery tests. Another fellow student I would like to give thanks to is Eric Huhn, who was both a team member in this project and serves as the UNC Charlotte, Facility and Laboratory Safety Engineer. Also helping to keep us safe, the Charlotte Fire Department met with our team to discuss general lithium-ion battery fire safety and their involvement in our proposed large scale battery fire tests in the future, their support for this research and expertise is greatly appreciated. A big thanks is extended to Dr. Paul Sumitro for facilitating, and personally delivering, the Fire Early Detection System's equipment and prototype design. Dr. Sumitro also trained our team to use the system and was continually able to provide technical support throughout the study. The US Department of Transportation (USDOT) and Federal Railroad Association's (FRA) grant financial support (FRA grant number: 693JJ621C000002) made this research a reality, and I would like to thank our FRA project advisor Dr. Omar Terek for his support. Our rail-industry sponsors' passion and support for this project has also helped make this FRA project possible, with much help from Dave Cook at Rail Propulsion Systems RPS, and Lynn Harrus from Deutsche Bahn. Our team is also highly appreciative of the city of Belmont, NC, and their battery-trolley development team on their inclusion of multiple UNC Charlotte lithium-ion battery projects and studies, with their exciting and revolutionary lithium-battery public rail project. All our local suppliers (Batteries + Bulbs) and donators of the various lithium-ion batteries tested in this study, contributed to both current and future research. Lastly, I would like to thank the University of North Carolina at Charlotte, without their facilities, faculty, and support, and the combined efforts of everyone listed on this page and beyond, this impactful research would not have been possible.

Table of Contents

LIST OF TABLES x

LIST OF FIGURES xii

LIST OF ABBREVIATIONS xx

CHAPTER 1: INTRODUCTION 1

1.1 Background 1

1.2 Problem Statement 5

1.3 Research Methodology 5

1.4 Scope of Work 6

1.5 Organization of the Report 7

CHAPTER 2: LITERATURE REVIEW 9

2.1 History of Reported LIB Fires 9

2.2 LIB Characteristics 16

2.3 State of Research Methods 25

CHAPTER 3: EXPERIMENTAL DESIGN AND SETUP 28

3.1 Experimental Setup 28

3.2 Instrumentation and Data Acquisition 33

3.3 Individual Cell Test Setup 36

3.4 Multi-cell Propagation Test Setup 42

CHAPTER 4: CELL LEVEL DATA AND RESULTS 46

4.1 Sample Prismatic Test Results 46

4.2 Sample Cylindrical Test Results 53

4.3 Intra-chemistry Results 60

CHAPTER 5: MODULE LEVEL PROPOGATION DATA AND RESULTS 62

5.1 Multi-pouch Tests 63

5.1.1 Four-Pouch Test (6.8.22) 65

5.1.2 Four-Pouch Test (6.11.22) 81

5.2 Multi-cylinder Tests 100

5.2.1 Three-18650 Test (6.4.22) 100

5.2.2 Four-18650 Test (6.11.22) 111

CHAPTER 6: DISCUSSION 119

6.1 General Test Procedure and Equipment 119

6.1.1 Digital Recordings 119

6.1.2 IR Recordings 120

6.1.3 Thermocouples and DAQ 121

6.1.4 Batteries 123

6.1.5 Hot Plate 124

6.2 General Prismatic and Selected 5.4.22 Discussion 125

6.3 General 18650 and Selected 4.27.22(3) Discussion 126

6.4 Inter-chemistry Comparison 128

6.5 SOC Comparison 132

6.5 Multi-cell Propagation Discussion 138

CHAPTER 7: CONCLUSION 141

CHAPTER 8: RECOMMENDATIONS FOR FUTURE STUDIES 144

REFERENCES 153

APPENDIX: SMARTCONNECT INSTRUCTION GUIDE 160

LIST OF TABLES

Table 2-1: EUCAR LIB failure hazard levels [34] 18

Table 2-2: Brand et al., heating rate temperature of onset/increase [4] 21

Table 2-3: Brand, overcharge buffer resistance [4] 21

Table 4-1: Prismatic ICR 5.4.22 matrix excerpt 52

Table 4-2: 18650 INR 4.27.22 (3) matrix excerpt 59

Table 4-3: Matrix excerpt of all reported ICR tests 60

Table 4-4: Matrix excerpt of all reported IMR tests 60

Table 4-5: Matrix excerpt of all reported IMR tests 61

Table 5-1: Excerpt 1/2 of combined TC raw data [383-425sec] (6.8.22) 66

Table 5-2: Excerpt 2/2 of combined TC raw data [426-459sec] (6.8.22) 67

Table 5-3: Excerpt 1/3, combined TC raw data [327-352sec] (6.11.22) 82

Table 5-4: Excerpt 2/3, combined TC raw data [530-587sec] (6.11.22) 83

Table 5-5: Excerpt 3/3, combined TC raw data [588-631sec] (6.11.22) 84

Table 5-6: DAQ raw data excerpts at key times, 6.4.22 104

Table 5-7: Combined TC raw data excerpt, at hiss, 6.11.22 (18650) 113

Table 5-8: Combined TC data excerpt, explosion and errors 6.11.22 (18650) 114

Table 6-1: Comparison of chemistry averages 129

Table 6-2: INR SOC averages 133

LIST OF FIGURES

Figure 1-1: Cylinder and hard prismatic LIB shapes, layers [7] 2

Figure 1-2: Pouch LIB shapes, layers [7] 2

Figure 1-3: 18650 cell layering detail [9] 3

Figure 1-4: Prismatic cell layering detail [10] 4

Figure 2-1: Packing of LIB shapes [34] 17

Figure 2-2: ARC vs. SOC for batteries with different cathode makeups [36] 19

Figure 2-3: Brand et al., study on chemistry heating rate [4] 20

Figure 2-4: Brand et al., CID diagram [4] 22

Figure 2-5: SOC impact on TR in 16 Ah automotive pouch cells [36] 23

Figure 2-6: SOC relationships [36] 24

Figure 3-1: Thermal abuse test system schematic 28

Figure 3-2: Typical testing environment 29

Figure 3-3: Box furnace detail 29

Figure 3-4: Hot plate schematic 30

Figure 3-5: Hot plate temperature data w/ adjusted average curve 32

Figure 3-6: Rijer prismatic charger 37

Figure 3-7: EASTSHINE cylindrical charger 37

Figure 3-8: Single prismatic cell placement 39

Figure 3-9: Single 18650 placement 39

Figure 3-10: end cap placement 5.3.22 40

Figure 3-11: First-person view, mid-test 41

Figure 3-12: Typical propagation test setup 43

Figure 3-13: Multi-18650 plate setup 44

Figure 3-14: Multi-pouch plate setup 45

Figure 4-1: TC data prismatic ICR 100% 2450mAh 5.4.22 47

Figure 4-2: 1sec before rapid expansion/explosion [4:23 (vid.), 245sec (data)] 5.4.22 48

Figure 4-3: Maximum expansion before explosion [4:24 (vid.), 246sec (data)] 5.4.22 48

Figure 4-4: Large flames after explosion [4:27 (vid.), 249sec (data)] 5.4.22 49

Figure 4-5: Sustained flame size 5.4.22 49

Figure 4-6: IR video during large flames [4:22 (IR vid.), 4:27 (digital vid.)] 5 4.22 50

Figure 4-7: Flames about to extinguish [8:12 (IR vid.), 2:04 (digital vid)] 5.4.22 50

Figure 4-8: 5.4.22 post-condition photo 1 51

Figure 4-9: 5.4.22 post-condition photo 2 51

Figure 4-10: TC data 18650 INR 100% 2600mAh 4.27.22 (3) 53

Figure 4-11: Moment of explosion [8:15 (vid.), 399sec (data)]4.27.22 (3) 54

Figure 4-12: 5sec after explosion [8:20 (vid.), 404sec (data)] 4.27.22 (3) 55

Figure 4-13: 50sec after explosion [9:06 (vid.), 449sec (data)]4.27.22 (3) 55

Figure 4-14: 1sec pre-explosion [7:52 (IR vid.), 398sec (data)] 4.27.22 (3) 56

Figure 4-15: Moment of explosion [7:53 (IR vid.), 399sec (data)] 4.27.22 (3) 57

Figure 4-16: 1sec post-explosion [7:54 (IR vid.), 400sec (data)] 4.27.22 (3) 57

Figure 4-17: Post-test condition 4.27.22 (3) 58

Figure 5-1: IR video display types for computer ID 63

Figure 5-2: Label of multi-pouch test cells 64

Figure 5-3: Combined DAQ and SmartConnect TC data plot 6.8.22 65

Figure 5-4: First hiss after 1sec, bottom cell [6:59 (vid.), 384sec (data)] 6.8.22 68

Figure 5-5: First hiss heavy smoke [7:00 (vid.), 386sec (data)] 6.8.22 68

Figure 5-6: IR first hiss, bottom cell [6:51 (IR vid.), 386sec (data)] 6.8.22 69

Figure 5-7: First ignition, bottom cell [7:05 (vid.), 391sec (data)] 6.8.22 70

Figure 5-8: IR first ignition, bottom cell [6:56 (IR vid.), 391sec (data)] 6.8.22 70

Figure 5-9: First jet after 2sec, bottom cell, [7:13 (vid.), 399sec (data)] 6.8.22 71

Figure 5-10: IR first jet after 1sec, bottom cell, [7:04 (IR vid.), 399sec (data)] 6.8.22 71

Figure 5-11: Additional jets other side [7:15 (vid.), 401sec (data)] 6.8.22 72

Figure 5-12: IR jets other side [7:06 (IR vid.), 401sec (data)] 6.8.22 72

Figure 5-13: Mini jets the second before jet 2 [7:22 (vid.), 408sec (data)] 6.8.22 73

Figure 5-14: IR mini jets the second before jet 2 [7:13 (IR vid.), 408sec (data)] 6.8.22 74

Figure 5-15: Approx. max point jet 2, (2^{nd} cell?) [7:27 (vid.), 413sec (data)] 6.8.22 74

Figure 5-16: IR Approx. max point jet 2, (2^{nd} cell?) [7:18 (IR vid.), 413sec (data)] 6.8.22 75

Figure 5-17: Top-cell DAQ TC detaching [7:31 (vid.), 417sec (data)] 6.8.22 75

Figure 5-18: IR top-cell DAQ TC detaching [7:22 (IR vid.), 417sec (data)] 6.8.22 76

Figure 5-19: 3^{rd} and final jets both sides, (top cell only?) [7:40 (vid.), 426sec (data)] 6.8.22 77

Figure 5-20: IR 3^{rd} and final jets both sides, (top cell only?) [7:31 (IR vid.), 426sec (data)] 6.8.22 ... 77

Figure 5-21: Approx. max point jet 3 [7:44 (vid.), 430sec (data)] 6.8.22 78

Figure 5-22: IR approx. max point jet 3 [7:35 (IR vid.), 430sec (data)] 6.8.22 78

Figure 5-23: Red-hot top-cell w/ subsiding flames [7:55 (vid.), 441sec (data)] 6.8.22 79

Figure 5-24: IR red-hot top-cell w/ subsiding flames [7:46 (IR vid.), 441sec (data)] 6.8.22 79

Figure 5-25: Post-condition of all 4 cells (order unknown) 6.8.22 80

Figure 5-26: Combined DAQ and SmartConnect TC data plot 6.11.22 81

Figure 5-27: ~5sec into first hiss/smoke (bottom cell) [6:15 (vid.), 335sec (data)] 6.11.22 85

Figure 5-28: IR ~5sec into first hiss/smoke (bottom cell) [5:54 (IR vid.), 335sec (data)] 6.11.22 86

Figure 5-29: Bottom cell post-hiss condition, no fire [7:44 (vid.), 424sec (data)] 6.11.22 86

Figure 5-30: IR bottom cell post-hiss condition, no fire [7:23 (IR vid.), 424sec (data)] 6.11.22..... 87

Figure 5-31: Middle of 2nd hiss/expans. (2nd cell) [9:35 (vid.), 535sec (data)] 6.11.22..... 88

Figure 5-32: Red-hot innards after hiss/expans. (2nd cell) [9:38 (vid.), 538sec (data)] 6.11.22 88

Figure 5-33: IR red innards after hiss/expans. (2nd cell) [9:17 (IR vid.), 538sec (data)] 6.11.22..... 89

Figure 5-34: IR burst of flames (2nd cell) [9:19 (IR vid.), 540sec (data)] 6.11.22 90

Figure 5-35: 1st second after burst of flames (2nd cell) [9:40 (vid.), 540sec (data)] 6.11.22 90

Figure 5-36: 3rd hiss w/ instant jet flames (3rd cell) [10:13 (vid.), 573sec (data)] 6.11.22 91

Figure 5-37:IR 3rd hiss w/ instant jet flames (3rd cell) [9:52 (IR vid.), 573sec (data)] 6.11.22 92

Figure 5-38: Jet flames from both ends (3rd cell) [10:16 (vid.), 576sec (data)] 6.11.22..... 92

Figure 5-39: IR jet flames from both ends (3rd cell) [9:55 (IR vid.), 576sec (data)] 6.11.22 93

Figure 5-40: After jets, partially blue flame (3rd cell) [10:25 (vid.), 585sec (data)] 6.11.22..... 94

Figure 5-41: IR after jets, partially blue flame (3rd cell) [10:04 (IR vid.), 585sec (data)] 6.11.22..... 94

Figure 5-42: Start of jet flames before falling (4th cell) [10:44 (vid.), 604sec (data)] 6.11.22 95

Figure 5-43: IR start of jet flames before falling (4th cell) [10:23 (IR vid.), 604sec (data)] 6.11.22.... 96

Figure 5-44: Fallen cell flames, TCs off (4th cell) [10:51 (vid.), 611sec (data)] 6.11.22 96

Figure 5-45: IR fallen cell flames, TCs off (4th cell) [10:30 (IR vid.), 611sec (data)] 6.11.22 97

Figure 5-46: Hot internal cell layers (cell unknown) 6.11.22..... 98

Figure 5-47: Hot internal cell layers, flipped open (cell unknown) 6.11.22 98

Figure 5-48: Hot intact cells (cells unknown) 6.11.22 98

Figure 5-49: Approx. 4-week post-test condition 6.11.22..... 99

Figure 5-50: Zoomed in view of crystalline buildup, 4-weeks 6.11.22..... 100

Figure 5-51: 6.4.22 multi-cell test setup..... 101

Figure 5-52: SensorConnect TC data plot..... 103

Figure 5-53: DAQ TC data plots 6.4.22..... 103

Figure 5-54: Moment of 1st ignition bottom cell, initial sparks [13:22 (vid.), 757sec (data)] 6.4.22. 105

Figure 5-55: Second after 1st ignition bottom cell, jet flames [13:23 (vid.), 758sec (data)]..... 106

Figure 5-56: Moment of 2nd ignition, 2nd cell, sparks [1:24 (2nd vid.), 1061sec (data)]..... 107

Figure 5-57: IR Moment of 2nd ignition, 2nd cell, sparks [18:16 (IR vid.), 1061sec (data)] 107

Figure 5-58: 2nd ignition, rocket of cells into chamber wall [1:26 (2nd vid.), 1063sec (data)] 108

Figure 5-59: IR 2nd ignition, rocket of cells into chamber wall [18:18 (IR vid.), 1063sec (data)] 108

Figure 5-60: 2nd ignition, after jet, cell red-hot, dual-end flames [1:29 (2nd vid.), 1066sec (data)].... 109

Figure 5-61: IR 2nd ignition, after jet, red-hot, dual-end flames [18:21 (IR vid.), 1066sec (data)] 110

Figure 5-62: Post-condition all, 6.4.22 110

Figure 5-63: Post-condition middle cell, 6.4.22 111

Figure 5-64: Combined TC data plots, 6.11.22(18650) 112

Figure 5-65: Explosion bottom cell, ¼ speed still shot 1 [16:40 (1st vid.), 973sec (data)] 6.11.22 115

Figure 5-66: Explosion bottom cell, ¼ speed still shot 2 [16:40 (1st vid.), 973sec (data)] 6.11.22 116

Figure 5-67: IR Explosion bottom cell [16:27 (IR vid.), 973sec (data)] 6.11.22 116

Figure 5-68: Post-explosion cell position, small flames [16:44 (1st vid.), 977sec (data)] 6.11.22 117

Figure 5-69: Post-condition photo, implanted (+) end cap, 6.11.22(18650) 117

Figure 5-70: Post-condition photo, emptied bottom cell, 6.11.22(18650) 118

Figure 5-71: Post-condition photo, bottom cell w/ ejected innards, 6.11.22(18650) 118

Figure 6-1: Phase 1, no expansion, ICR 3.2.22 131

Figure 6-2: Phase 2, medium expansion, ICR 3.2.22 131

Figure 6-3: Phase 3, full expansion, ICR 3.2.22 131

Figure 6-4: INR pressure and explosion average temperature and time 134

Figure 6-5: INR pressure release (hiss) temps, box and whisker (inclusive) 135

Figure 6-6: INR pressure release (hiss) times, box and whisker (inclusive) 136

Figure 6-7: INR explosion temps, box and whisker (inclusive) 137

Figure 6-8: INR explosion times, box and whisker (inclusive) 138

Figure 8-1: Engine room replaced, LIB powered train schematic 144

Figure 8-2: Belmont battery trailer car 145

LIST OF ABBREVIATIONS

ARC	accelerated rate calorimetry
BEL	Battery-Electric Locomotive
BESS	battery energy storage system
BMS	battery management system
CID	current interruption device
CO	carbon monoxide
CO2	carbon dioxide
DAQ	National Instruments Compact Data Acquisition (short)
ESC	external short circuit
ESS	energy storage system
EUCAR	European Council for Automotive Research and Development
EV	electric vehicle
FAA	Federal Aviation Administration
FEDS	Fire Early Detection System
FRA	Federal Railroad Administration

GM	General Motors
HVAC	heating, ventilation, and air conditioning
ICR	Manufacturer Acronym (LCO)
IFR	Manufacturer Acronym (LFP)
IMR	Manufacturer Acronym (LM)
INR	Manufacturer Acronym (NMC)
IR	infrared
ISC	internal short circuit
LCD	liquid crystal display
LCO	lithium cobalt oxide
LFP	lithium iron phosphate
LIB	lithium-ion battery
LM	lithium manganese oxide
LMO	lithium manganese oxide
LTO	lithium titanate oxide
mAh	milliampere hour

NCA	lithium nickel cobalt aluminum oxide
NCO	lithium nickel cobalt oxide
NHSTA	National Highway and Traffic Safety Administration
NI	National Instruments
NI-CDAQ	National Instruments Compact Data Acquisition
NMC	lithium manganese nickel
OBS	Open Broadcaster Software
PPE	personal protective equipment
RAM	random-access memory
SCBA	self-contained breathing apparatus
SMV	slow-motion video
SOC	state of charge
TC	thermocouple
TR	thermal runaway

CHAPTER 1: INTRODUCTION

Lithium-ion battery (LIB) fire and explosion hazards are a substantial concern amongst industry producers and consumers. A better understanding of how LIBs behave leading up to and during explosion/fire events may lead to more effective detection, prevention, and suppression of the events of concern. In almost all cases LIB fire hazards are caused by short circuiting the battery which in turn causes thermal runaway (TR) [5]. Short circuits may occur externally or internally, and are caused by mechanical abuse, defects, high temperatures, and electrical abuse [5]. Thermal runaway occurs when the rate of heat production during LIB operation is faster than the rate of heat dissipation and is generally classifiable when heating occurs at greater than 20 degrees centigrade per minute [6]. Once a state of TR has been entered it typically cannot be stopped or controlled and can cause dangerous side effects such as: ejection of gas, shrapnel, or smoke, extreme temperatures, and fire [6].

LIBs come in various shapes, arrangements, and chemistries (design topology). These variables come with their own individual sets of pros and cons. Determining the behavior characteristics of different types of LIBs is paramount in assessing the TR risks involved with each individual battery.

1.1 Background

LIBs can be typically found in two different cell shapes and classified as three different types. The two standard shapes are cylindrical and prismatic. The prismatic cell can further be divided into a hard case (metal or hard plastic) or soft pouch style, which is surrounded in a lightweight foil, where cylindrical batteries are typically only in hard metal cases, see Figure 1-1 and 1-2. Note, that pouch cells do typically not contain liquid electrolyte [7].

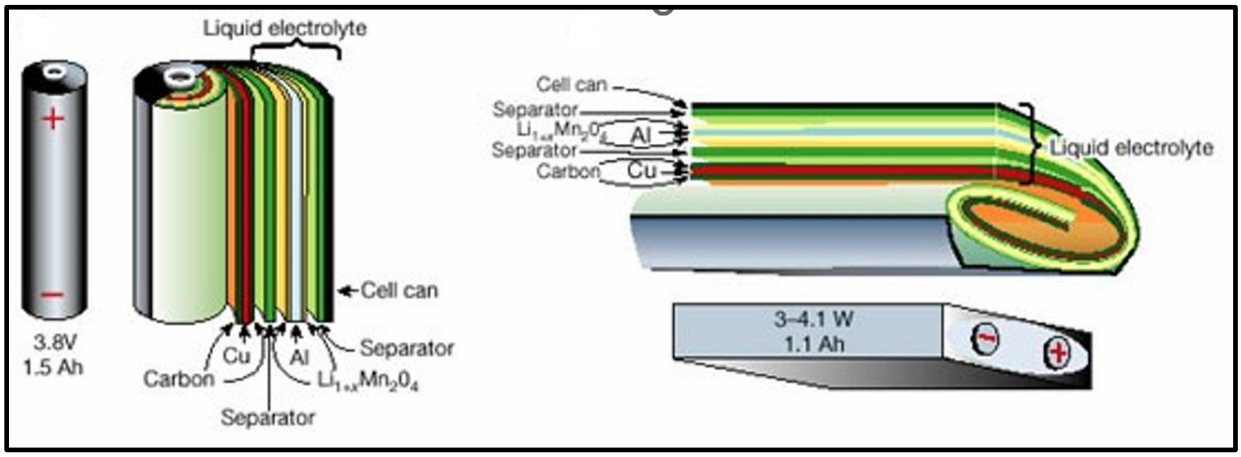

Figure 1-1: Cylinder and hard prismatic LIB shapes, layers [7]

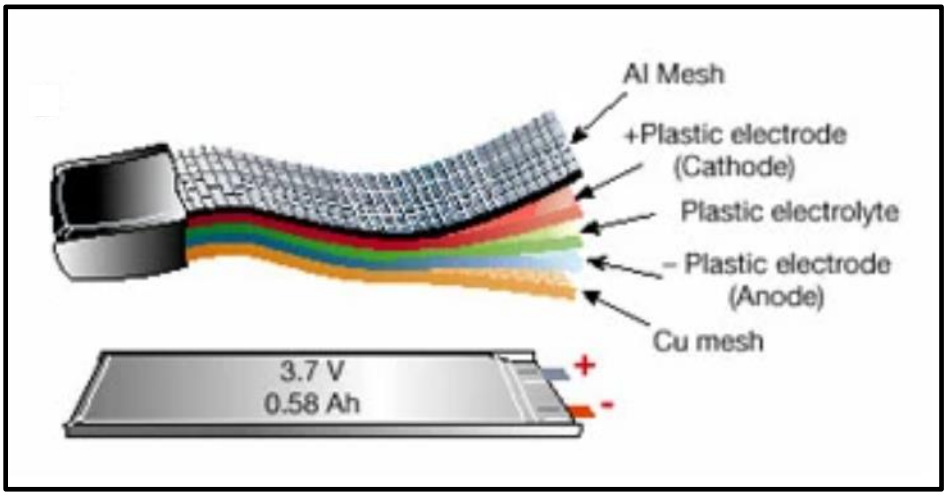

Figure 1-2: Pouch LIB shapes, layers [7]

At the individual level, prismatic cells are commonly found in thinner electronic devices like cell phones, where cylindrical cells may be found in flashlights or electronic cigarettes. Different geometric constraints and energy capacity needs in devices using individual cells creates a demand for both shapes, and different size options within each shape. Cylindrical cells are typically only produced in a standardized range of sizes, with the 18650 (18mm diameter x 65mm length) being the most common, where the battery dimensions can dictate the design of the device using it. Prismatic cell production sizes are often more customizable to conform with constant variations in handheld electronic device designs. When energy needs exceed the capacities of single cells, both cylindrical and prismatic cells can be arranged into modules

that are comprised of multiple cells. For instance, the original Tesla Roadster's (electric motor vehicle) main battery system is comprised of 6,831 individual cylindrical cells [8]. A detailed schematic of typical 18650 cell interiors is shown in Figure 1-3 [9]; detailed schematics of prismatic cells are shown in Figure 1-4 [10].

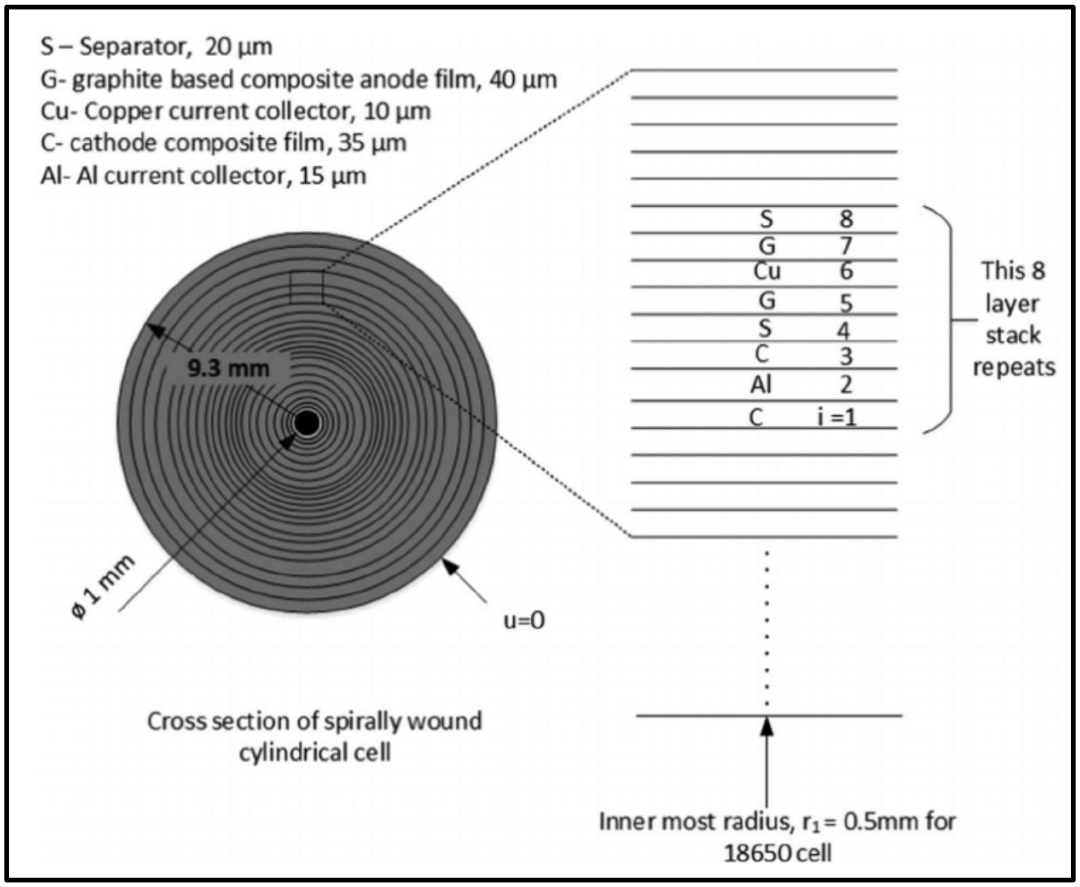

Figure 1-3: 18650 cell layering detail [9]

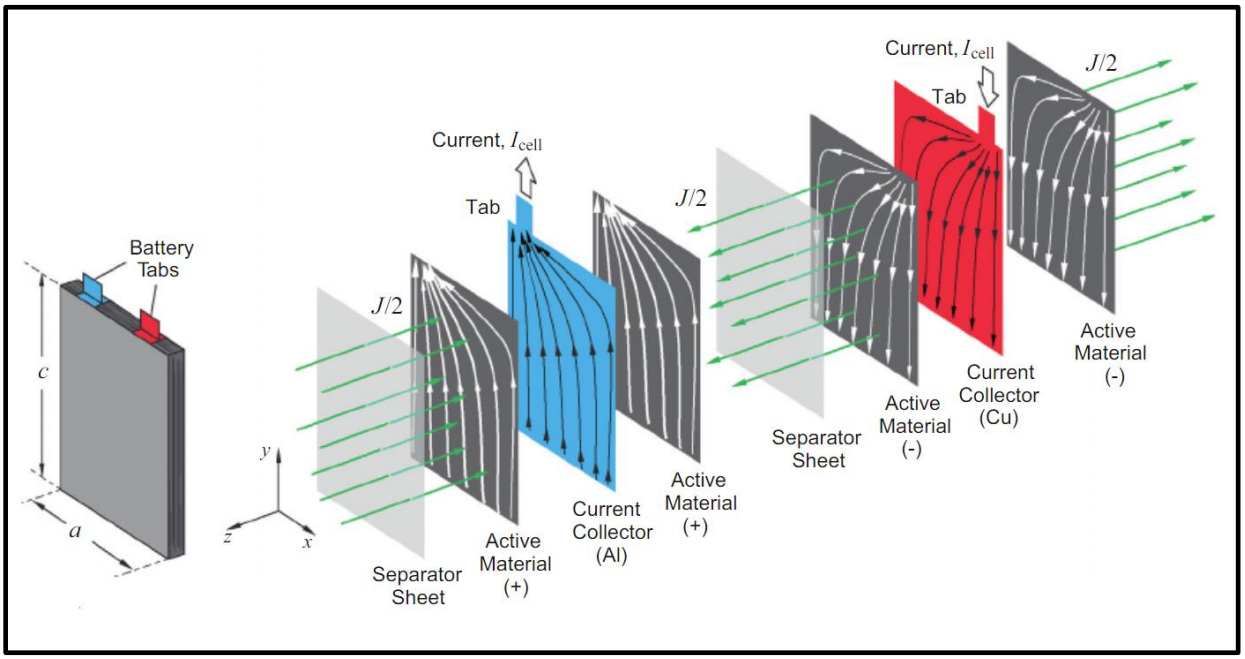

Figure 1-4: Prismatic cell layering detail [10]

Separate from their shape, all LIBs can be further characterized by their cathode oxide chemistry. Common cathode chemical makeups and their industry and chemical compound abbreviations are listed below. Note that "I" and "L" both indicate Li-Ion, and some manufacturers drop the "I" or "L" completely. Also, while all Li-Ion batteries are rechargeable, some manufacturers include an "R" for rechargeable to disambiguate from non-rechargeable Lithium batteries.

- Lithium manganese oxide (IMR, LM, LMO)
- Lithium manganese nickel (INR, NMC, - contains cobalt)
- Lithium nickel cobalt aluminum oxide (NCA)
- Lithium nickel cobalt oxide (NCO)
- Lithium cobalt oxide (ICR, LCO)
- Lithium iron phosphate (IFR, LFP)

Some of these cathode chemistries have advantages in terms of sustainability and higher energy density over others. At the same time, some chemistries hold disadvantages in terms of low thermal runaway temperature and high energy release during runaway in comparison to others.

1.2 Problem Statement

Predicting and preventing LIB fire hazards is the most important and challenging issue at the consumer level with an overarching goal of improving human safety related to LIB use. To approach solving this issue, a need for research into the fundamental mechanisms of LIB fires was deemed necessary. The objective of this research was to develop a wireless battery monitoring system that can be used to investigate LIB behavior leading up to and during battery fire incidents. This system, and its collected data, will be used to make recommendations toward general LIB use, storage, and future research. Specific recommendations will also be related to LIB powered locomotives.

1.3 Research Methodology

To determine key parameters during TR of various types of LIBs, short circuiting of tested batteries was required. In all tests, thermal abuse was used to catalyze an internal short circuit (ISC), in turn starting the TR process. Thermal abuse was performed by placing the LIBs on an electric hotplate. Individual LIBs with various chemistries, shapes, and states of charge were investigated. Similar tests were also performed on LIBs combined physically to emulate multi-battery modules and understand their thermal propagation behavior. Various forms of wireless data collection were employed during each test including digital video recording, infrared (IR) video recording, on-battery thermocouple(s) (TC), and handheld IR devices (video thermometer, IR thermometer, and compact IR camera).

1.4 Scope of Work

All instrument accuracies were validated during initial unreported battery tests and during "dry runs" of the hotplate with no battery. The handheld IR devices are not shown in the schematic as the locations varied while they were used to determine the hot plate's heating magnitude and rate consistency, to determine temperature of battery remains when a TC fell off during explosion events, and spot check temperatures. To confirm and build upon referenced literature, the heating of three battery chemistry types (ICR, IMR, INR), with varying states of charge between 0-100%, were evaluated for the following parameters: the occurrence of fire (ignition and sustained flame), smoke and smell (off-gassing), physical expansion of cells, pressure release (piercing of battery casing), explosion, battery temperature, the time at parameter occurrence, the length of occurrence, the post-test condition of batteries, and the mass lost during fire and/or off-gassing when applicable. All the batteries tested were used batteries that were donated or purchased locally. The quantity of all reported tests performed in this research, categorized by cell cathode chemistry and test type are as follows:

- Single-cell, hard-cased plastic ICR (prismatic) – 5
- Single-cell, 18650 IMR (cylindrical) – 6
- Single-cell, 18650 INR (cylindrical) – 24
- Multi-cell, pouch ICR (prismatic) – 2, four-pouch tests
- Multi-cell, 18650 INR (cylindrical) – 1, three-cylinder test, and 1, four-cylinder test

The findings from these tests are used to determine the effectual capacity of test parameters on battery safety, and to make recommendations on battery selection, use, train applications, and future test methods or research.

It should be noted that the originally proposed testing system included gas sensors to evaluate the profile of any released gasses and their potential toxicity concerns as additional parameters; however, our initial

gas detection instruments could not be validated for accuracy. Hence, subsequent testing continued without gas detection but plans for future implementation of a gas-to-bag collection system has been discussed. This method could allow for a detailed analysis of more individual gasses, than real-time gas detectors. From this data, better recommendations could be made for specific battery chemistries and types.

1.5 Organization of the Report

In chapter 1, section 1.1 outlines background information describing Li-ion batteries and their associated hazards. Section 1.2 defines the problem statement of the research. Sections 1.3 and 1.4 define the overall approach and scope of work for the research, respectively.

Chapter 2 overviews the literature review conducted to demonstrate a need, and develop test methods, for the research discussed in this report. Section 2.1 surveys reported cases of LIB fires amongst consumers and manufacturers, and how they relate to emerging LIB-powered rail technology. Section 2.2 references important foundational information on LIB characteristics. Section 2.3 cites the state of research related to LIB fire testing and safety.

Chapter 3 covers the experimental design and setup of the tests performed. Section 3.1 details the experimental setup, while section 3.2 details instrument functionality, methods used to validate instruments, and safety guidelines used to optimize the overall data acquisition process. Section 3.3 describes the single-cell test process, while 3.4 describes the multi-cell, propagation test process.

Chapter 4 presents the data results of the single-celled tests, where section 4.1 details a selected prismatic cell test, and section 4.2 details a selected 18650 cell test. Section 4.3 compiles the data of all single-cell tests, and groups them by cathode chemistry.

Chapter 5 presents the propagation testing results, where section 5.1's subheadings detail the two multi-pouch tests, respectively. Section 5.2's subheadings detail the two multi-18650 tests, respectively.

Discussion on the overall test processes, categorized groupings of the results, and specific tests occurs in Chapter 6.

Conclusions based on test results are made in Chapter 7, where chapter 8 overviews recommendations toward future studies, along with recommendations on general LIB use, and train-specific LIB use.

CHAPTER 2: LITERATURE REVIEW

2.1 History of Reported LIB Fires

Before testing and FEDS development began, an extensive investigation into reported LIB battery fires was undertaken. For efficiency and relevance, only LIB fires at the electric vehicle (EV) scale or larger were considered. Reports were found from 2011 (soon after EVs were first available on the consumer market) to 2021 (beginning of this research). These reports were catalogued and are available supplementally to this research, but while the 69 entries of this catalogue are believed to be most of the serious EV (or bigger) fires in this time frame, there are likely instances that were not discovered. One website is dedicated to Tesla fire reports and is currently tallied with 97 reports and 38 deaths. [11] While every report of fire and death on the site has not been verified, it is believed to be accurate since every Tesla fire found in the separate review conducted for this research, is also on the site. The goal of this incident review was to learn more about the causes and behavior of LIB fires. This knowledge was considered in both the cell experiment design, and development of the FEDS. A list of selected representative and useful reports is as follows:

- May 2011: Chevy Volt catches fire a week after crash testing, in a NHTSA parking lot, burning multiple nearby cars [12].
- Two similar 2013 Tesla incidents: A Tesla collided with tow hitch damaging beneath the car, (minimal damage yet puncture) [13]; another Tesla hit debris on highway causing fire [14].
- February 2014: Tesla Model S caught fire while parked and not charging or plugged in [15].
- August 2016: A Tesla Model S 90D spontaneously caught fire during a promotional test drive in Biarritz, France. The fire completely destroyed the Tesla Model S 90D within 5 minutes [16].
- April 2017: Large explosion and fire on Union Pacific train car carrying recycled LIBs. Only one car damaged, but a man was thrown into side of his house while standing outside, 350 feet away [17]. (Note, only LIB fire related to trains found in research.)

- December 2017: VW e-Golf caught fire in Triangel, Germany. This incident was the first EV fire that the firefighters had ever responded to. They first cooled the vehicle then moved it into a container which they then filled with water [18].
- May 2018: The first reported Hyundai Kona fire took place in Hyundai's Ulsan production plant, (second battery fire in the same plant reported later that year) where 25,000 were eventually recalled [19].
- June 2018: Pedestrians alert Tesla Model S driver of smoke coming from the vehicle. The driver was able to pull over and exit the vehicle before flames began shooting from beneath the car [20].
- February/April 2019: A Tesla Model S first caught on fire in a garage (February). Two months later (April), it caught on fire again, even after a Tesla engineer had removed the battery fuse before transport by towing company. The second fire lasted over four hours [21].
- April 2019: Tesla Model S exploded in an underground garage in Shanghai, China, damaging five surrounding cars. This event was captured on security camera footage, in the video thick smoke begins emitting from beneath the car, increase in smoke progresses over a few seconds into a large explosion that "whites-out" the cameras entire view. Large flames immediately follow the explosion and are expelled in every direction from below the car [22]. (In this incident, a similar failure progression to many of the battery tests performed in this research, can be seen.)
- April 2019: McMicken NMC (INR) battery energy storage system
- (BESS) fire and subsequent explosion (LG Chem batteries) [23]. (Full third-party incident report available for this test, detailed later in this section)
- April 2021: Beijing LFP BESS fire and explosion that killed two firefighters [24]. (Full translated report published on cited website.)
- 2021: By 2021 General Motors (GM) had issued recalls on every single Chevy Bolt EV model ever made totaling almost 142,000 vehicles [25], while Hyundai had recalled 77,000 vehicles by 2020

[26], and added another 82,000 in 2021, where both car manufacturers' LIBs were supplied by LG Chem [25].

The LIB fire incidents above are a fraction of the total fires reported, but are representative of the different causes, dangers, and challenges related to LIB fires. While most events point to impact, charging, or manufacturing defects (or a combination of the three) as the root cause, for many cases a definite cause of the fires could not be determined. Most of these unknowns likely stem from destruction of evidence due to the violent nature of LIB fires, combined with a lack of knowledge and resources from first responders and local investigators.

For some of the more devastating and expensive incidents, professional investigative reports were conducted. For all the battery fires listed known to contain LG Chem LIBs, South Korean government investigations were conducted on the LG Chem cells, along with a third-party investigation report by Norway based, DNV (DNV GL at time of report), for the McMciken BESS fire (Arizona). For some of the earlier Hyundai recalls, LG Chem made a statement that a defect in the manufacturing process was found where the anode tab was folded in some cells produced at their Nanjing plant, but independent testing by the Ministry of Land, Infrastructure, and Transport of the Republic of Korea was unable to reproduce fires in cells with the defect [27]. LG claimed this defect was discovered early in production and had already been fixed and pointed to an error in programming logic for fast charging in the Kona BMS, designed by Hyundai, as a possible cause. The recent recall of 82,000 Hyundai vehicles worldwide was mostly 2018-2020 Hyundai Konas (76,000), where the rest consisted of Hyundai Ioniqs and city busses. The Chevy Bolt recalls occurred effectively at the same time due to similar LG Cells, only they were produced in LG's Michigan and Ochang plants [28]. Ultimately LG assumed $1.2 billion of the estimated $2 billion recall cost for GM [29], while also covering an estimated 70% of Hyundai's $900 million recall cost [28]. In a statement on the monetary settlement, GM claimed two different defects, a torn anode tab and a folded separator, were the cause of the increased fire risk in the Bolts. (SAME GM cite as before) Through the direction of LG, both car manufacturers recommended to charge all recalled vehicles no more than 90%

until battery modules could be replaced [28]. It is important to note that the recall of the142,000 Bolts was in response to only 13 battery fires amongst them; thus, highlighting the second-hand economic impact LIB fires can have, on top of their first-hand damage to expensive property; however, the most important impact of these fire comes from endangering human lives.

Regarding the McMicken BESS (or commonly called an ESS for energy storage system) explosion, a more extensive report was provided by DNV for Arizona Public Service, the energy company that owned the system. According to the report, prepared and authored by Hill [23], the facility, which was a containerized system approximately the size of a standard shipping crate, consisted of 36 racks, where 27 racks contained 14 battery modules, and each module consisted of 28 NMC, pouch LG Chem cells and a module-level BMS. The BESS was used to store solar energy produced by nearby panels during the day, and then redistribute the stored energy into the local power grid at night. The timeline of the explosion at the facility, which was 25 months old at the time of event, states that a suspected fire was reported at the BESS at 17:48 local time, from which first responders soon arrived. At 20:04 an explosion occurred inside the BESS, which injured several firefighters and effectively destroyed the BESS and container. DNV [23] presented “factual conclusions” they were able to make from the investigation, and they are summarized as follows:

- An internal cell failure, caused by lithium metal deposits and dendrite growth in the cell, occurred in one cell that initiated a propagating TR event.
- The total flooding clean agent fire suppression system installed in the BESS operated correctly, early on in the event, but these clean agent systems are designed to prevent incipient fire and are not capable of preventing TR in LIB cells.
- Propagation advanced through every cell and module in Rack 15, which was facilitated by the lack of a sufficient thermal barrier between the cells, which they predicted may have stopped or slowed the spread.

- With TR present throughout Rack 15, a large quantity of flammable gasses was released into the container. Through modelling it was determined these gasses were able to create a flammable atmosphere in the BESS. This atmosphere was ignited when firefighters opened the container doors 3 hours after TR occurred, where a spark or heat source contacted the gasses. They also noted no ventilation means were present, and emergency response teams had no plans for an extinguishing, ventilating, or entry procedure.

While a report was also conducted for the Chinese BESS explosion [24], investigators state they were not able determine a cause for the event that saw two separate explosions, on two sides of the large rooftop-solar and storage system. Investigators did point to the system's outdoor exposure to weather elements as a possible cause. It should be noted that the batteries were LFP.

Throughout many of the reported LIB fire incidents, a first responder and fire fighter lack of knowledge and experience for handling LIB fires is evident, which in some cases, may have caused a loss of human lives. In a response to several EV fires since the company's inception, Tesla has released emergency response guides for every model car they have produced, and they also provide guides for their supercharging stations, solar roof, and battery storage (Powerwall, Powerpack, Megapack) products. Citing Tesla's Model S guide [30], important behavioral aspects of LIBs are detailed, along with information on monitoring failed or failing modules, and LIB fire suppression recommendations. Tesla states using copious amounts of water as the ideal method of cooling the batteries that have been exposed to high heat, are generating heat of gasses, or have caught fire. Tesla warns that it can take between 3,000 to 8,000 gallons of water, applied directly to the battery, to extinguish and completely cool the battery fire; recommending to always request for more water ahead of time, if this amount is not readily available at the scene. If water is not immediately available, Tesla recommends carbon dioxide suffocation (CO2), dry chemicals, or other common fire-extinguishing agents, however, they do not recommend use foam extinguishers or fully submerging the car in water. Tesla cites submersion as a cause of LIB fires, using submersion as fire

suppression tool can create new fires in different cells not affected by original fire. To provide better water access to the batteries, which are located along the underside of the car, tilting the car to expose the battery area is recommended if it is possible to do safely. Note Tesla advises against removing the module cover to expose the cells. Once the car is tilted, displaying the full area cells are present, Tesla recommends using IR thermometer devices to monitor the battery temperature during cooling. Water should be continually applied until all areas of the battery have reached ambient temperatures or lower. When cooling is believed to have been achieved and water application has stopped, time must be given for water to clear the surface and for any heat transfer still active to be picked up by IR devices. Tesla warns that battery fires can take up to 24 hours to completely cool, and that a minimum of 45 minutes consisting of no fire, smoke, audible battery failures (popping/hissing), or increase in heat must pass before the vehicle can be released to second responders or vehicle transporters. While Tesla does not state for how long after the fire, they note that the vehicle/battery pack should be stored 50 feet from any vulnerable objects. Based on the listed Tesla incident where a Model S re-ignited after 2 months of static storage [21], the time frames in the previous Tesla emergency response guide are not guaranteed and should be taken as such. For the 2-month re-ignition event, it's likely that moving experienced from riding on and being placed on a tow truck, disturbed remaining active yet damaged cells.

Tesla also mentions the potential for chemical hazards stemming from LIB fires [30], and issues a warning that LIBs can release gasses and particulates at high pressures and dangerous temperatures, which may include volatile organic compounds, hydrogen gas, carbon dioxide, carbon monoxide, soot, particulates containing oxides of nickel, aluminum, lithium, copper, cobalt, and hydrogen fluoride. The guide states that correct personal protective equipment (PPE) and self-contained breathing apparatus (SCBA) should be used for all LIB fire encounters.

While the Tesla response guide can be considered mostly standard across all electric cars, applying some aspects to LIB powered train fires would be more challenging. While most designs for LIB trains are still in the development phase, there are three main design options being considered for locations of the

cells. A Siemens, 120-passenger, LIB train is scheduled to be delivered for operation in Baden-Württemberg, Germany, in 2023 [31]. This press release from Siemens states the train is a hybrid between electric overhead-wire powered, and LIB powered, with the ability to travel around 80 kilometers on only the LIB's, which are mounted underfloor in two separate packs.

A different battery design option can be seen in Wabtec's press release on their new FLXdrive Battery-Electric Locomotive (BEL) [32], which has also received order for delivery in 2023. Wabtec states this order will contain an upgraded version of their pilot BEL, which was the world's first 100-percent battery-powered, freight locomotive. While the locomotive itself is fully battery powered, its intended use is to supplement traditional diesel-electric locomotives (or other fuel source locomotives) due to the large loads seen in freight transportation; specifically, the company who placed the order (BHP, Australia) will combine two of the BEL locomotives with their current four-diesel-electric locomotives, who together will haul a 270-car consist that is used to carry 38,000 tons of iron ore. In Wabtec's general specifications for the pilot BEL, that operated in a similar diesel-electric-BEL hybrid system and completed successful testing in 2021, the consist's total fuel consumption was reduced by 10 to 15 percent, and greenhouse gas, particulate matter, and nitrogen oxide(s) emissions also reduced by 10 percent [33]. The specifications for prototypical version are as follows:

- Engine room replaced with 20 battery racks, which are made up of approximately 20,000 LIB cells.
- On-board BMS and HVAC system in the container car.
- 30–40-minute capacity for full, 4400 horsepower output.
- Maximum hauling weight of 430,000 lbs.
- Maximum speed of 75 mph.
- Both wayside and regenerative breaking capabilities for charging.
- Tested on 350-mile route.

The arrangement of the Siemens cells is similar to a typical electric car, where the cells make up the undercarriage of the vehicles; where the Wabtec locomotive can be likened to a BESS system on wheels, similar to the non-mobile McMicken BESS discussed previously. Both arrangements present significant access challenges during a theoretical battery fire event. Tipping the Siemens train, to better expose the cells for water application, would require detachment of the unaffected cars and heavy machinery. For the Wabtec layout, access to the inside of the container would be required, which poses safety risks. Trains often travel in remote areas that could also present further access challenges. In theory the structure of typical trains would be more durable against fire damage, but the Union Pacific recycled LIB train fire shows the possible danger to surrounding areas of the train [17]. Possible forest fire ignition should also be a concern.

A third design concept has been proposed for the Belmont, NC, single-car, passenger trolley, where a small rail trailer with EV batteries will be pulled behind the trolley car it powers. This trolley, currently in development, is local to UNC Charlotte and is discussed further in Chapter 8. While this car still presents battery access challenges, they may be less difficult to overcome due to the smaller size of the trailer and lower number of batteries.

2.2 LIB Characteristics

To effectively perform LIB fire testing, a fundamental understanding of their design, and electrical and thermal properties is required. In research conducted on the fire safety of LIBs in road vehicles, Bisschop et al., describes some of the structural and geometric properties of the three main types of LIBs [34]. Pouch cells are sealed in foil which makes them flexible, and while this design is cheaper and lighter, it also allows for easier puncturing, and the cells may require a support structure to resist bending stresses. Pouch cells have an efficient internal layer design, which sees their current collector assembly stacked, instead of rolled like in some hard-cased prismatic and cylindrical cells, although some hard-cased cell also see stacking. This stacked layering allows for higher energy density per cell. This energy density translates into the

module level for both soft (pouch) and hard prismatic cells, since they can be packed directly next to each other with their thin, rectangular design.

Bisschop et al. also cited cylindrical cells as having higher mechanical stability than their prismatic counterparts, due to their round shape distributing both internal and external pressure around the circumference [34]. Relating this round shape to module packing, the authors note a decrease in efficiency is seen in terms of unused space between the batteries when they are placed next to each other at their long round edges. This loss of useable space likely provides an advantage however, since these air gaps allow for cooler air to circulate between the cells, aiding in their temperature regulation. Tightly packed prismatic cells provide virtually no room for heat dissipation between them, which can reduce the time needed to reach thermal runaway. A generalized graphic by Bisschop et al. demonstrating this packing comparison, can be seen in Figure 2-1.

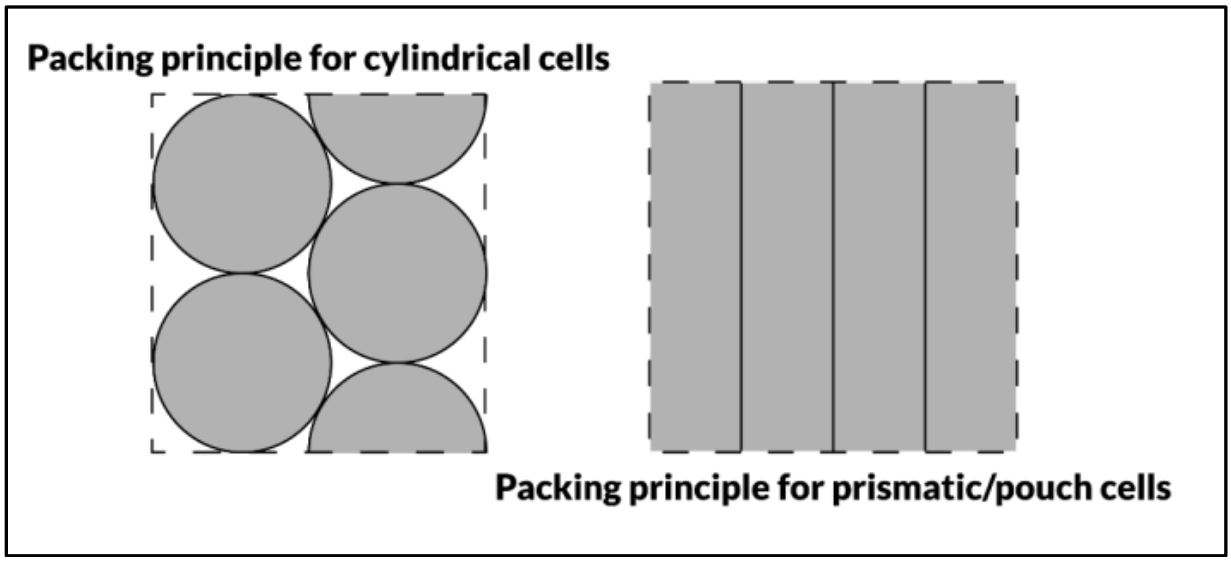

Figure 2-1: Packing of LIB shapes [34]

Note, that most modern cylindrical cells, and all tested in this research have built in safety vents at their positive end caps. In a reviewed study on 18650 vents, Ouyang concluded that vented cells helped to delay TR when compared to 18650s without vents [35]; and when SOC levels of 0, 50, and 100 percent were tested, a key finding was that higher SOC cells saw reduced effectiveness from vents in delaying TR.

Continuing reference from Bisschop et al. [34], a brief section discusses anode materials in typical LIBs, stating there are only two, general options commercially available. These two anode makeups are carbon based and lithium titanate oxide (LTO), where the latter is more expensive, it delivers better performance in thermal stability, charge/discharge rate, and life cycle.

Anode type was not considered as an investigative parameter for this scope. but may be an effective parameter to investigate in future research.

The internal failure of LIBs in thermal runaway can differ between chemistry and geometry but can also differ from cell-to-cell in the same model of batteries. The European Council for Automotive Research and Development (EUCAR) has classified each failure mode with a numerical, "hazard level" ranking system, where the descriptions of each level and certain criteria to be classified at a level are also given. This tabulated information, given by Bisschop et al. [34], can be seen in Table 2-1.

Table 2-1: EUCAR LIB failure hazard levels [34]

Hazard Level	Description	Classification Criteria and Effect
0	No effect	No effect. No loss of functionality.
1	Passive protection activated	No defect; no leakage; no venting, fire, or flame; no rupture; no explosion; no exothermic reaction or thermal runaway. Cell irreversibly damaged. Repair of protection device needed.
2	Defect/damage	No leakage; no venting, fire, or flame; no rupture; no explosion; no exothermic reaction or thermal runaway. Cell irreversibly damaged. Repair needed.
3	Leakage, $\Delta mass < 50\%$	No venting, fire, or flame[8]; no rupture; no explosion. Weight loss <50% of electrolyte weight (electrolyte = solvent + salt)
4	Venting, $\Delta mass \geq 50\%$	No fire or flame[8]; no rupture; no explosion. Weight loss ≥ 50% of electrolyte weight (electrolyte = solvent + salt).
5	Fire or flame	No rupture; no explosion (i.e., no flying parts).
6	Rupture	No explosion, but flying parts of the active mass.
7	Explosion	Explosion (i.e., disintegration of the cell).

If a consumer wanted to choose what type of cell to use with thermal safety as a priority, the most likely way to accomplish this would be by selecting on cathode chemistry. Several studies were found comparing different chemistries under different tests. In research by Orendorff et al., Figure 2-2 shows the results from accelerated rate calorimetry (ARC) of different battery chemistries at a state of charge (SOC) of 100%, where the internal, self-heating rate of the batteries was investigated.

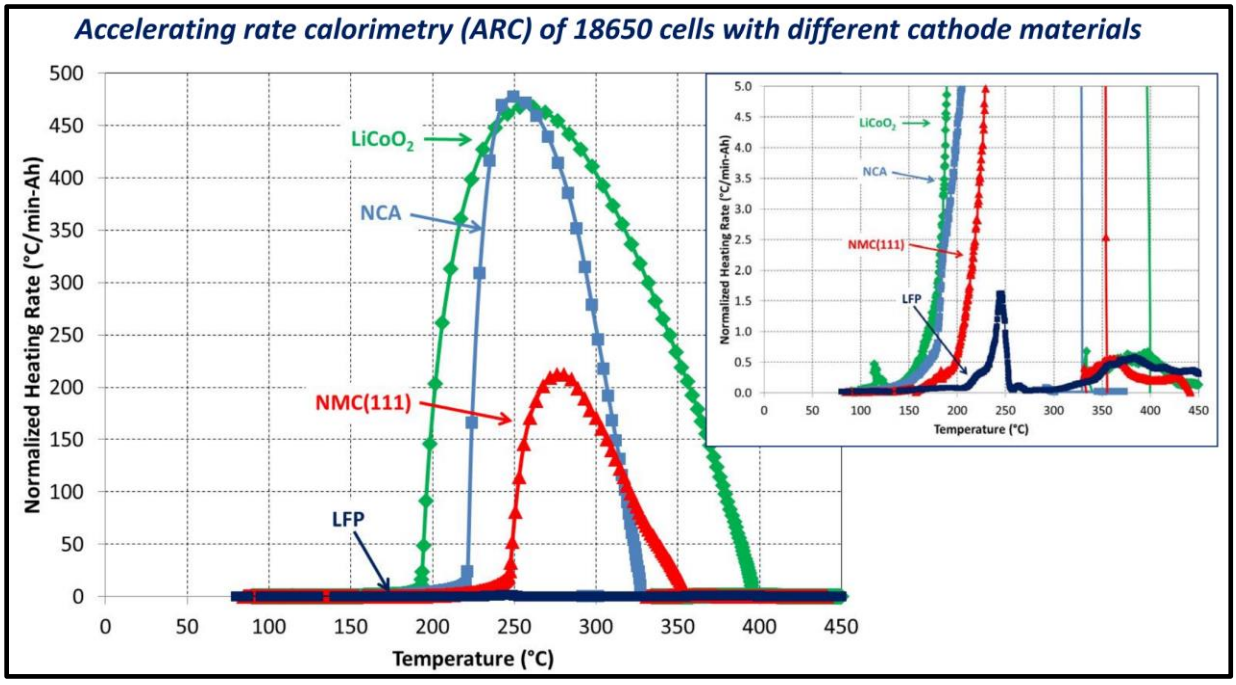

Figure 2-2: ARC vs. SOC for batteries with different cathode makeups [36]

The NMC cell in Figure 2-2 shows a maximum heating rate that is approximately half the maximum heating rates of the LCO and NCA cells, where the two latter cells reached their max rate at a lower temperature [36]; however, the LFP cell's max heating rate was approximately 130 times less than the NMC and 270 times less than the NCA and LCO cells. This alludes to a significant advantage in thermal stability in the LFP cells, which was also concluded by the authors. A key demonstration in Figure 2-2 sees the sudden rate change of the LCO cells occur at the lowest temperature (below 190 °C), while the LCO rate stays high through higher temperature exposure as well.

In the similar previously referenced study and test by Brand et al. [4], ARC was used to test NMC, NCA, and two different LFP cell types. For the LFP cells, a maximum temperature rate of 28 °C/min was found in "LFP1" by these researchers, and a maximum rate of 7 °C/min was found for LFP2. In comparison to the tested NMC and NCA cells, which saw temperature rates of more than 400 °C/min, both LFPs showed significant advantages in terms of thermal stability. This means, that the investigated LFP/C cells show a significantly higher thermal stability in this test as well. The plot of the findings in Brand's study, seen in Figure 2-3, shows similarities to the Orendorff et al. study [36], meaning the findings are likely consistent across the chemistries tested

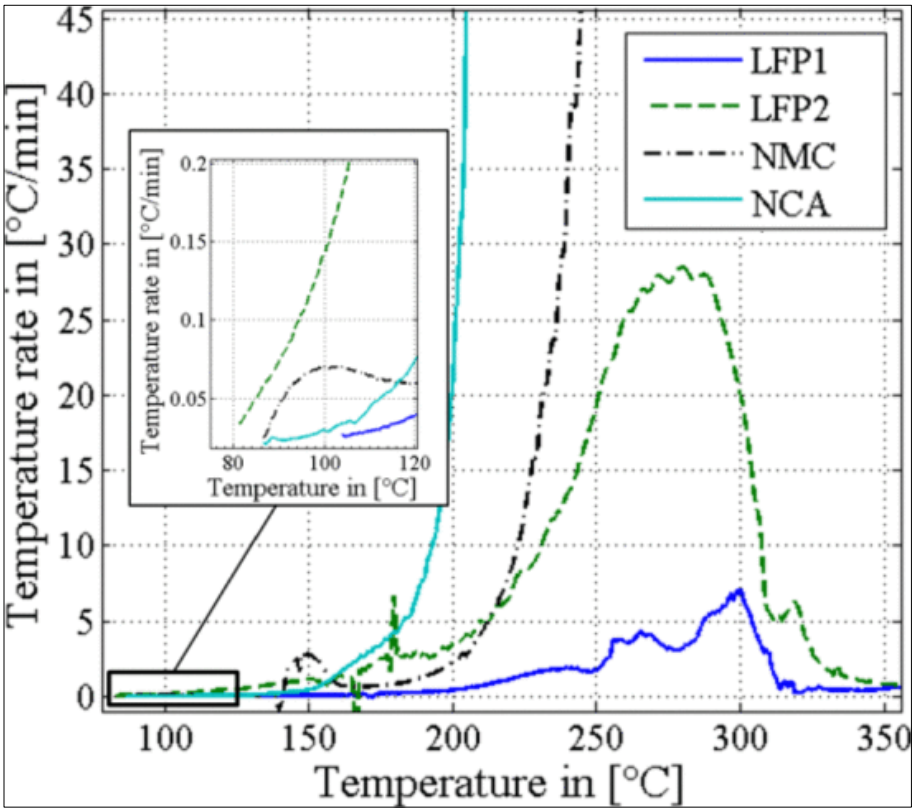

Figure 2-3: Brand et al., study on chemistry heating rate [4]

A tabulated breakdown of the plots in Figure 2-3, for the self-heating onset temperature and the temperature when self-heating surpassed 5 °C/min was provided, and seen in Table 2-2 [4].

Table 2-2: Brand et al., heating rate temperature of onset/increase [4]

	Type	T_{onset}	T when rate >5 °C/min
1	LFP/C	104 °C	287 °C
2	LFP/C	81 °C	212 °C
3	NMC/C	88 °C	212 °C
4	NCA/C	86.5 °C	183 °C

Brand et al. stated that the LFP cathode material has an olivine structure, which did not display an exothermal decomposition reaction [4]. During overheating no oxygen gas was released and the rate declines in LFP1 at 250 °C and 280 °C, the researchers attributed this to safety vent activation in the first drop, and complete removal of the positive end cap in the second.

Throughout the multi-study, literary review conducted for this research, LFP cells consistently demonstrated to be the safest chemistry in term of fire safety. It should be noted however, that Brand et al. found a disadvantage in these cells besides energy density, which occurred in a separate, overcharge test of the same cells used in their ARC tests [4]. Both LFP cells showed an effectively immediate exothermic reaction once full SOC was reached, whereas the NMC and NCA cells demonstrated a buffer effect against overcharging, which can be seen in the referenced Table 2-3.

Table 2-3: Brand, overcharge buffer resistance [4]

	Type	SOC onset	T rate after onset
1	LFP/C	1	0.8 °C per % SOC
2	LFP/C	1.05	0.77 °C per % SOC
3	NMC/C	1.35	1.02 °C per % SOC
4	NCA/C	1.3	1.74 °C per % SOC

Both nickel chemistries demonstrated a buffer of 30% over full charge or more [4]. Brand et al. noted that overcharging can be one of the severest failures to occur, due to the ability of over loaded anodes to deposit lithium metal onto the carbon in the cell which can reduce thermal stability. Recall that lithium deposits were also cited as the cause of TR in the McMicken BESS fire by investigators [23]. While the Brand et al. tested LFPs showed no overcharge buffer [4], all cells were equipped with a current interruption device (CID), which is common amongst most 18650 cell designs. CIDs activate similar to vent cells, where internal pressure exceeds a certain limit in the cell, causing the CID to push outward creating discontinuity in the cell circuit, terminating current flow. Brand et al. provided a diagram that illustrates the functional design of a CID in an 18650 cell, shown here in Figure 2-4.

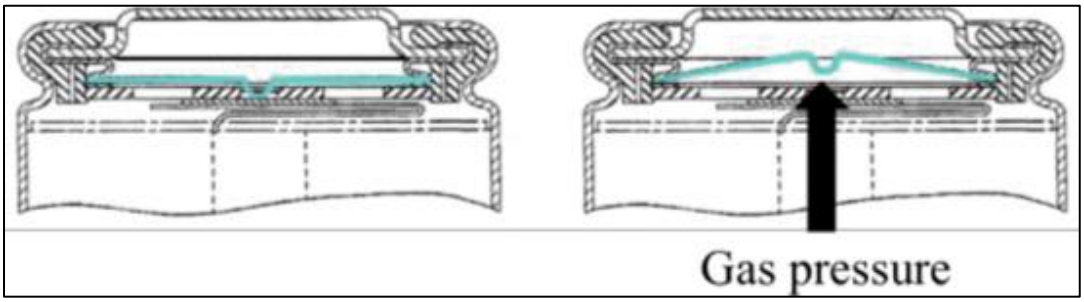

Figure 2-4: Brand et al., CID diagram [4]

Orendorff et al.'s study also made comparisons between different SOC levels within the same cell type [36];from their tests, Figure 2-5 shows the reference heating rate versus temperature plot of the same IMR pouch cells at different SOCs, where

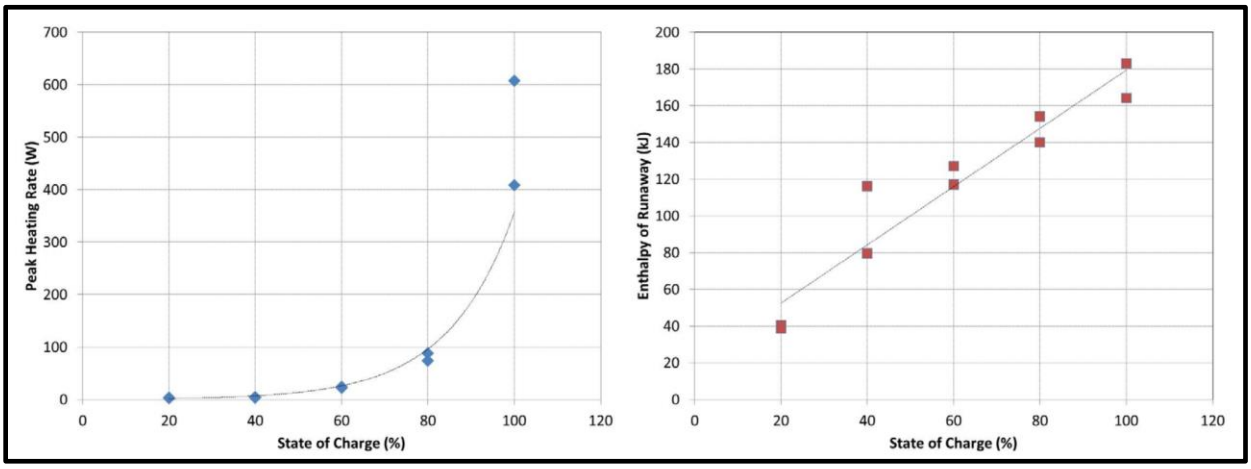

Figure 2-6 shows the peak rate for each SOC level tested.

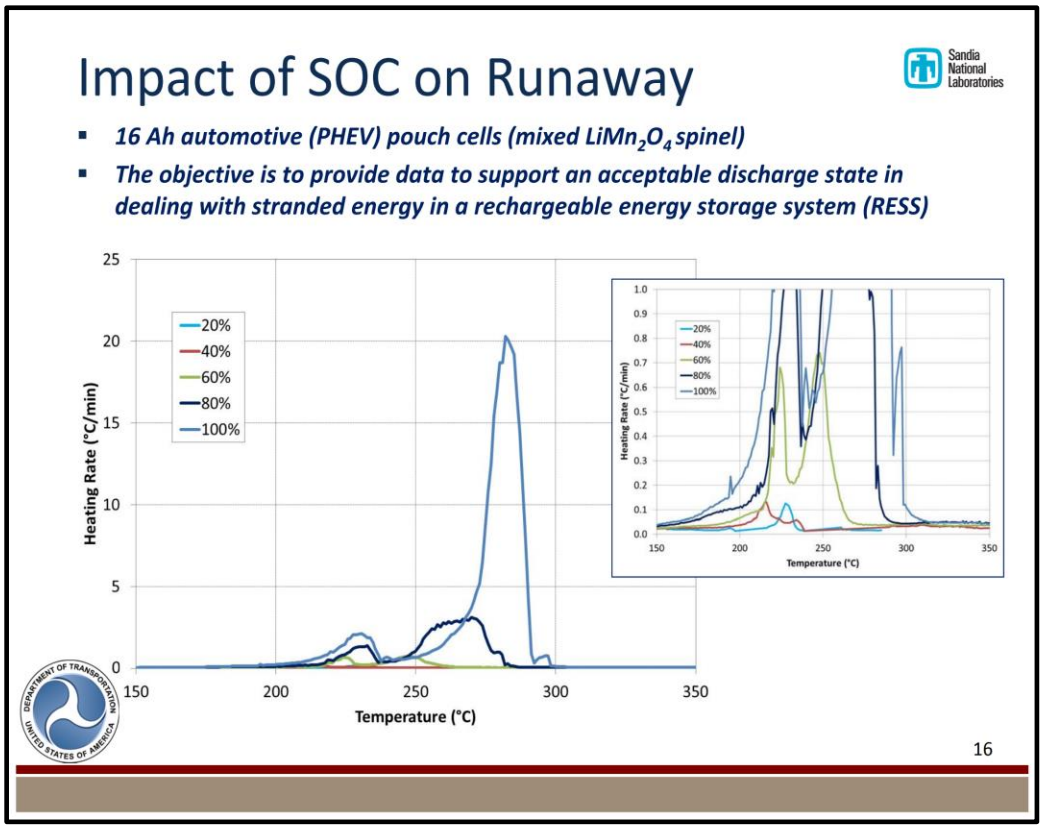

Figure 2-5: SOC impact on TR in 16 Ah automotive pouch cells [36]

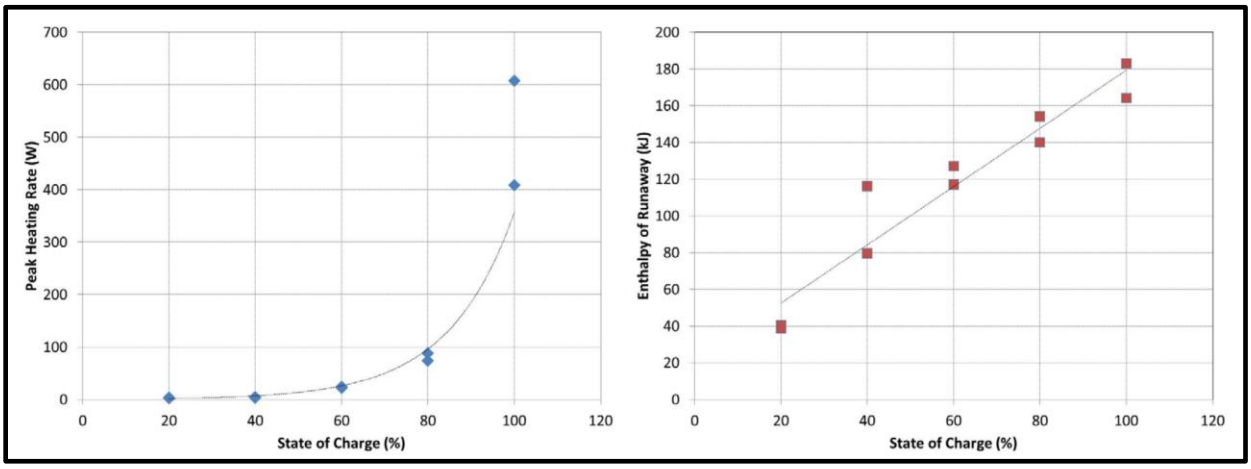

Figure 2-6: SOC relationships [36]

The scaled in view in Figure 2-5 shows that for the higher SOC cells the initial heating rate starts off larger and that rapid increases in heating start at a lower temperature [36]. Effectively, there is an exponential correlation between the maximum heating rate and the SOC, as seen in

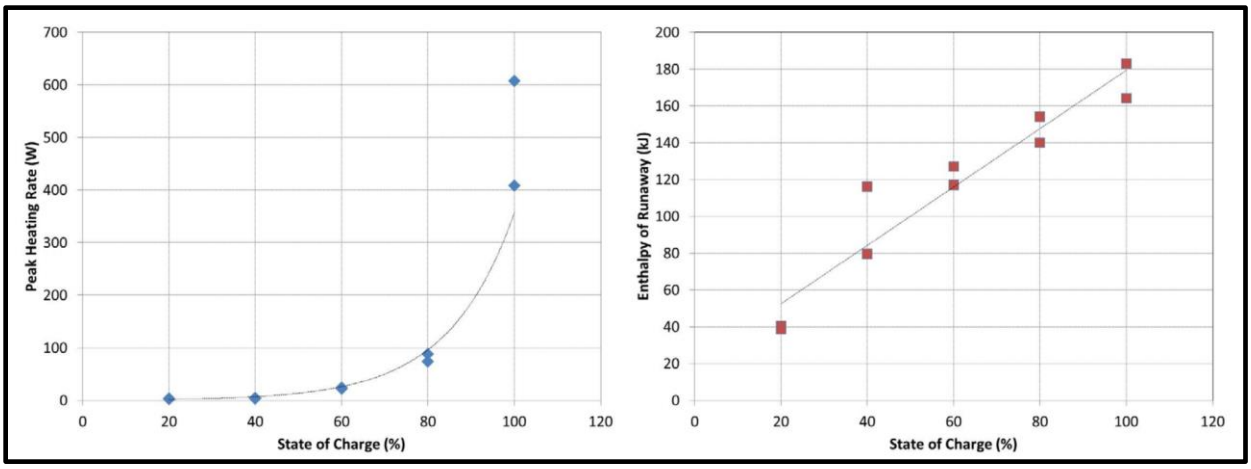

Figure 2-6. In the same figure a linear relationship between the total release of energy and SOC can be seen, and these researchers note a significant decrease in heating rate around 40-60% SOC and recommend a standard shipping and handling SOC of approximately 50%.

2.3 State of Research Methods

While information on battery behavior seen in different studies was gathered, the experiment methods used to test the cells was also compiled. A study from Xiong et al. listed representative LIB fire incidents [37], similarly to section 2.1 of this paper, and they found internal short circuit (ISC) involves 52% of the accident probability, whereas the external short circuit (ESC) involves 26% of the accident probability. Different types of cell safety and qualification testing often aim to recreate ISC and ESC, to investigate TR and fire in LIBs. The general test methods seen throughout this literature review of the field of LIB fire safety research are as follows:

- ARC testing (previously discussed 2.2)
- Nail penetration testing
- Indentation testing
- Pinch testing
- Forced internal short circuit testing
- Overcharge, over-discharge testing (previously discussed 2.2)
- Equivalent short resistance testing
- Heating element (hot plate) contact testing

The Xiong et al.-study investigates many of these test methods in detail [37], where they claimed nail penetration to be a widely used method, also stating this test to be a standard in battery qualification. These researchers found that depth of penetration does not correlate to temperature increase but speed and location of puncture does. Middle-cell penetration caused faster propagation, and in general repeatability for nail testing is important.

Xiong et al. found that the indentation test was developed to investigate different layers of the cell, in terms of mechanical stability [37]. Xiong et al. warned that an indentation of just 1mm could lead to TR hazard, while also being virtually invisible to the human eye. The nature of this test method also causes ISC

to occur in the outer layers of the cell, where the researchers note that heat can dissipate quicker from these exterior layers than from the middle of the cell, thus, the initial temperature results may ineffectively show the seriousness of the failure. The pinch test produces a similar effect but by applying force at two opposite sides of the cell, here researchers were able to create ISC with smaller than 1mm indentations.

Non-ARC heating of the cells, which is the method used for this paper's research, was not discussed in Xiong et al.'s meta-study, and was not found to be used in most other studies; however, direct heating of LIBs was used in research by the Federal Aviation Administration (FAA) [38]. In this FAA research single-cell, ignition, and propagation tests were performed. For the single-cell cylindrical tests, a 100-watt cartridge heater was used to instigate TR, while a 240-watt hot plate was used to start TR for the lithium-ion-pouch cells and button cells. For the single-cell tests, two $1/16^{th}$-inch, type-K, inconel TCs were used, one on the heating element and one on the cell surface. For the propagation tests, the cylindrical cells (5) were placed next to each other along their long edge with a TC on the battery next to the heater and the battery at the other end, the pouch cells were stacked vertically by their largest face and held down with a steel plate. In this research some of the cell types tested will not self-ignite their gasses released during TR, so for these tests an oil-burner spark gap was situated about an inch up and inch away from the cells' vent locations. These igniter tests were performed in a pressure vessel with a volume of almost 11 cubic meters. At first signs of venting the burner was activated and left to remain on for the duration of the test, while TC application similar to their single-cell tests recorded TR activation. Additionally, hydrocarbon presence and pressure with the chamber were also recorded, where a fan within the cell helped circulate vented gasses to increase readings by the gas detection instruments. Notably this FAA research also concluded that LFP cells show advantages in thermal stability.

In the report by Bisschop et al. [34], a similar external heat abuse test on LIBs was referenced. In this test LIBs were placed in an over that heated to 300 ^{o}C in a consistent amount of time. This study found that all the LCO cells reached TR by 190 ^{o}C, and that about 15 seconds later gasses in the oven ignited in over half of the tests. For the 18650 cells tested in a similar fashion, TR was found to occur around 220 ^{o}C, which

resulted in an immediate fire. The 18650 cells also displayed a discharge of liquid electrolyte leading up to TR. In this study and the FAA study [38], the point of TR activation was determined by the first sign of rapid temperature increase of the cells. LFP cells were also applied to Bisschop et al.'s oven method [34], and again this chemistry displayed little-to-no signs of TR.

CHAPTER 3: EXPERIMENTAL DESIGN AND SETUP

3.1 Experimental Setup

A schematic of the general test system and environment is shown in Figure 3-1, along with a functional view of the equipment and test safety measures shown in Figure 3-2. The main components of the setup include a test chamber (box furnace) containing a hot plate for application of thermal abuse, thermocouples and cameras, and wireless data acquisition system. The ThermoScientific box furnace contained a ceramic fiber interior capable of withstanding high temperatures and impact. The door was propped open during testing to allow clear views for the image recording devices at a safe distance. A dimensioned schematic of the box furnace is shown in Figure 3-3. Nearly all individual cell tests were performed in the box furnace save for a few that were performed in the large steel containment (see section 3.3).

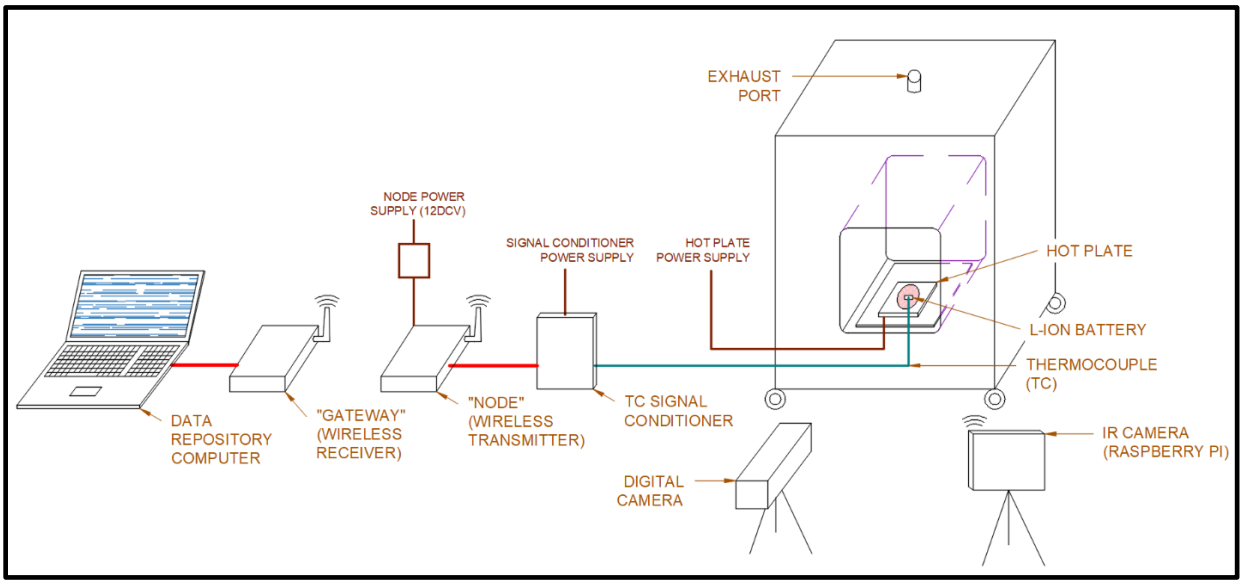

Figure 3-1: Thermal abuse test system schematic

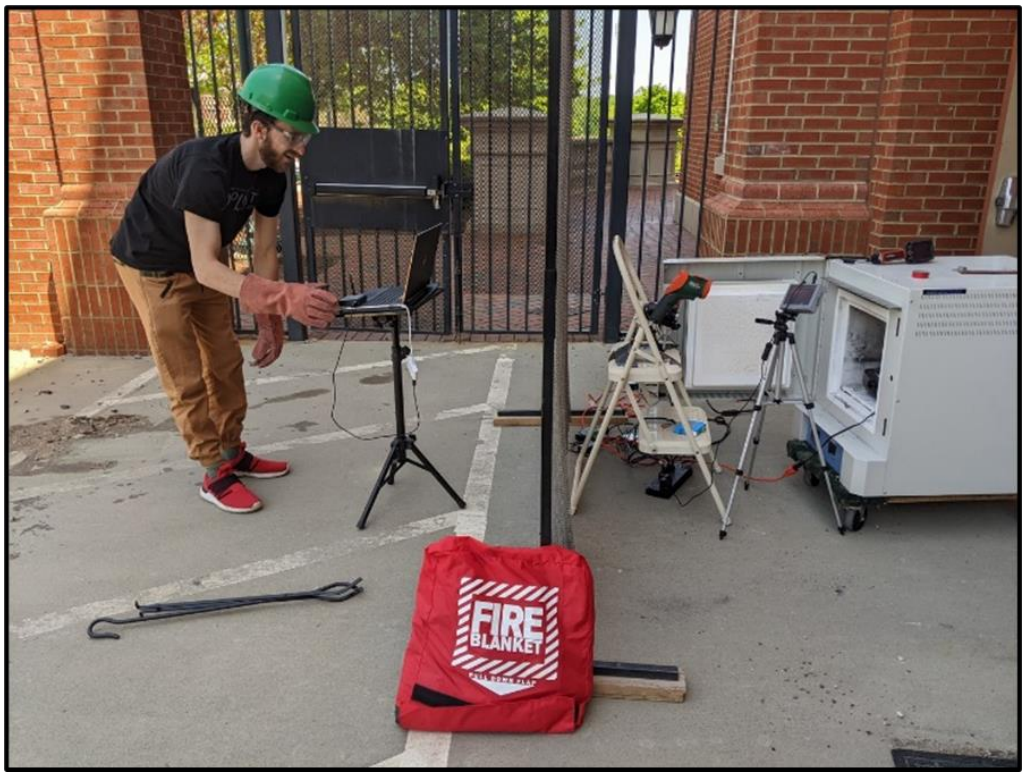

Figure 3-2: Typical testing environment

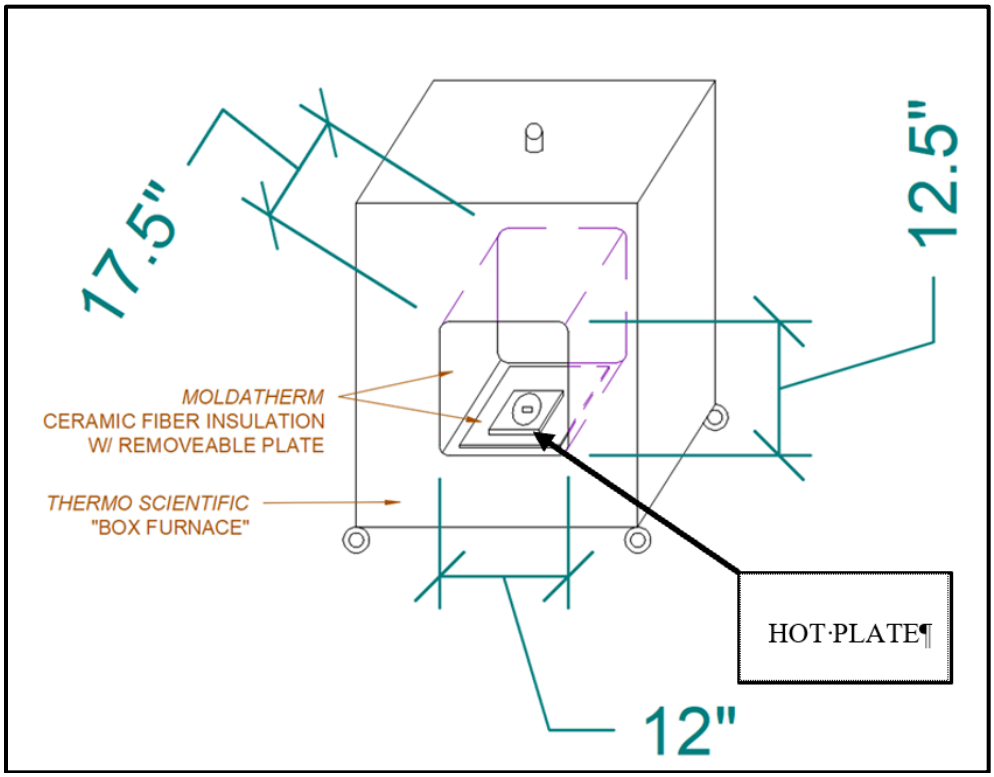

Figure 3-3: Box furnace detail

For all tests performed, an Oster brand electric hotplate was used to create thermal abuse to facilitate an ISC, simulating a real-world LIB failure mode. An initial analysis of the hot plate by itself was conducted using the same temperature measuring devices applied to battery tests, which are discussed in detail later in this section. Inconsistent temperature readings across the surface of the plate were seen on the first test run of the plate. Thermal images from multiple IR thermography devices showed the location of a smaller, sub-surface heating element. The same location was also the point of maximum plate surface temperature at any time in the heating process. A schematic of the hot plate dimensions and hot spot location is shown in Figure 3-4.

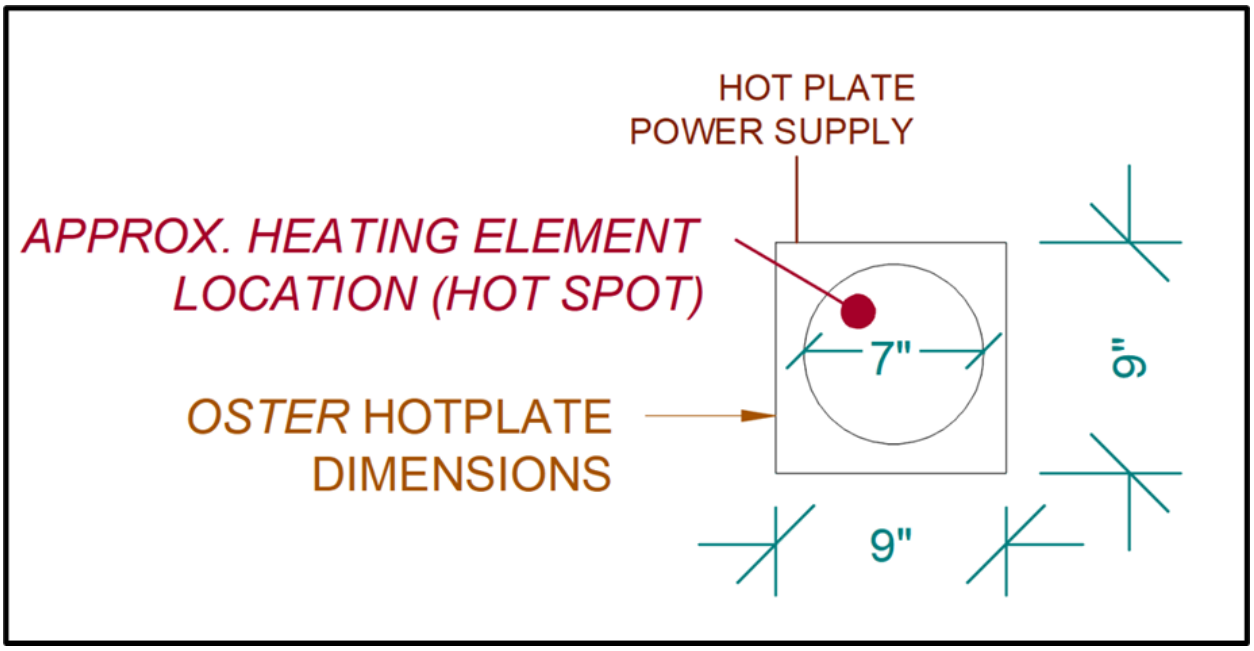

Figure 3-4: Hot plate schematic

Upon seeing the temperature profile of the plate surface, the hot spot was chosen to be the consistent location of battery placement throughout testing. To determine the controllability of this heating method, the heating rate of the hot spot and its rate consistency was investigated. To determine the heating rate, an IR thermometer (brand: EXTECH) with data logging capabilities was placed on a stable tripod positioned at an angle above the plate; upon confirming proper calibration of the thermometer's guiding lasers, it was

aimed at the hot spot and activated, while the plate was allowed to heat from an inactive ambient temperature to its maximum temperature, which was determined after no increase in temperature was observed for some time. A plate heating rate was plotted using the time of plate activation, after first activating the temperature logging device, with the timestamp of the first data point logged. This process was repeated to determine the heating consistency of the plate. While the plate consistency was deemed sufficient to begin testing, the same plate temperature recording method was used during several subsequent battery tests to monitor any depreciation in performance of the plate over time. To improve efficiency of the test procedure, plate temperature was spot checked but not recorded in some tests as extended consistency was confirmed. The data sets used to check plate consistency were plotted together, along with the average heat rate adjusted for outliers caused by interruptions in some plate data logging sessions, which can be seen in Figure 3-5.

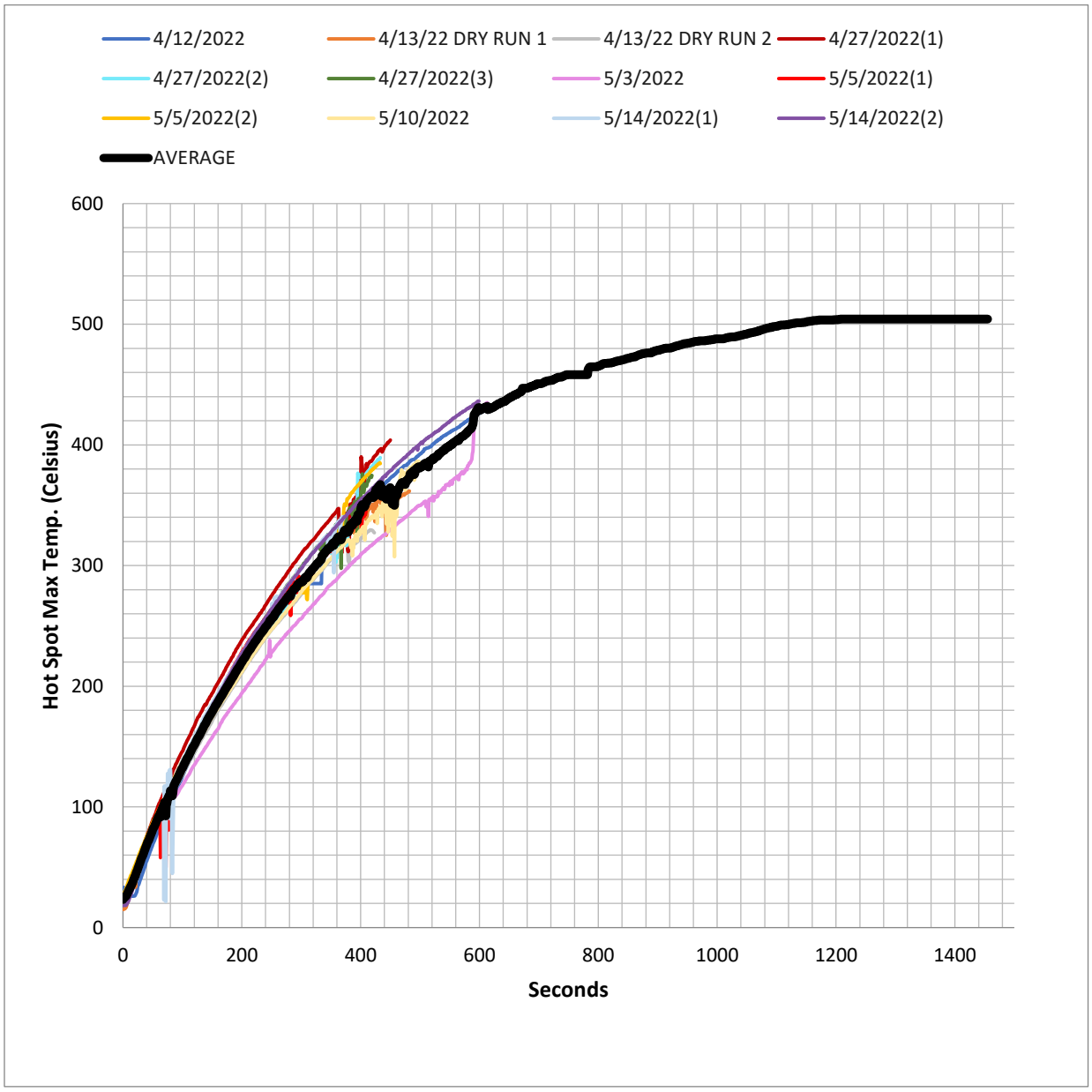

Figure 3-5: Hot plate temperature data w/ adjusted average curve

A large portion of the tests performed used the same plate (26 reported tests), except for tests on or before 4.8.22 (method development phase, two reported tests), and, on or after 6.23.22 (nine reported tests), which used different plates of the same make and model. The plate cooling rate quickly proved to be too slow for bringing the plate back down to safe levels to leave unattended, and for efficient back-to-back tests. To expedite the cooling process, a metal pan filled with ice was placed on the unplugged hot plate to

return the plate to ambient temperature for the next test or storage. A few different metal pans were available in the lab, some were lightly colored aluminum pans designed for use in soil drying ovens, while others were darker and designed for baking food. It should be noted that the simple pans were visually observed to cool the plate significantly faster than the food baking pans, which is predicted to be attributed to the food pans being designed to absorb heat.

3.2 Instrumentation and Data Acquisition

A TC and IR video camera with wireless transmitting capabilities were used as the LIB and fire event monitoring system. This system, with planned combination of gas sensors, was proposed with anticipated future applications to LIB powered trains. While the first generation of the monitoring system came with a probe style TC (Omega), this was replaced during the experiment design phase with two type-K surface TC (both Evolution). In the current system design, which was used for all tests, the TC is connected to an Omega brand signal conditioner which translates the TC signal for the "node" device to which it is wired. The "node" acts as a router which transmits all data to the "gateway" device which is located a safe distance away. The "gateway" is connected by a USB cord to the experiment monitoring computer, where the data logging software (SensorConnect) records and displays the data in real-time. The gas sensor that was used in the initial test runs of the system were also able to connect to the "node" and without a signal conditioner. The current node can receive 8 separate sensors. The two-in-one (CO, CO_2) gas sensor needed its own power supply, and so does the conditioner and node. When attempting to validate the gas sensor, by comparing its ambient air and human breath readings to expected, it was deemed to be insufficient for testing requirements. It was concluded that this was likely due to the sensor being designed for use in HVAC ducts, and gas detection was tabled for future research. In theory this system could be expanded to include more sensors and configured to be powered by the same batteries it is monitoring.

While the IR video camera (brand: ADAFRUIT) is considered part of the overall monitoring system and stores its data and images on the same computer as the TC data concurrently, the camera operates on

separate software and connectivity. The small camera is wired to a handheld tablet, on a tripod, which utilizes a RaspberryPi operating system. Its use is also wireless from a safe distance using a remote desktop connection to the IR camera tablet, established by the main monitoring computer that is also using a screen and audio recording software (currently Open Broadcaster Software, or OBS, set to record only the remote desktop viewer window and audio). Note that for some test no audio was recorded, and the cause is unknown at this time. This connectivity type differs from the TC radio frequency communication between the node and gateway, in that the current remote desktop function requires the main computer and IR camera tablet to be connected to the same stable Wi-Fi network throughout the test. So far using the C++ programming language to operate the camera and displays its images has shown to be best available option that was provided with the device. It should be noted that throughout all tests performed in this research, where an IR video was successfully recorded, the image being viewed is mirrored from the expected first-person view at the same location, and the digital camera recordings' views. For instance, if a person were standing at the same location as the digital camera and IR camera, all with similar trajectories of vision toward a battery test, and the person saw the battery rocket upwards and to the right, the digital camera recording would display the same battery path; however, the IR camera would display the cell travelling up and to the left. In cases where a test called for the IR camera to record for an extended length, the displayed live video would often freeze after 15 minutes, rendering the recording useless beyond this point. While few tests called for this much recording time, this occurrence happened nearly every time when it was required. For the tests covered in the scope of this research, these time and distance to reliable Wi-Fi limitations were an effective non-issue; however, these issues should be carefully considered for future similar studies and practical train applications, if not resolved completely.

To validate the TC and IR video camera temperature readings, three supplemental IR devices and three supplemental TCs were employed. The IR devices consisted of two handheld "gun" thermometers (EXTECH Video IR Thermometer, FLIR), and a handheld still thermal photograph camera (FLIR Compact Thermal Camera); the latter option gave a real-time display of two selectable location temperatures, and

the max/min temperature/location within its field of vision. The supplemental TCs were also type-k and were connected to a National Instruments Compact Data Acquisition (NI-CDAQ, referred to as DAQ throughout text) system; a similar device, yet non-wireless, to the node/gateway used with the main TC. These TCs reported to the National Instruments (NI) DAQ Express software on a separate computer from the main data collection computer. When validating the main TC, all supplemental devices reported the same temperature on both the heated hotplate and a human body within reasonable degrees of deviation; thus, both the main TC and supplemental devices were deemed valid for immediate testing or further use as validators. The IR video camera temperature readings did not have the same congruency to the other approved devices. The IR camera's distance from the desired temperature surface played a significant role in the magnitude of its inaccuracy compared to the other devices running concurrently with the same point of interest. Distance was not initially expected to be an issue, within reason, for this camera; but the issue is believed to stem mainly from the lower resolution quality of the camera and possibly not being able to focus the camera with the current setup. While its temperature readings are inaccurate, the camera was still deemed beneficial to tests performed as it provides a secondary timestamp reference for visual and audible "landmarks" during specific tests (see result interpretation in chapters 4 and 5), a somewhat accurate account of temperatures when TCs may have been removed during fire events, and functional practice of similar IR devices used in the future. These procedures conducted for the main test system, in turn also validated the supplemental IR devices for the hot plate heating analysis and spot checking of plate temperature, and displaced battery casing temperatures after explosions/fires. For most tests an attempt was made to record the temperature of any pieces of the battery that been displaced and/or separated from any TCs, using the listed handheld thermal devices. It should be noted that many times, the capacity range of the available handheld devices was exceeded. The DAQ TCs were likewise validated for use in multi-battery propagation tests.

A digital camera was used to capture audio and visual recording of the heating tests which proved to be essential in lining up the separate datasets provided by the various instruments used during each test, on

top of the ability to go back and slowly breakdown each important reaction of the battery that cannot be recorded by the human eye. While not immediately apparent, it was found that turning the digital camera on and recording first, combined with providing clear voice callouts when activating the other equipment reduced the difficulty of processing the results. Result processing is further aided by starting TC data collection and turning on the hotplate at the exact same time, which was achievable since at least two people were present for each test, which is highly recommended for test safety. Other forms of test safety used or on-hand in every test include: PPE (hard-hat, facemasks, thick high-temperature gloves, protective eyewear), a chain-linked steel curtain, fire blanket, large and long high-temperature forceps (hot battery handling), plenty of ice close by (plate and heated battery cooling), performing tests outside yet in Wi-Fi range, and placing the batteries and hot plate in a durable and fireproof containment that allows for instrumentation and viewing of tests.

Regarding the general experiment setup, a troubleshooting note should be made about an issue encountered on the computer used in most tests that is pictured above. The SensorConnect software, used for data recording from the node/gateway system, would not immediately recognize the standard USB port connection between the computer and gateway. A USB-to-USB-C adapter was required to meet the minimum bitrate of 921,600 baud (bits per second) for the port connecting the gateway. The baud rate capacity was focused more on the newer USB-C type ports and lacked capacity in outdated ports. An automatic connection to the gateway still did not occur and had to be created manually in the SensorConnect settings menu. A detailed instruction manual for the SensorConnect software and hardware setup and operation is in the appendix.

3.3 Individual Cell Test Setup

The prismatic, hard-cased ICRs and both cylindrical chemistries (IMR, INR) were tested individually. Before setting up the test system, the SOC of each battery was checked and increased if desired. Two “universal” chargers with SOC displays were used, one designed for prismatic LIBs (brand: Rijer), and the

other designed for multiple sizes and types of cylindrical cells, not just LIBs (brand: EASTSHINE), can be seen in Figure 3-6 and Figure 3-7 respectively.

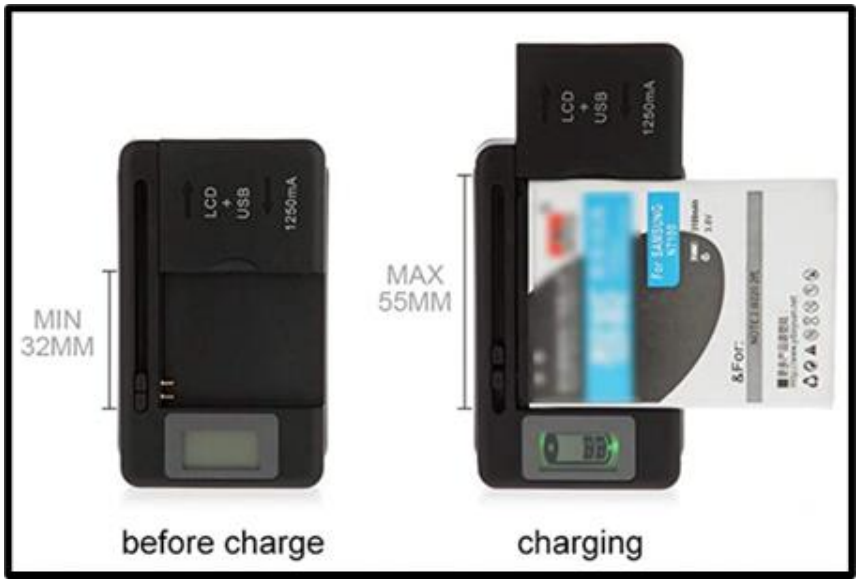

Figure 3-6: Rijer prismatic charger

Figure 3-7: EASTSHINE cylindrical charger

The Rijer charger was also able to be used as a battery discharge device by unplugging the charger with a non-zero SOC battery still connected, the battery becomes the liquid crystal display (LCD) screen power source. The 18650 cells were not able to be discharged by the EASTSHINE charger. The Rijer charger had disadvantages as well; it would not charge some prismatic cells with 4 charging prongs, which were more common (compared to 3-prong), its SOC display intervals were only every 25%, compared to the more accurate 20% for the EASTSHINE charger.

After a few tests it was decided to record the mass lost from the cell during off-gassing or fire events that did not render the cell unweighable. The mass was recorded in grams before each test along with the battery's capacity in milliampere hour (mAh), and any other notable information to each battery (date, defects, brand when applicable). After a test was completed and the area was safe, batteries were carefully moved with gloves and forceps to the tray of ice being used to cool the hot plate. This quickly cooled the battery, but care needed to be taken when moving the battery to be weighed, while also making sure water did not invade any battery cavities, causing errors in recorded mass.

The surface TC is applied to the batteries along its longest edge opposite of the hot plate, using heat resistant tape in addition to the self-adhesive included by the manufacturer. The batteries were placed on the approximate surface hot spot location before activating the plate. For the cylindrical 18650 cells, pointing the positive end cap left and angled slightly toward the digital camera, kept the safety vent activation in view. This specific placement was not adopted immediately, but as the vents were found to be the consistent first point of 18650 failure under thermal abuse (see chapters 4 and 6), this placement proved most advantageous. An image of both cell types placed for testing can be seen in Figure 3-8 and Figure 3-9 and, where an alternative 18650 placement in Figure 3-10from the 5.3.22 test was only used once for individual testing due to safety concerns (see chapters 4 and 6).

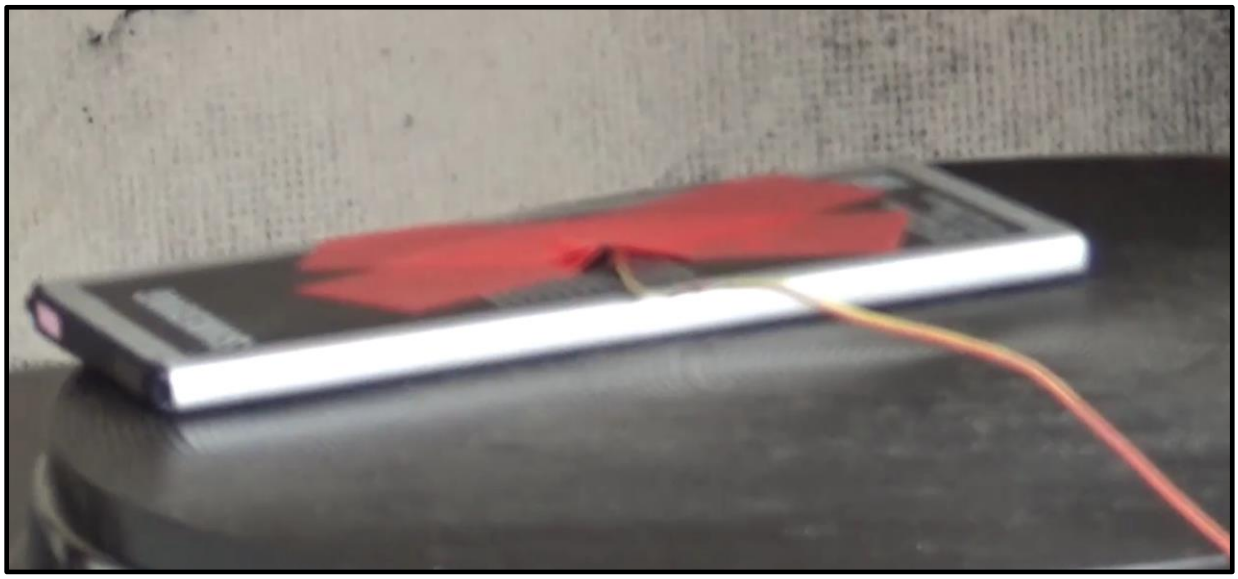

Figure 3-8: Single prismatic cell placement

Figure 3-9: Single 18650 placement

Figure 3-10: end cap placement 5.3.22

Upon placement of batteries and confirming all equipment was ready, all data recording devices were activated starting with the digital camera. The hot plate should be turned on last or at the same time as TC network, in every test the hot plate was turned immediately to its highest setting. A typical first-person view during the test can be seen in Figure 3-11, but note this picture is inside with no steel curtain for clarity.

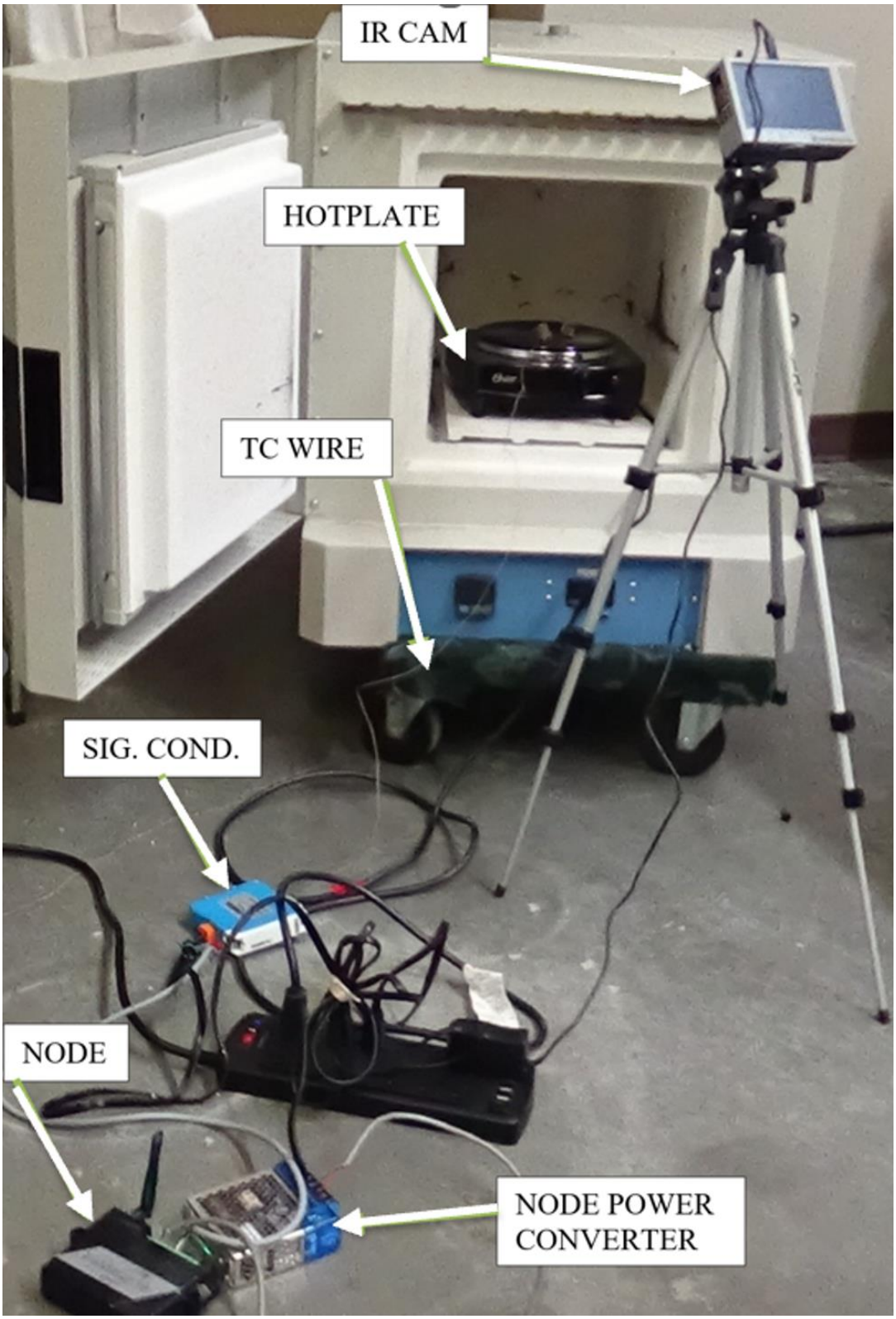

Figure 3-11: First-person view, mid-test

Those performing the experiment were alerted to notice important events throughout the test and called them out clearly to reidentify events in saved videos. While the containment box and curtain were highly effective safety tools; everyone in the test area, on every test, should be prepared for a flaming projectile that may escape the confinement area. Take care to make sure high-temperature battery pieces do not land and stay on equipment and their chords for an extended time, while also unplugging the hot plate as soon as safe to do so after fire event becomes stable. After unplugging plate, make sure to return the temperature dial to the off position to prevent hazards when plugged in later. Data collection devices should be stopped soon after important events have passed or if the TC is removed during the test to reduce data size. The TC was often removed during violent explosions and/or fire; if this occurred supplemental IR thermometers and devices were used when possible. Upon cooling, all tested batteries are stored in the box furnace for safekeeping and reinspection. Recycling and disposal of any LIBs should always be handled professionally.

3.4 Multi-cell Propagation Test Setup

The multiple-cell tests, intended to investigate thermal propagation, followed many of the same steps and processes of the individual cell tests, and used all the same equipment except for the containment box and supplemental TCs. A typical equipment setup, including the supplemental NI CDAQ TCs and computer, can be seen in Figure 3-12 (steel curtain was used but not shown).

Figure 3-12 also shows the large, insulated, steel containment box used instead for the test environment. A plywood cover was placed over its open top to aide in containment and block the wind, while allowing a small gap for light and camera view. A small air ventilation opening was present in the front wall and an exhaust hole was present in the back wall—serving as additional viewing ports as well. For three of the four propagation tests (two 18650, one pouch) the digital camera was placed on the upper rim of the box, looking down on the hotplate which gave a wider view angle. This box and camera angle was also used for a few individual cell tests but made no change to battery behavior. In all tests the IR camera and TCs were used through the side viewport. For the second pouch propagation test (6.11.22), the side viewport was also

used for the digital camera, which gave a better close-up view to witness the pronounced expansion of the pouch cells.

Figure 3-12: Typical propagation test setup

Based on the consistent failure of previously tested single-cell 18650s at their positive end caps, for multi-18650 tests, batteries were connected at their end caps with the positive ends pointing up towards the next battery (when applicable). This configuration focused any high temperature material from lower batteries into the battery it was touching. The bottom battery was placed on the hot plate maximum point on its negative end while a retort stand was used to support the tall column of batteries, see Figure 3-13 that also shows TC connectivity along the sides of each battery.

Figure 3-13: Multi-18650 plate setup

For pouch propagation tests, the batteries were stacked by their broad surface directly above each other with surface TCs placed in between each layer at the center of the batteries. The digital camera still in Figure 3-14 shows this configuration and alternate viewing angle.

Figure 3-14: Multi-pouch plate setup

While the larger containment area and weight of combined batteries reduced the overall risk of projectiles, the overall magnitude of fires and smoke were dramatically increased and should be carefully considered. These tests took longer overall, so enough time for the reaction of all batteries must be allotted to ensure that the test area is not entered before it is safe to do so.

CHAPTER 4: CELL LEVEL DATA AND RESULTS

Typical nomenclature to identify a specific test referenced in text, tables, plots, and figures, both included in this document or any supplemental documents, is the date of the battery test. Only if multiple tests were performed in one day will a parenthetic value follow the date, indicating the sequential order of the tests performed. For example, 4.27.22(1) was the first test performed this day (three total).

Once the experiment design and procedure were finalized, all individual cells tested after this point were logged into a data matrix. Each row of the matrix is a single test identified by battery shape, chemistry, and date tested. The main test matrix is grouped by shape and cathode chemistry, and these categories will be stated where specific tests are referenced elsewhere. The reportable parameters of each test are as follows: SOC, mAh, expansion (time to first sign, time to max expansion), smoke/smell (plate temp, battery temp, time), pressure release (plate temp, battery temp, time), explosion (plate temp, battery temp, time), occurrence of fire, fire length, fire description, battery temp after, post condition of cell, loss of mass, distance travelled, test notes. This matrix was completed using the aid of audio/video recordings (both IR and regular), TC data logging, IR thermographs and thermometers, pictures, and visual inspection. Due to battery variability, occasional human error, and violence of some reactions; some of the data and media options were not obtained for a few tests and are noted in the matrix; however, the majority of performed tests produced sufficient data to highlight behavioral trends by categories of the LIBs tested, and their outliers.

4.1 Sample Prismatic Test Results

The following information details a selected individual test (5.4.22) of a prismatic LIB. The TC temperature recordings for the ICR (NMC) hard-case battery, with 100% SOC, is plotted over the time from hotplate activation, shown in Figure 4-1.

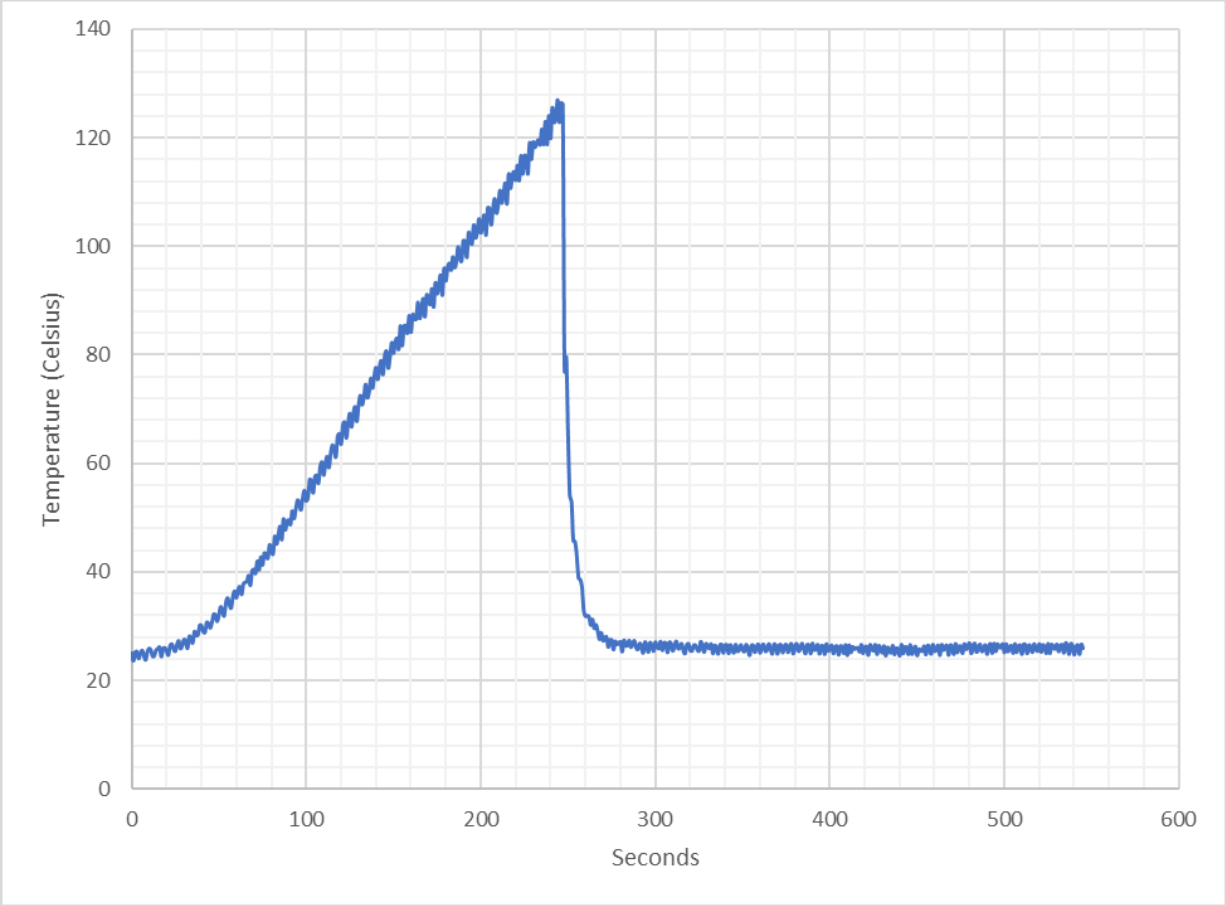

Figure 4-1: TC data prismatic ICR 100% 2450mAh 5.4.22

The TC readings from the top of the battery show a steady increase up to the point of explosion where the TC was ejected from the battery surface, dropping its reading to ambient air temperature. In the first 4 minutes of heating, minimal and gradual expansion of the cell can be seen along with the deformation of the plastic wrapper. About 7 seconds after the fourth minute of heat application, the cell expanded orthogonally to the plate surface, over 1-inch in a less than a second. This expansion led directly into a loud explosion, displacing all pieces of the battery just behind the plate in the box furnace, where large flames immediately erupted. Significant flames lasted roughly 5 seconds, but once they had reduced to a safe level, the plate was removed from the containment area to both protect its wiring and unblock the view of the still burning battery. In total flames where present for 237 seconds after explosion, where a small flame was sustained near the main casing of the battery.

Video stills showing physical observations are given in Figure 4-2 through Figure 4-5. Digital camera recording was briefly stopped accidentally 35 seconds after the explosion, but recording was restarted 74 seconds later, which was determined using the continuous IR video. Nothing significant was missed in this filming gap. It should be noted that the digital camera used for all tests would sometimes break videos into two separate files on its own, but there is no loss of footage between the first and second video (see 6.2.22[1] videos). This consistently happened around 17 minutes and 2 seconds of recording, which is an uncommonly long test length, but it did occur a few times.

Figure 4-2: 1sec before rapid expansion/explosion [4:23 (vid.), 245sec (data)] 5.4.22

Figure 4-3: Maximum expansion before explosion [4:24 (vid.), 246sec (data)] 5.4.22

Figure 4-4: Large flames after explosion [4:27 (vid.), 249sec (data)] 5.4.22

Figure 4-5: Sustained flame size 5.4.22

An IR video still shot corresponding to the maximum temperature reading during the 5 seconds of large flames can be seen in Figure 4-6, while Figure 4-7 shows the camera's reading in the few seconds before the flames fully extinguished (approximately 230 seconds apart). In both the TC had already been removed.

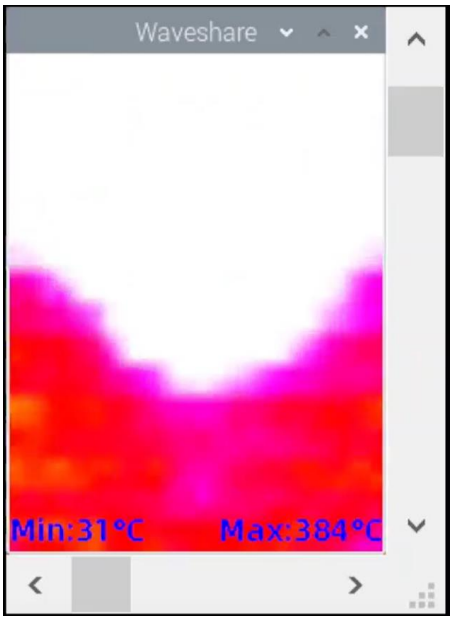

Figure 4-6: IR video during large flames [4:22 (IR vid.), 4:27 (digital vid.)] 5 4.22

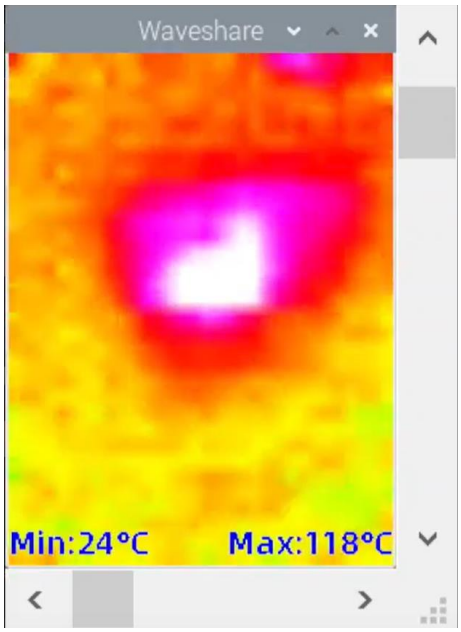

Figure 4-7: Flames about to extinguish [8:12 (IR vid.), 2:04 (digital vid)] 5.4.22

Since most battery shrapnel pieces landed behind the hot plate, on the box furnace's removeable, ceramic-fiber plate, examination of the fragile pieces was able to occur without disturbing them. Figure 4-8 shows the charred, book-like inner layers, and the cavity in the casing from where they were expelled, while the silver-colored foil is believed to have been the outermost layer just inside the casing.

Figure 4-8: 5.4.22 post-condition photo 1

The opposing view, shown in Figure 4-9, displays the melted, plastic end-tab where the charging prongs were located, which is also where the small flame occurred for the duration of the fire.

Figure 4-9: 5.4.22 post-condition photo 2

A transposed excerpt of the recorded data and observations that were entered into the test matrix is displayed in Table 4-1. The matrix parameters discussed at the beginning of this chapter were filled in with their corresponding data points using a combination of recorded data, voice callouts, videos, and photography. Notably there was no sign of smoke or smell leading up to the explosion. The mass was lost was not recorded due to the complete removal of innards, and no distance travelled was recorded, as is typical of all tests where the cell did not travel more than 5 feet.

Table 4-1: Prismatic ICR 5.4.22 matrix excerpt

ALL TEMPS (C °) *ALL TIME (sec)* *ALL MASS (g)*		*5.4.22*
S.O.C.		100
mAh		2450
EXPANSION	*FIRST SIGN TIME*	137
	TIME-TO-MAX	247
SMOKE/SMELL	*PLATE TEMP*	-
	BATTERY TEMP	-
	TIME	-
PRESSURE RELEASE (HISS)	*PLATE TEMP*	252
	BATTERY TEMP	126
	TIME	247
EXPLOSION	*PLATE TEMP*	252
	BATTERY TEMP	126
	TIME	247
FIRE		YES
FIRE LENGTH		237
FIRE DESCRIPTION		LARGE FLAMES ENGULFED BAT. FOR 5 SEC THEN FLAMES DECREASED SIGNIFICANTLY
BATTERY TEMP AFTER		-
POST CONDITION		CASING EXPANDED OVER AN INCH, CHARRED INNER LAYERS EXPELLED BUT STAYED TOGETHER
MASS LOST		-
DISTANCE TRAVELLED		-
NOTES		VIDEO STOPPED 35 SEC AFTER FIRE FOR 74 SEC

4.2 Sample Cylindrical Test Results

The following information details a selected individual test (4.27.22[3]) of a cylindrical LIB. The TC temperature recordings for the INR (NMC) 18650 battery with 100% SOC is plotted over the time from hotplate activation, shown in Figure 4-10, where key failure events are called out.

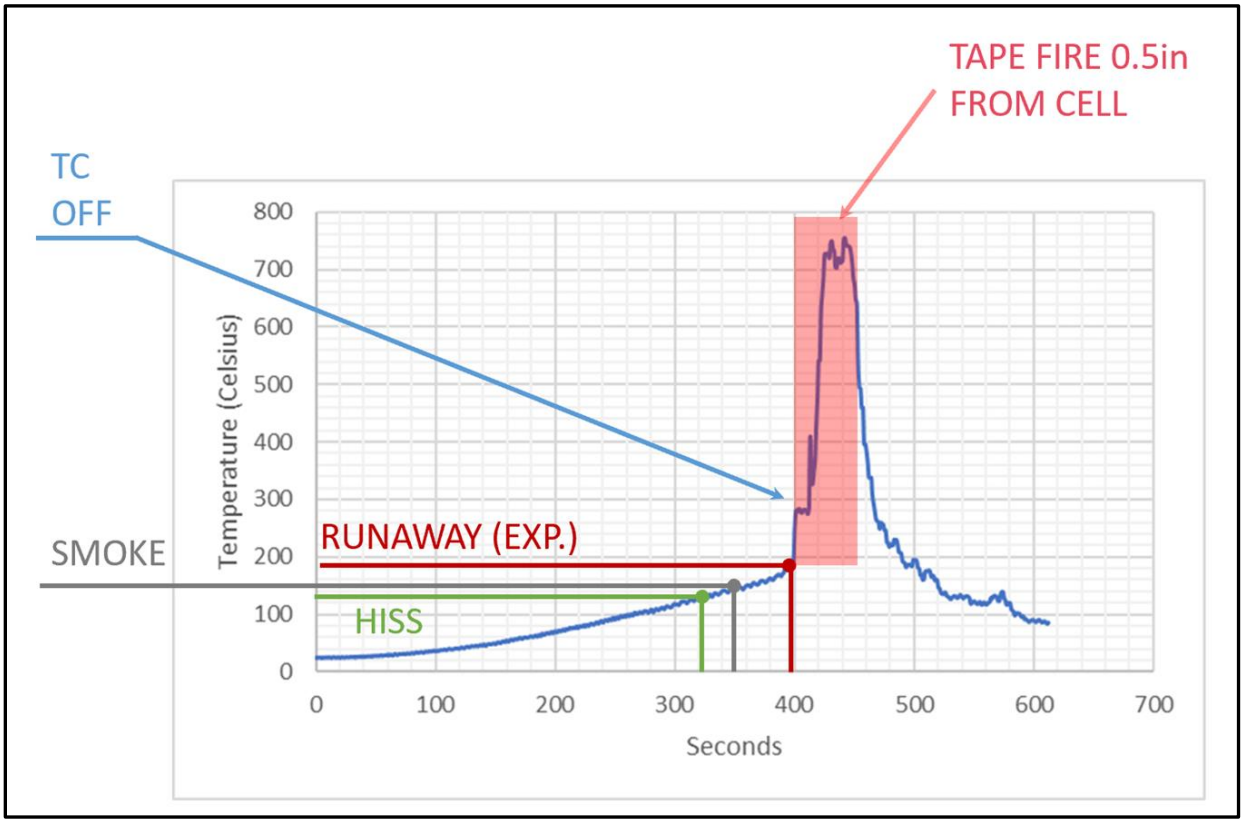

Figure 4-10: TC data 18650 INR 100% 2600mAh 4.27.22 (3)

At the beginning of the test and video, the hotplate was turned on but was not plugged in from the previous test, so the SmartConnect TC network was restarted 96 seconds (called out at 90 seconds) into the video, leading to the difference in video-to-TC time of events. The IR video was not restarted. This mistake highlights the need for clear voice callouts of actions in the video, along with the utilization of timestamps for all equipment. The first rapid spike in temperature between 399 and 400 seconds, signifies the time of the explosion event, which in this case was a rapid explosion of sparks causing a projectile action by the battery, shown in Figure 4-11.

Figure 4-11: Moment of explosion [8:15 (vid.), 399sec (data)]4.27.22 (3)

The battery became red hot for over a minute and a maximum temperature of 755 ^{o}C was recorded. In this instance the TC was less than a half inch away from the resting, but burning, battery. The battery became lodged in between the hotplate and ceramic wall allowing a fraction of the TC tape to remain in contact with the battery for a few seconds. Soon after the tape and TC were disconnected but came to rest on the hotplate right next to the battery. This moment of TC disconnect can be seen clearly in the temperature data plot, where just after the 400-second mark, the plot suddenly plateaus from its rapid increase in heat for a few collection cycles, before the tape it is connected to catches fire causing the second rapid increase in temperature. The only visible flames were that of the burning tape, which lasted just under a minute. When the TC data is viewed alongside the video, the approximate 440-445 (sec) TC point coincides with the extinguishing of tape flames; this leads to the rapid drop in recorded temperature to the cooler air in the test chamber, which also validates the response and accuracy of the TC. Note that a slow-motion video (SMV) of the fire event in this test was captured and is available as a supplemental file, however, this is the only test a SMV is available. The video stills showing these physical observations are given in Figure 4-12 and Figure 4-13.

Figure 4-12: 5sec after explosion [8:20 (vid.), 404sec (data)] 4.27.22 (3)

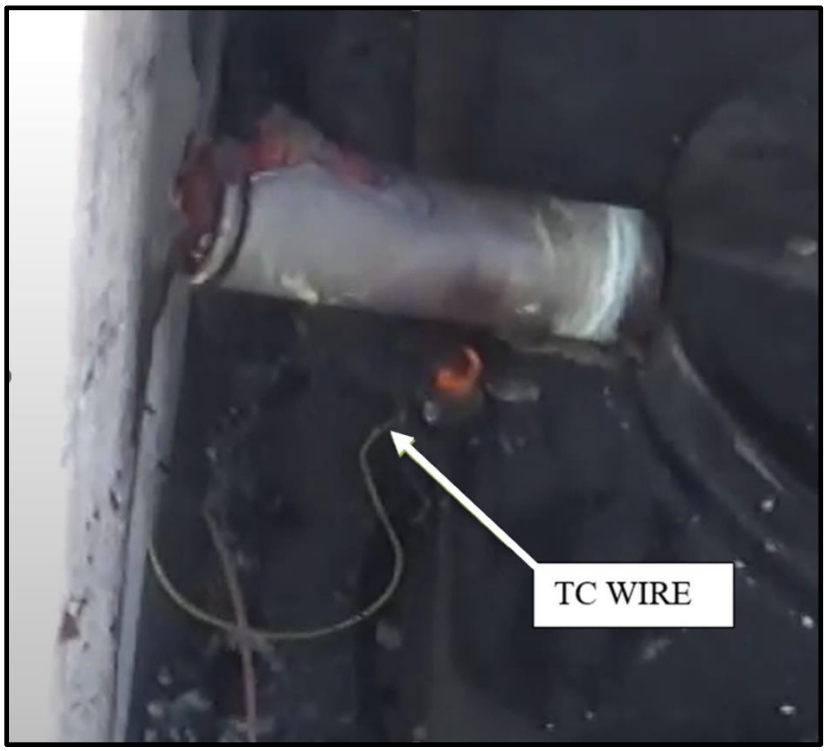

Figure 4-13: 50sec after explosion [9:06 (vid.), 449sec (data)]4.27.22 (3)

Approximately 1.25 minutes after the explosion and flames were extinguished, it was deemed safe to repurpose the IR thermometer being used to monitor plate heating, and its focus was adjusted to the surface of the battery. The sights were pointed at the middle of the length of the battery and read an initial maximum temperature of 359 °C; the sights were then pointed at the "gash end" of the battery briefly reading a temperature of 481 °C. Over 4 minutes after the explosion, thermometer readings on the battery had cooled to about 200 °C. Temperatures between this time can be heard in corresponding video callouts and the logged IR thermometer data (supplemental files).

IR camera recording stills from this test are shown in Figure 4-14 through Figure 4-16, showing the second before explosion, moment of explosion, and the second after explosion, respectively.

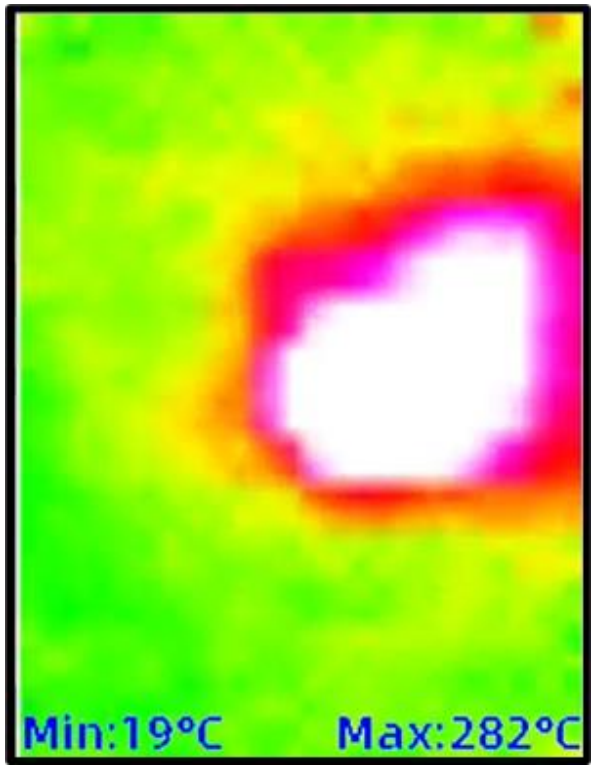

Figure 4-14: 1sec pre-explosion [7:52 (IR vid.), 398sec (data)] 4.27.22 (3)

Figure 4-15: Moment of explosion [7:53 (IR vid.), 399sec (data)] 4.27.22 (3)

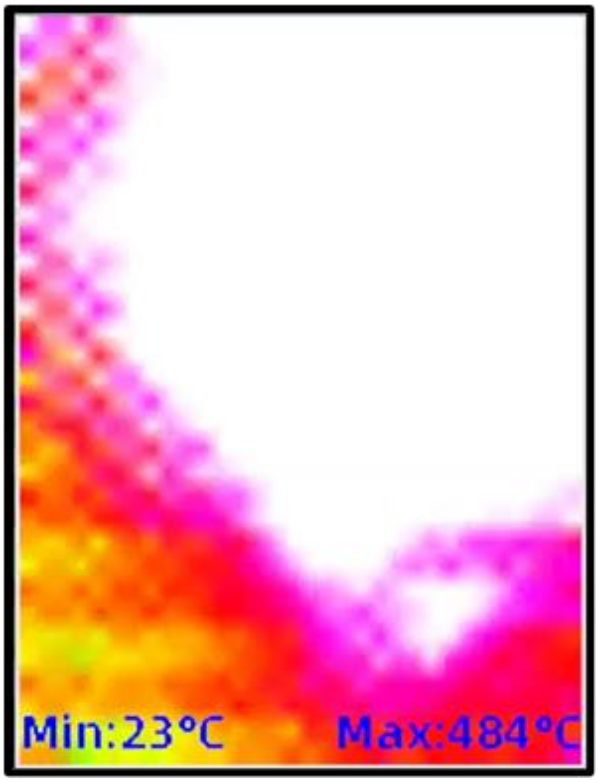

Figure 4-16: 1sec post-explosion [7:54 (IR vid.), 400sec (data)] 4.27.22 (3)

In the second before the explosion, the general shape of the hotplate can be seen with the upper-right corner of the plate (mirror image of actual upper-left corner) showing a raised area with higher (white) temperature. This corner piece is the battery, and this depiction is common amongst all 18650 tests performed in the same hotspot. The moment of explosion, which was notably violent, filled the entire IR camera view space with high temperatures, providing the white-out image. In the subsequent seconds, the IR camera read a maximum temperature of 518 ^{o}C for a split-second but then immediately dropped below 400 ^{o}C and hovered around 300 ^{o}C for the remaining 2 minutes of the video.

Once the battery had sufficiently cooled for handling, its post-test condition was noted, and its mass was recorded and compared to its pre-test mass. For this test, 15.4 grams of mass was lost during the test. Upon inspection a significant gash in the battery casing was seen travelling from the edge of the positive end cap, down the side of the casing for over an inch. A post condition picture can be seen in Figure 4-17.

Figure 4-17: Post-test condition 4.27.22 (3)

As for all 18650 tests, expansion of the cell is virtually non-existent, so this parameter was not considered. A transposed excerpt of all the recorded data and observations that were entered into the test matrix is displayed in Table 4-2.

Table 4-2: 18650 INR 4.27.22 (3) matrix excerpt

ALL TEMPS (C°) *ALL TIME (sec)* *ALL MASS (g)*		*4.27.22 (3)*
S.O.C.		100
mAh		2600
EXPANSION	*FIRST SIGN TIME*	-
	TIME-TO-MAX	-
SMOKE/SMELL	*PLATE TEMP*	318
	BATTERY TEMP	147
	TIME	354
PRESSURE RELEASE (HISS)	*PLATE TEMP*	301
	BATTERY TEMP	130
	TIME	326
EXPLOSION	*PLATE TEMP*	342
	BATTERY TEMP	182
	TIME	397
FIRE		YES
FIRE LENGTH		54
FIRE DESCRIPTION		RAPID EXPLOSIONS WITH AMPLE SPARKS OUT +END, RED HOT CASING 1min
BATTERY TEMP AFTER		481
POST CONDITION		PRESSURE CAUSED A 1in GASH DOWN THE SIDE OF BATTERY FROM POSITIVE END, LESS THAN HALF OF INNARDS BURNED AND COULD NOT ESCAPE, GASH CAUSED BY END CAP BEING LODGED SHUT
MASS LOST		15.4
DISTANCE TRAVELLED		-
NOTES		BATTERY COOLED TO 200 AFTER 4min

4.3 Intra-chemistry Results

Transposed matrix excerpts of important time and temperature recordings for all reported prismatic, ICR tests are shown in Table 4-3, where they are organized by SOC in descending order from left to right.

Table 4-3: Matrix excerpt of all reported ICR tests

ALL TEMPS (C°) ALL TIME (sec)		PRISM ICR (LCO)			
		4.12.22	5.4.22	4.13.22 (DEFECT)*	4.8.22 (OLD PLATE)^
S.O.C.		100	100	75	50
mAh		3300	2450	2800	2600
EXPANSION	FIRST SIGN TIME	123	137	107	180
	TIME-TO-MAX	373	247	292	390
SMOKE/SMELL	PLATE TEMP	262	-	-	-
	BATTERY TEMP	128	-	-	100
	TIME	263	-	-	246
PRESSURE RELEASE (HISS)	PLATE TEMP	-	252	275	-
	BATTERY TEMP	-	126	123	133
	TIME	-	247	282	366
EXPLOSION	PLATE TEMP	349	252	275	-
	BATTERY TEMP	164	126	123	162
	TIME	407	247	282	487
FIRE		YES	YES	YES	?

*4.13.22 battery appeared to have already expanded about ½ inch.
^The original hot plate was used for 4.8.22 test and extreme smoke blocked view of possible fire.

Transposed matrix excerpts of important, time and temperature recordings for all reported 18650 IMR tests are shown in Table 4-4, where they are organized by SOC in descending order.

Table 4-4: Matrix excerpt of all reported IMR tests

ALL TEMPS (C°) ALL TIME (sec)		18650 IMR (NM)					
		5.14.22	4.20.22	4.26.22 (1ST HEATING)**	4.26.22 (2ND HEATING)**	6.25.22 (1)	5.14.22
S.O.C.		100	80	60	60	20	0
mAh		2600	3000	3000	3000	2400	2400
PRESSURE RELEASE (HISS)	PLATE TEMP	304	328	328	360	387	337
	BATTERY TEMP	131	146	141	181	191	184
	TIME	332	375	375	424	518	390
EXPLOSION	PLATE TEMP	331	351	-	-	-	-
	BATTERY TEMP	167	201	-	-	-	-
	TIME	380	427	-	-	-	-
FIRE		YES	NO	NO	NO	NO	NO

**First release of pressure caused battery to immediately fall off plate but was reheated upon cooling.

Transposed matrix excerpts of important time and temperature recordings for all reported 18650 IMR tests are shown in Table 4-5, where they are organized by SOC in descending order.

Table 4-5: Matrix excerpt of all reported IMR tests

ALL TEMPS (C °) ALL TIME (sec)	S.O.C.	mAh	PRESSURE RELEASE (HISS)			EXPLOSION			FIRE
			PLATE TEMP	BATTERY TEMP	TIME	PLATE TEMP	BATTERY TEMP	TIME	
4.27.22 (1)	100	2500	321	130	360	338	158	393	YES
4.27.22 (2)	100	2500	302	132	328	333	173	386	YES
4.27.22 (3)	100	2600	301	130	326	342	182	397	YES
5.5.22 (1)	100	2500	309	132	337	342	172	397	YES
5.5.22 (2)	100	2500	286	124	299	321	167	359	YES
6.23.22 (3)	80	2500	339	163	344	-	-	-	NO
6.27.22 (2)	80	2500	309	188	298	-	-	-	NO
6.25.22 (2)	60	2500	331	152	332	380	182	409	YES
6.25.22 (3)	60	2500	360	149	379	370	157	408	YES
5.29.22 (2)	40	2500	320	144	357	358	240	419	NO
5.31.22 (2)	40	2500	318	184	354	357	256	418	YES
6.27.22 (1)	40	2500	322	158	317	371	216	392	YES
6.27.22 (3)	40	2500	292	107	275	342	150	348	YES
5.29.22 (1)	20	2500	315	145	349	-	-	-	NO
5.31.22 (1)	20	2500	357	171	418	-	-	-	NO
6.18.22 (1)	20	2600	366	211	466	384	268	507	NO
6.18.22 (2)	20	2600	363	144	427	379	186	489	NO
6.23.22 (1)	20	2500	342	172	348	366	182	388	NO
6.23.22 (2)	20	2500	346	146	355	371	196	399	NO
6.2.22 (1)	0	2100	349	193	401	-	-	-	NO
6.2.22 (2)^^	0	2500	305	161	333	-	-	-	NO

^^First release of pressure caused battery to immediately fall off plate, no reheating performed.

While the descriptive parameters that are not included in this matrix excerpt are important, they are more variable and are easier to compare on a test-by-test basis. The data points listed together above are quantifiable and will provide graphical visualization options not only for each individual test, but for categorized groupings of cells and their averages.

CHAPTER 5: MODULE LEVEL PROPOGATION DATA AND RESULTS

For the following propagation tests, the SOC of neither the individual cells nor the combined module of cells, was able to be obtained due to their connection in series with current SOC devices. The physical behavior of these grouped cells under thermal abuse was investigated without this parameter. None of the following multi-cell tests are in the single-cell matrix nor do they have their own matrix as a group. The TC datasets (DAQ, SmartConnect) are combined for each test leaving one excel for each test, except the 6.4.22 test where the two datasets were left separated due to technical difficulties.

Note that for many of the test performed in June, a different computer, compared to many of the May (and earlier) single-cell tests, was used to wirelessly communicate between the SmartConnect system and the IR camera device. Of the two different computers used in June, one was an older laptop with less random-access memory (RAM) capacity, and it was used for both 6.11.22 multi-cell tests (18650, pouch). This is believed to be the cause of the reduced quality in the IR video recordings for the 6.11.22 tests, however in other tests using this computer the image quality is better than these two tests (6.4.22 test before freezing), yet still worse than IR videos recorded by the other two computers. To identify which computer was used, differences in the IR videos can be used. In the IR videos recorded and uploaded by the first computer, used for most of the single-cell tests, the screen-recorded image is displayed towards the middle of the video pane with clear display of temperature readings and scroll bars bordering the thermal image (see Chapter 4). IR recordings by the newer computer used in June display the thermal image box at the top left corner of the video pane, also with high quality but thinner scroll bars than the first, main computer. For the older June computer, the image is also displayed in the upper-left corner, with the same size, but the image is pixelated, and the numerical temperature display is often unreadable. Since all the IR video stills in this paper crop out the void space in the full video pane, an uncropped screenshot of the full-size IR video for the 6.11.22 pouch test is shown in Figure 5-1, where the approximate location of the first computer image location is drawn.

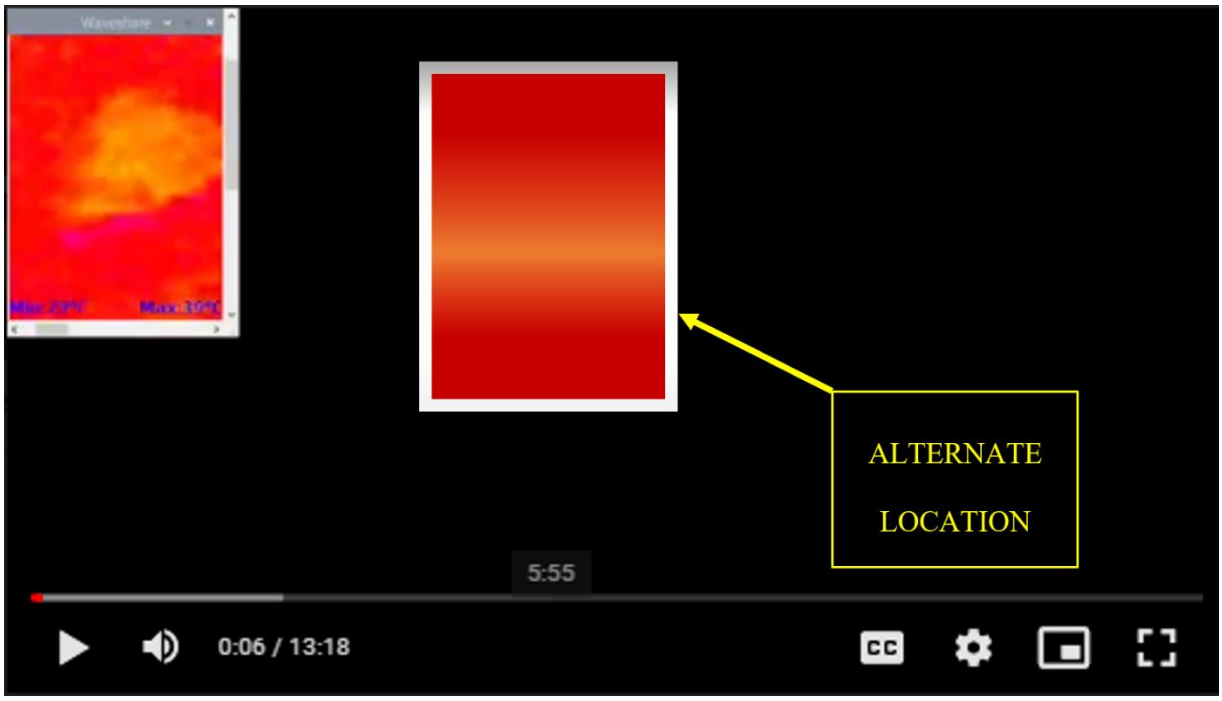

Figure 5-1: IR video display types for computer ID

While the 6.11.22 IR video still shots are not ideal, the general thermal outline of the test environment can still be seen, and most of the digital camera stills in these tests will be accompanied by their corresponding IR image.

5.1 Multi-pouch Tests

The following information details the two multi-pouch LIB tests performed, where both tests consisted of four Samsung (model #: EB-BA505ABU) ICR (LCO) cells extracted from a used laptop battery module, seen in Figure 5-2.

Figure 5-2: Label of multi-pouch test cells

While these pouches' chemistry is not listed on the label, their cathode materials were confirmed using the manufacturers safety data sheet [39]. These are the only pouch cells that were tested throughout the scope of this research.

5.1.1 Four-Pouch Test (6.8.22)

The following information details the first multi-pouch LIB test performed (6.8.22). The TC temperature recordings from both the DAQ and SmartConnect systems, were combined and plotted over the time from hotplate activation and are shown in Figure 5-3.

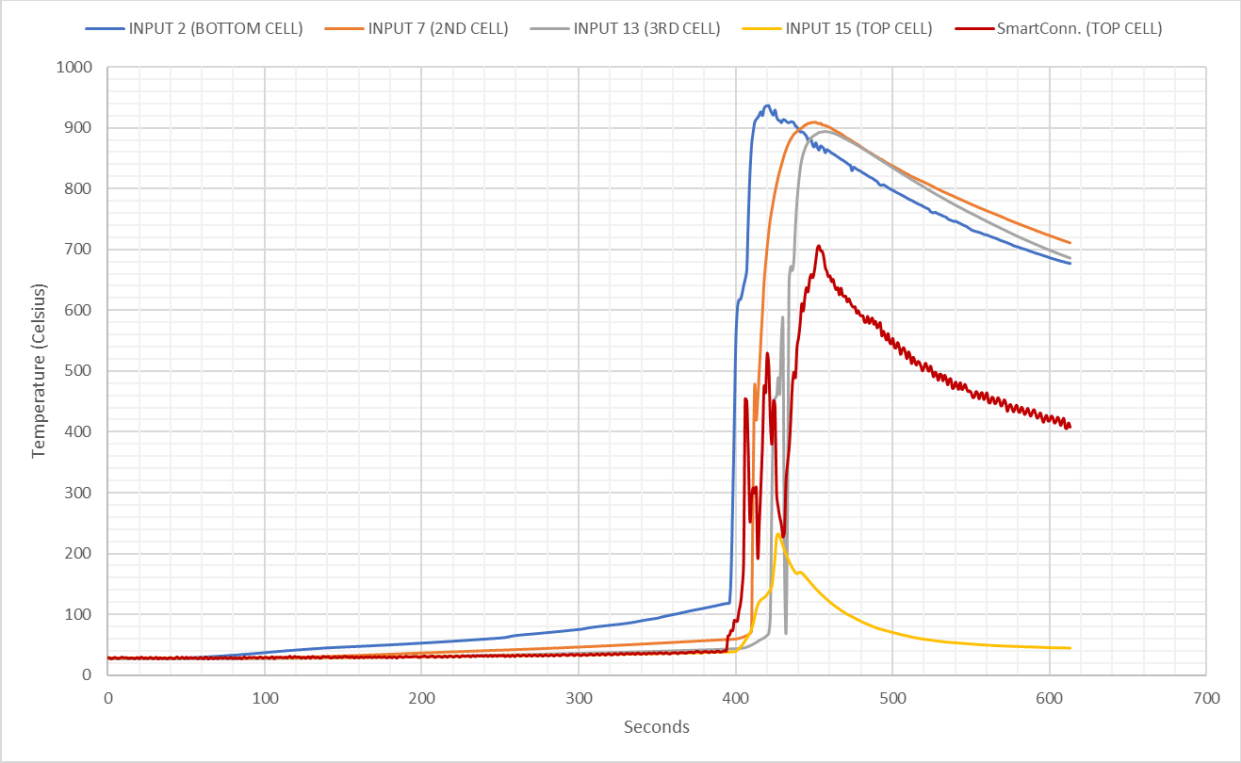

Figure 5-3: Combined DAQ and SmartConnect TC data plot 6.8.22

Each of the four DAQ TCs were placed on the top of one of the four cells tested, meaning the lower three TCs were between cell-to-cell contact surfaces, while the top was exposed. The SmartConnect TC was also placed on the top cell as validation tool and backup since the top TCs were predicted to fall off easier without the weight of a cell(s) above them. Excerpts from the raw data for the four DAQ TCs and

the single SmartConnect TC are shown in Table 5-1 and Table 5-2, highlighting key points from the Figure 5-3 plot and test videos.

Table 5-1: Excerpt 1/2 of combined TC raw data [383-425sec] (6.8.22)

Input 2 (Bottom Cell)		Input 7 (2nd Cell)		Input 13 (3rd Cell)		Input 15 (Top Cell)		Notes	SmartConn. (Top Cell)
Seconds	°C	Seconds	°C	Seconds	°C	Seconds	°C		°C
383	113	383	58	383	42	383	37		37
384	113	384	58	384	42	384	37	HISS	39
385	114	385	58	385	42	385	37		39
386	114	386	58	386	43	386	37		38
387	115	387	58	387	43	387	37		38
388	115	388	58	388	43	388	37		40
389	116	389	58	389	43	389	37		39
390	116	390	59	390	43	390	37		38
391	117	391	59	391	43	391	37	1ST FIRE	38
392	118	392	59	392	43	392	38		39
393	118	393	59	393	43	393	38		41
394	118	394	59	394	43	394	38		40
395	119	395	59	395	43	395	38		64
396	120	396	59	396	44	396	38		66
397	166	397	60	397	44	397	38	1ST JET	74
398	282	398	60	398	44	398	38		73
399	411	399	60	399	44	399	38		90
400	546	400	60	400	44	400	39		89
401	603	401	60	401	44	401	41		89
402	618	402	61	402	44	402	43		105
403	619	403	62	403	44	403	46		118
404	628	404	63	404	45	404	49		143
405	641	405	63	405	45	405	52		185
406	652	406	64	406	46	406	57		454
407	668	407	66	407	47	407	61		451
408	751	408	67	408	48	408	64		364
409	824	409	69	409	49	409	69	2ND JET	254
410	871	410	73	410	50	410	76		291
411	893	411	298	411	51	411	84		308
412	910	412	475	412	53	412	96		299
413	915	413	420	413	54	413	107		308
414	918	414	455	414	56	414	116		193
415	922	415	503	415	58	415	121		251
416	927	416	552	416	59	416	124	<<	312
417	921	417	597	417	60	417	126	TC OFF	379
418	933	418	647	418	62	418	127		475
419	936	419	677	419	64	419	130		464
420	937	420	704	420	66	420	133		528
421	937	421	730	421	69	421	137		509
422	930	422	750	422	97	422	140		421
423	925	423	766	423	293	423	147	*	380
424	922	424	781	424	424	424	169		451
425	930	425	795	425	455	425	195		441

*Possible third cell fire starts here.

Table 5-2: Excerpt 2/2 of combined TC raw data [426-459sec] (6.8.22)

Input 2 (Bottom Cell)		Input 7 (2nd Cell)		Input 13 (3rd Cell)		Input 15 (Top Cell)		Notes	SmartConn. (Top Cell)
Seconds	°C	Seconds	°C	Seconds	°C	Seconds	°C		°C
426	918	426	808	426	460	426	228	LAST JET	298
427	913	427	819	427	490	427	233		276
428	913	428	829	428	464	428	228		260
429	909	429	839	429	550	429	221		248
430	914	430	848	430	585	430	213	^	227
431	914	431	857	431	192	431	206		235
432	912	432	864	432	70	432	199		319
433	910	433	871	433	293	433	193		349
434	909	434	876	434	650	434	187		374
435	911	435	882	435	672	435	182		419
436	911	436	886	436	666	436	177		476
437	909	437	890	437	682	437	172		498
438	904	438	892	438	739	438	169		489
439	902	439	894	439	780	439	167		539
440	898	440	897	440	810	440	168		555
441	894	441	899	441	832	441	170		578
442	894	442	900	442	848	442	168		610
443	893	443	902	443	858	443	166		598
444	890	444	905	444	866	444	163		621
445	887	445	905	445	872	445	160		637
446	880	446	908	446	877	446	157		630
447	883	447	908	447	881	447	154		650
448	881	448	909	448	884	448	151		658
449	872	449	909	449	886	449	148		653
450	869	450	909	450	888	450	145		664
451	876	451	909	451	890	451	142		682
452	868	452	908	452	891	452	139		702
453	864	453	907	453	893	453	137	FLAME OUT	706
454	871	454	908	454	893	454	134		698
455	869	455	905	455	894	455	132		696
456	867	456	905	456	894	456	129		687
457	860	457	904	457	894	457	127		670
458	865	458	903	458	894	458	125		663
459	863	459	902	459	894	459	122		655

^Possible loss of connection and reconnection of third TC.

With the overhead digital camera angle used for this test, clear identification of cell expansion was not available. The first notable activity occurred when the bottom cell casing failed and an audible release of pressure (hiss) was heard, which was immediately accompanied by heavy smoke which filled the containment box and momentarily blocked out the camera view. Video still shots of this event can be seen in Figure 5-4 and Figure 5-5, where the time of the video is listed along with corresponding time of TC data after the activation of the hot plate.

Figure 5-4: First hiss after 1sec, bottom cell [6:59 (vid.), 384sec (data)] 6.8.22

Figure 5-5: First hiss heavy smoke [7:00 (vid.), 386sec (data)] 6.8.22

A still shot from the IR camera recording that was concurrent with Figure 5-5 is shown in Figure 5-6, where the high-pressure plume of heated gasses being expelled from the bottom cell can be seen.

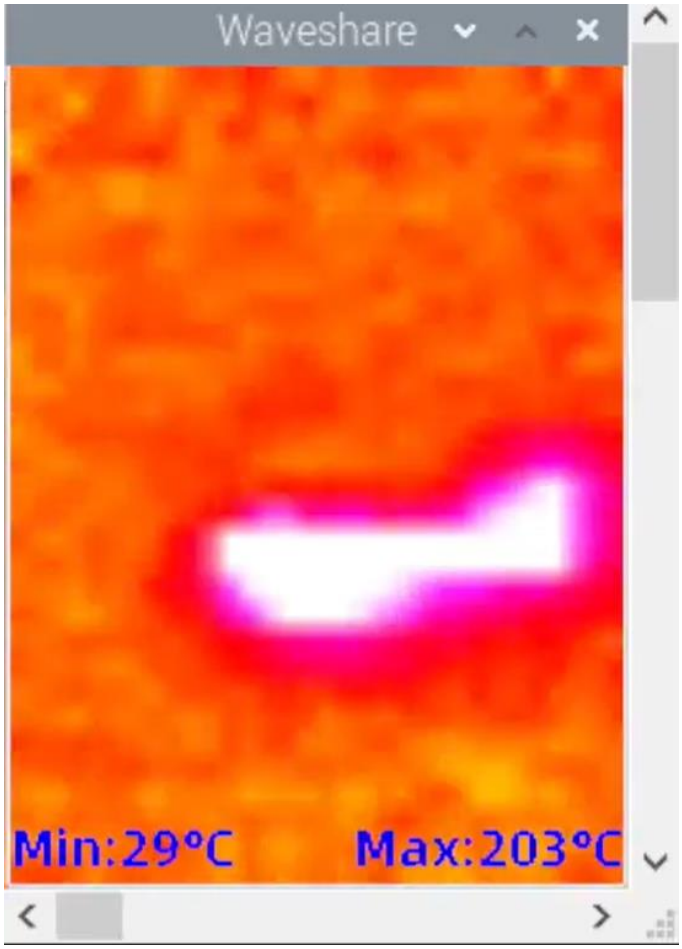

Figure 5-6: IR first hiss, bottom cell [6:51 (IR vid.), 386sec (data)] 6.8.22

Even though the digital camera view was blocked, the IR video was able to display the thermal environment of the test through the heavy smoke. Also seen in the individual test results, corresponding IR video stills will be typically shown for key events in the following multi-cell test results.

About 6 seconds after this first smoke event, a fire developed in the bottom cell which engulfed the stack of cells. After another 6 seconds, this fire had advanced into audible jet like flames, first coming from one side of the battery, but 2 seconds later jet-flames were emitting form both sides. Each stage of progression in the first fire event can be seen in order in Figure 5-7 through Figure 5-12.

Figure 5-7: First ignition, bottom cell [7:05 (vid.), 391sec (data)] 6.8.22

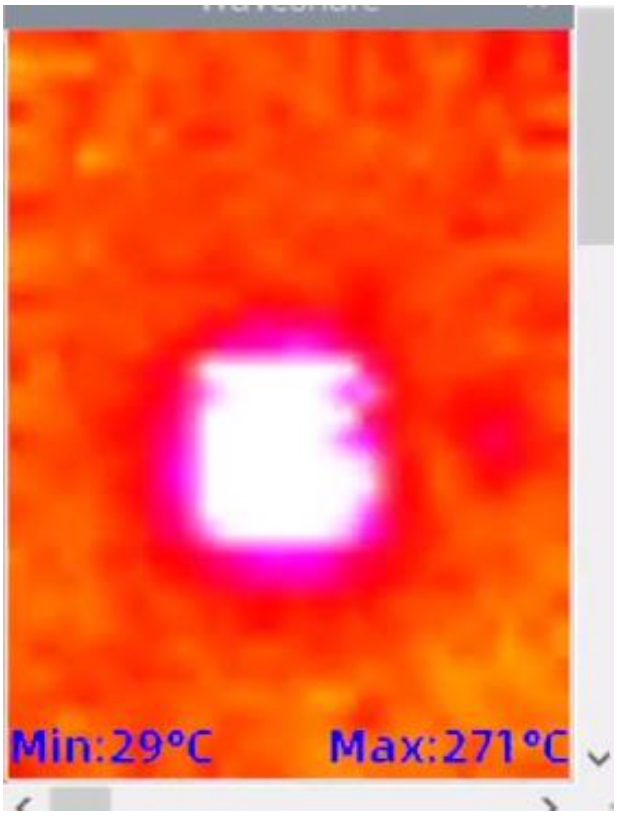

Figure 5-8: IR first ignition, bottom cell [6:56 (IR vid.), 391sec (data)] 6.8.22

Figure 5-9: First jet after 2sec, bottom cell, [7:13 (vid.), 399sec (data)] 6.8.22

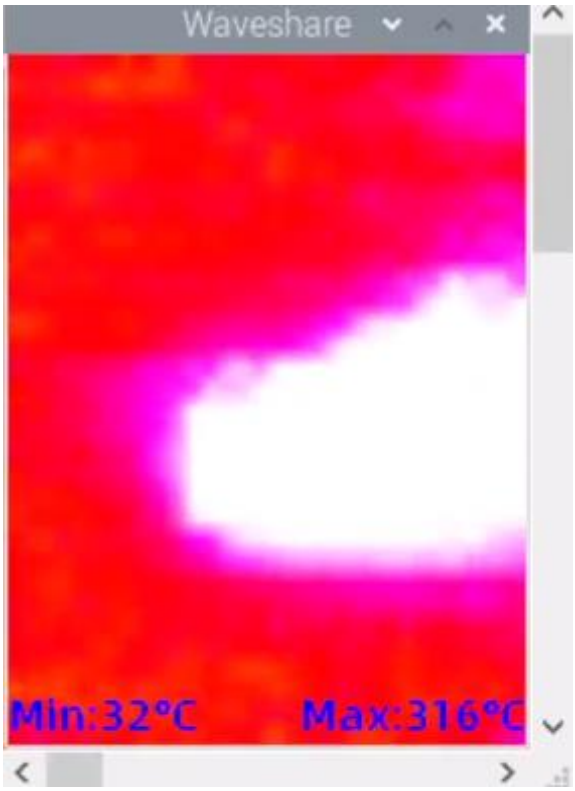

Figure 5-10: IR first jet after 1sec, bottom cell, [7:04 (IR vid.), 399sec (data)] 6.8.22

Figure 5-11: Additional jets other side [7:15 (vid.), 401sec (data)] 6.8.22

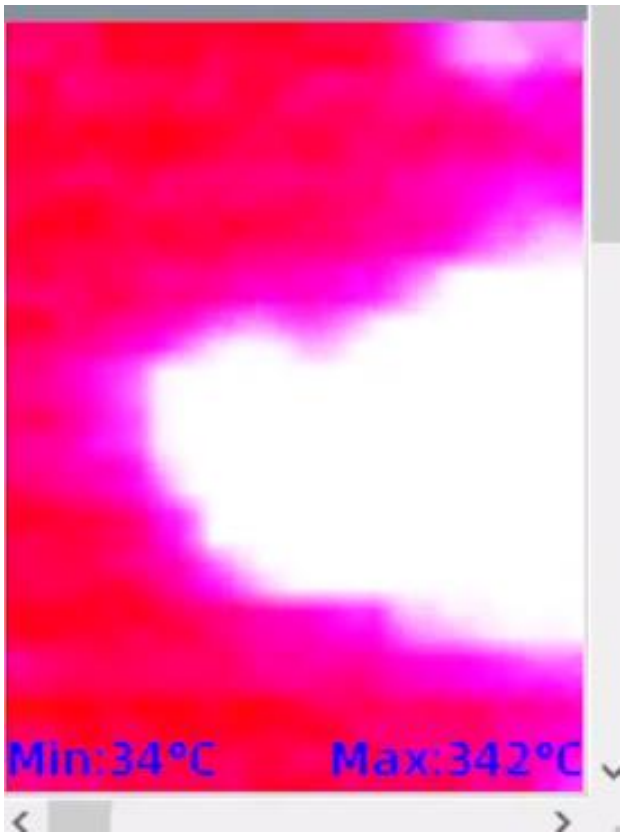

Figure 5-12: IR jets other side [7:06 (IR vid.), 401sec (data)] 6.8.22

After the first jets subsided, the stack was still mostly engulfed in flames which were originating from the bottom of the stack. Before the next jet-flames, some “mini-jets” were seen expelling from what is believed to be the second cell from the bottom for a second or two. The progression from the small to large jets is shown in Figure 5-13 through Figure 5-17.

Figure 5-13: Mini jets the second before jet 2 [7:22 (vid.), 408sec (data)] 6.8.22

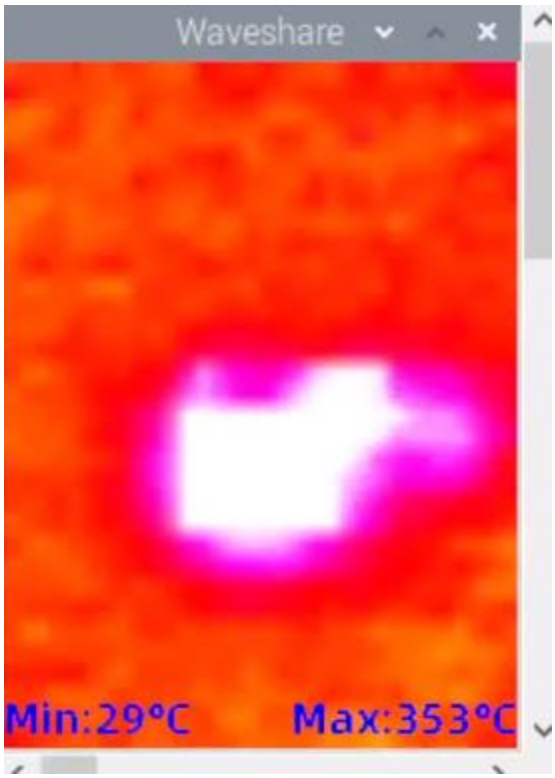

Figure 5-14: IR mini jets the second before jet 2 [7:13 (IR vid.), 408sec (data)] 6.8.22

Figure 5-15: Approx. max point jet 2, (2nd cell?) [7:27 (vid.), 413sec (data)] 6.8.22

Figure 5-16: IR Approx. max point jet 2, (2nd cell?) [7:18 (IR vid.), 413sec (data)] 6.8.22

About one second after the cessation of the second jet-flames, the top-level DAQ TC fell off and away from the batteries with flaming tape attached at its measuring end, which can be seen in Figure 5-17 (SmartConnect TC remained intact).

Figure 5-17: Top-cell DAQ TC detaching [7:31 (vid.), 417sec (data)] 6.8.22

Loss of the TC can also be seen in the IR video; however, it is minimally visible and only for a split second. The location of the TC moving across the screen (to the right due to mirror image) is shown in Figure 5-18, but it must be viewed frame-by-frame at a slower playback speed.

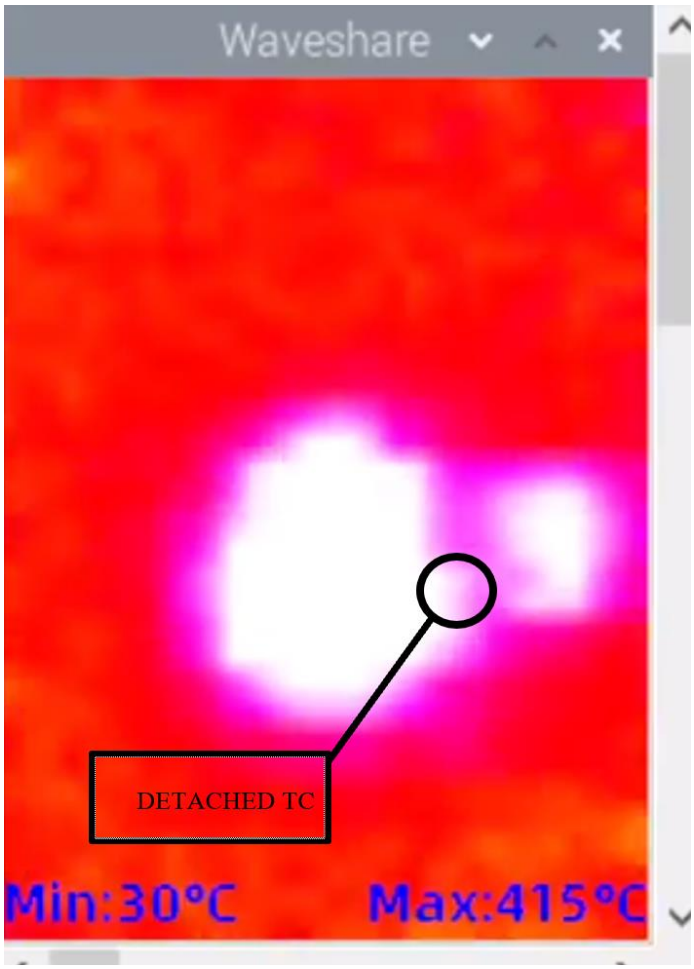

Figure 5-18: IR top-cell DAQ TC detaching [7:22 (IR vid.), 417sec (data)] 6.8.22

The third and final session of jet-flames again started on one side, but quickly progressed to a dual-sided jet. This 6-second jet event subsided into small flames flickering from each end of the top cell for a few seconds, while the tape used to secure the top TC's burned with a longer, larger, and more audible flame. Once the cell flames extinguished, the red-hot inner layers of the top cell could be seen across the elliptical endcap of the now expanded cell. This size of the red-hot area reduced concentrically toward the

center of the cell over 40 seconds. The progression of this final fire event is shown in Figure 5-19 through Figure 5-24.

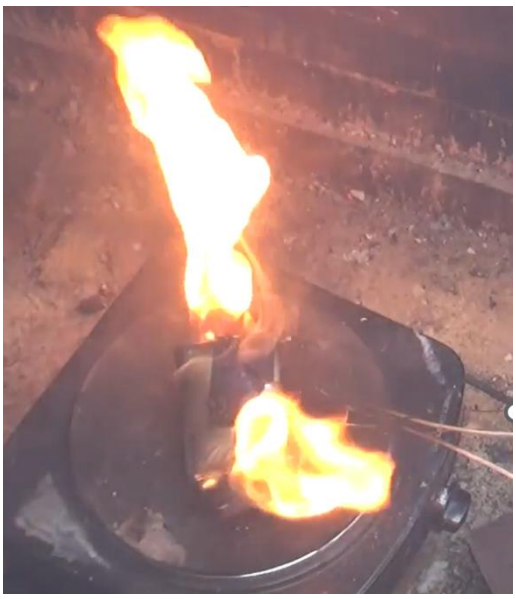

Figure 5-19: 3rd and final jets both sides, (top cell only?) [7:40 (vid.), 426sec (data)] 6.8.22

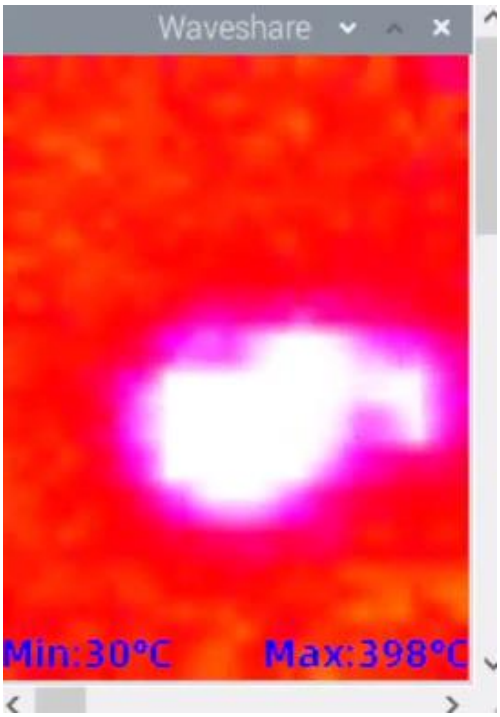

Figure 5-20: IR 3rd and final jets both sides, (top cell only?) [7:31 (IR vid.), 426sec (data)] 6.8.22

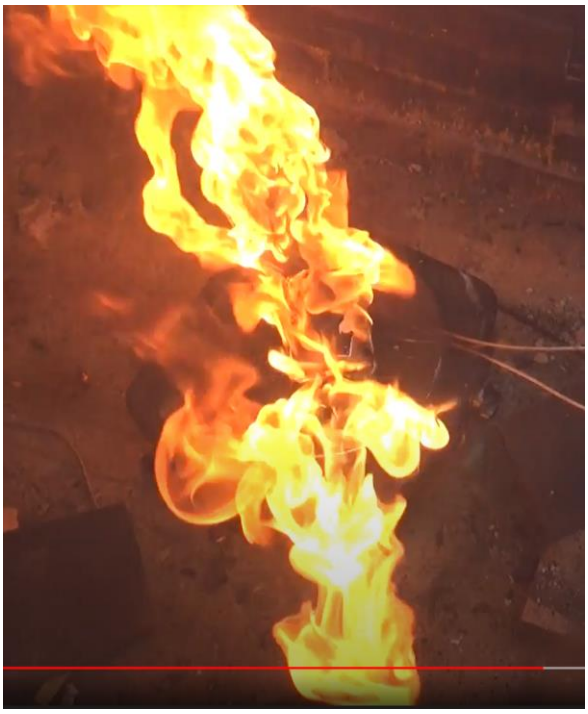

Figure 5-21: Approx. max point jet 3 [7:44 (vid.), 430sec (data)] 6.8.22

Figure 5-22: IR approx. max point jet 3 [7:35 (IR vid.), 430sec (data)] 6.8.22

Figure 5-23: Red-hot top-cell w/ subsiding flames [7:55 (vid.), 441sec (data)] 6.8.22

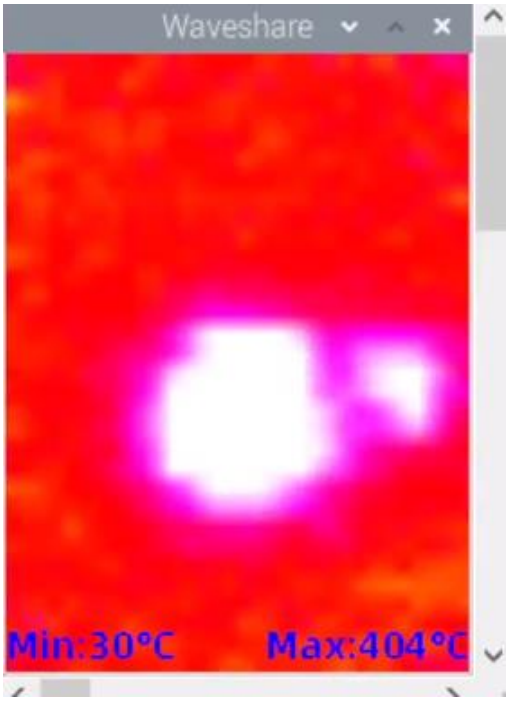

Figure 5-24: IR red-hot top-cell w/ subsiding flames [7:46 (IR vid.), 441sec (data)] 6.8.22

The post condition of all four cells can be seen in Figure 5-25, however their location in the original stack could not be determined.

Figure 5-25: Post-condition of all 4 cells (order unknown) 6.8.22

5.1.2 Four-Pouch Test (6.11.22)

The following information details the second multi-pouch LIB test performed [6.11.22 (note 18650 multi-cell test also performed this day)]. As detailed in section 3.3, the digital camera was moved down from the overhead view used in test 6.8.22, to a profile view of the cell stack through the steel containment box's side-port (similar to IR camera location). In this test tape was wrapped around the entire cell stack to both secure all TCs and simulate a more constrictive module design. The TC temperature recordings from both the DAQ and SmartConnect systems, were plotted over time, starting from hot plate activation, and are shown in Figure 5-26 (note SmartConnect system was started 5 seconds after plate activation).

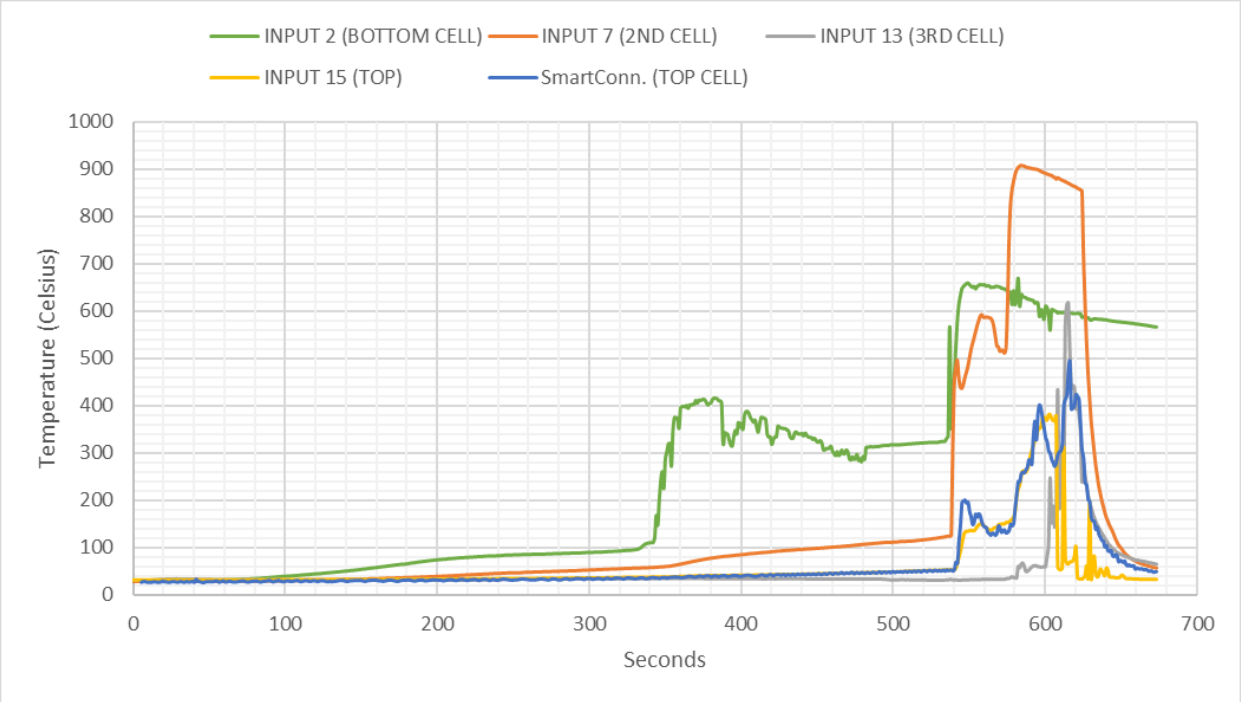

Figure 5-26: Combined DAQ and SmartConnect TC data plot 6.11.22

There was considerably more time between the first and second cell reactions, compared to the 6.8.22 multi-pouch test; therefore, three excerpts of the raw data were extracted to highlight the key events across the four cells. Theses excerpts are displayed in Table 5-3 through Table 5-5.

Table 5-3: Excerpt 1/3, combined TC raw data [327-352sec] (6.11.22)

Input 2 (Bottom Cell)		Input 7 (2nd Cell)		Input 13 (3rd Cell)		Input 15 (Top Cell)		Notes	SmartConn.
Seconds	°C	Seconds	°C	Seconds	°C	Seconds	°C		°C
327	94	327	57	327	33	327	37		37
328	95	328	57	328	33	328	37	1ST HISS	36
329	95	329	57	329	33	329	37		35
330	96	330	58	330	33	330	37		35
331	96	331	58	331	33	331	37		35
332	97	332	58	332	33	332	37		36
333	98	333	58	333	33	333	37		37
334	100	334	58	334	33	334	37		37
335	103	335	58	335	33	335	37		37
336	105	336	58	336	33	336	37		36
337	108	337	58	337	33	337	37		35
338	109	338	58	338	33	338	37		35
339	110	339	59	339	33	339	37		36
340	110	340	59	340	33	340	37		37
341	110	341	59	341	34	341	37		37
342	111	342	59	342	34	342	37		37
343	120	343	59	343	33	343	37		37
344	168	344	59	344	34	344	37		37
345	147	345	60	345	34	345	37		36
346	199	346	60	346	34	346	37		36
347	242	347	60	347	34	347	38	HISS ENDS	37
348	261	348	60	348	34	348	38		38
349	225	349	61	349	34	349	38		38
350	288	350	61	350	34	350	38		38
351	302	351	61	351	34	351	38		36
352	319	352	61	352	34	352	38		37

Table 5-4: Excerpt 2/3, combined TC raw data [530-587sec] (6.11.22)

Input 2 (Bottom Cell)		Input 7 (2nd Cell)		Input 13 (3rd Cell)		Input 15 (Top Cell)		Notes	SmartConn.
Seconds	°C	Seconds	°C	Seconds	°C	Seconds	°C		°C
530	324	530	122	530	30	530	52		53
531	324	531	122	531	30	531	52	2nd HISS/EXP	51
532	324	532	123	532	30	532	52		52
533	325	533	123	533	30	533	52		53
534	325	534	124	534	31	534	53		51
535	332	535	125	535	31	535	53		54
536	337	536	125	536	31	536	53	2nd CELL	52
537	568	537	125	537	32	537	53	RED HOT	53
538	357	538	127	538	32	538	53		54
539	410	539	308	539	31	539	53	1st FIRE	51
540	460	540	450	540	30	540	53		54
541	523	541	480	541	30	541	56		70
542	578	542	497	542	30	542	67		67
543	615	543	460	543	30	543	79		115
544	633	544	440	544	30	544	91		148
545	648	545	438	545	31	545	107		196
546	653	546	447	546	31	546	124		199
547	656	547	461	547	31	547	133		201
548	659	548	472	548	31	548	134		195
549	660	549	485	549	31	549	134		197
550	657	550	502	550	31	550	135		177
551	653	551	520	551	31	551	136		166
552	651	552	533	552	31	552	135		150
553	653	553	544	553	31	553	135		155
554	648	554	558	554	31	554	139		172
555	653	555	570	555	31	555	144		165
556	655	556	581	556	31	556	148		172
557	657	557	590	557	32	557	150		168
558	656	558	594	558	32	558	149		155
559	657	559	588	559	32	559	147		148
560	657	560	588	560	32	560	144		144
561	654	561	589	561	32	561	141		143
562	654	562	588	562	32	562	139		133
563	654	563	587	563	32	563	138		131
564	651	564	586	564	32	564	136		127
565	652	565	581	565	32	565	138		132
566	651	566	568	566	32	566	141		130
567	653	567	548	567	32	567	142		127
568	653	568	528	568	32	568	143		132
569	653	569	526	569	32	569	148		147
570	652	570	516	570	32	570	149		142
571	649	571	518	571	32	571	150		133
572	649	572	518	572	32	572	150		137
573	648	573	512	573	32	573	150	HISS	138
574	646	574	522	574	33	574	153	INTO INSTANT JET FLAMES	132
575	643	575	607	575	34	575	153		133
576	641	576	747	576	34	576	153		137
577	641	577	828	577	36	577	157		150
578	615	578	858	578	38	578	160		147
579	644	579	876	579	35	579	163		152
580	615	580	891	580	36	580	177		185
581	633	581	900	581	35	581	207		212
582	670	582	905	582	60	582	223		241
583	611	583	908	583	56	583	232		240
584	636	584	910	584	64	584	251		257
585	632	585	909	585	66	585	262		260
586	630	586	908	586	60	586	259		259
587	629	587	906	587	49	587	259		265

Table 5-5: Excerpt 3/3, combined TC raw data [588-631sec] (6.11.22)

Input 2 (Bottom Cell)		Input 7 (2nd Cell)		Input 13 (3rd Cell)		Input 15 (Top Cell)		Notes	SmartConn.
Seconds	°C	Seconds	°C	Seconds	°C	Seconds	°C		°C
588	627	588	905	588	49	588	264		270
589	626	589	905	589	51	589	277		286
590	625	590	904	590	56	590	294		285
591	624	591	903	591	58	591	305		277
592	623	592	902	592	61	592	316		337
593	617	593	902	593	61	593	327		368
594	619	594	901	594	61	594	335		328
595	618	595	900	595	59	595	348		385
596	589	596	899	596	59	596	351		402
597	604	597	896	597	58	597	355		394
598	599	598	895	598	58	598	372		373
599	583	599	894	599	59	599	376		354
600	611	600	893	600	59	600	372		333
601	608	601	891	601	80	601	369		325
602	593	602	890	602	106	602	381	3RD FIRE 4TH CELL	306
603	560	603	889	603	247	603	381		300
604	604	604	888	604	153	604	373		287
605	603	605	885	605	188	605	368		280
606	601	606	884	606	143	606	369		273
607	600	607	881	607	158	607	378	4TH CELL	281
608	597	608	884	608	435	608	60	FELL OFF	297
609	598	609	882	609	183	609	54		303
610	597	610	880	610	197	610	53	TCs	305
611	597	611	878	611	302	611	57	DETACH,	320
612	598	612	877	612	184	612	313	IN	402
613	598	613	875	613	571	613	78		414
614	597	614	873	614	614	614	67		423
615	598	615	872	615	619	615	65		473
616	596	616	870	616	516	616	69		493
617	596	617	868	617	438	617	70		393
618	596	618	867	618	443	618	72		397
619	596	619	865	619	440	619	80		400
620	596	620	864	620	393	620	102		424
621	596	621	861	621	412	621	36		420
622	596	622	860	622	380	622	34	TC	414
623	595	623	858	623	343	623	33	PULLED	360
624	588	624	855	624	240	624	33	OUT	308
625	589	625	718	625	277	625	35		289
626	586	626	618	626	252	626	41		239
627	586	627	537	627	231	627	61		233
628	587	628	468	628	211	628	36		202
629	583	629	415	629	196	629	192		199
630	581	630	369	630	184	630	34		165
631	584	631	335	631	172	631	53		157

The first reaction occurred at the bottom cell where a prolonged hiss and heavy smoke event lasted about 20 seconds. In the minutes leading up to this event minimal expansion of the bottom cell was seen, but there was a quick increase in its size, between one and two centimeters, just before the first hiss. As smoke began pouring out, the expansion reduced. It appeared that the cell casing failed along its longer edge, different from the first 6.8.22 pouch hiss, where the yellow tape wrapped around the cell forced the jet of smoke out in two directions. A still-shot 5 seconds into the smoke event is shown in Figure 5-27, and the congruent IR still 5 seconds into the first hiss event can be seen in Figure 5-28. The condition of the bottom cell once most of the heavy smoke had cleared is shown in Figure 5-29, with the thermal imaging at this time seen in Figure 5-30.

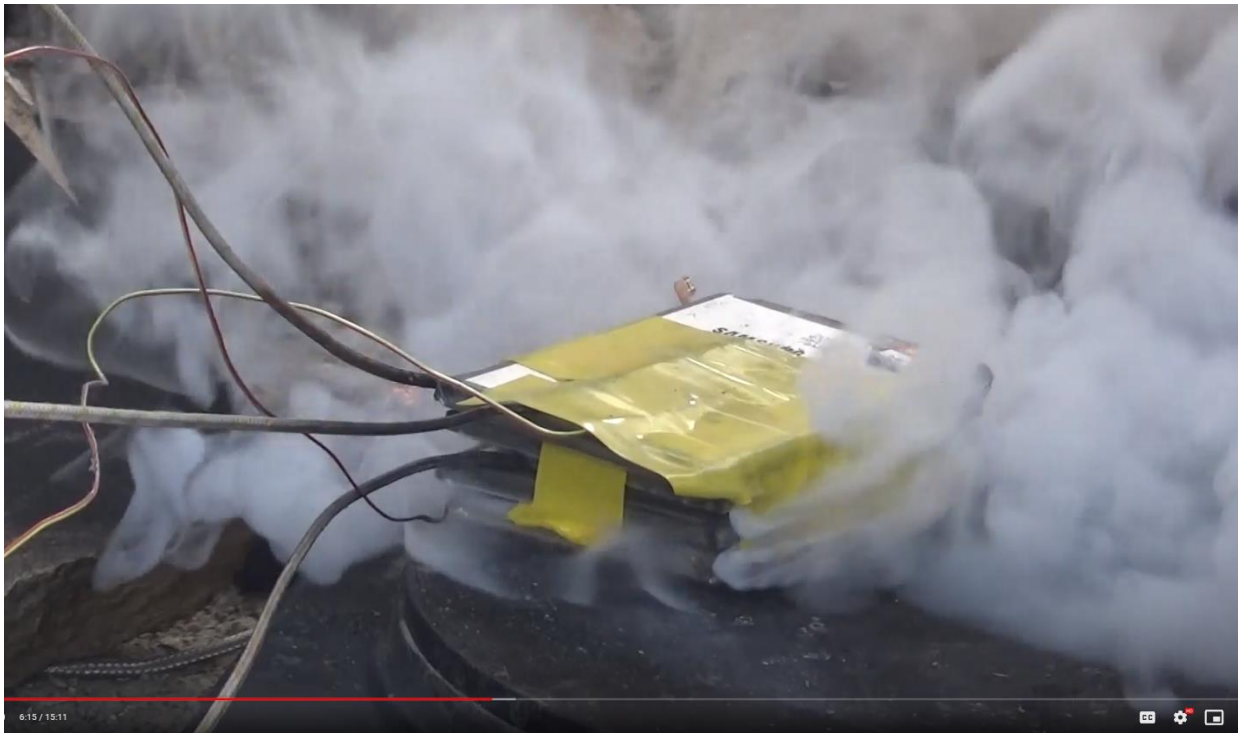

Figure 5-27: ~5sec into first hiss/smoke (bottom cell) [6:15 (vid.), 335sec (data)] 6.11.22

Figure 5-28: IR ~5sec into first hiss/smoke (bottom cell) [5:54 (IR vid.), 335sec (data)] 6.11.22

Figure 5-29: Bottom cell post-hiss condition, no fire [7:44 (vid.), 424sec (data)] 6.11.22

Figure 5-30: IR bottom cell post-hiss condition, no fire [7:23 (IR vid.), 424sec (data)] 6.11.22

Over the next 3 minutes, the second battery expanded minimally, with light smoke, believed to be from the melting tape below, swirling about the stack of cells; until the second cell's end cap, opposite the camera view, was heard ripping open from sudden, rapid expansion. A release-of-pressure hiss immediately followed the failure of the second cell casing. Smoke did not jet out from the failure, but instead it billowed out as spark like flaming particles shot outward from within the cell. After 2 seconds the opposite end of the cell was pulled open exposing the red-hot inner contents of the cell. The progression from sparking hiss, to exposed battery layers is shown in Figure 5-31 and Figure 5-32.

Figure 5-31: Middle of 2nd hiss/expans. (2nd cell) [9:35 (vid.), 535sec (data)] 6.11.22

Figure 5-32: Red-hot innards after hiss/expans. (2nd cell) [9:38 (vid.), 538sec (data)] 6.11.22

There is effectively no difference in the IR image from spark-hiss to red layers since the temperature readings cannot be seen, therefore only one IR still is shown that corresponds to Figure 5-32, which is Figure 5-33.

Figure 5-33: IR red innards after hiss/expans. (2nd cell) [9:17 (IR vid.), 538sec (data)] 6.11.22

Three seconds after the exposure of the second cell's innards, flames shot out from both ends of the battery, engulfing the stack with a radius of about 4 inches. When attempting to capture the digital video moment of flame outburst, the entire view of the camera is consumed with flames for an instant; therefore, only an IR still shot, that better shows the size of the flame burst, is shown in Figure 5-34; while Figure 5-35 shows a digital video image of the flames one second later.

Figure 5-34: IR burst of flames (2nd cell) [9:19 (IR vid.), 540sec (data)] 6.11.22

Figure 5-35: 1st second after burst of flames (2nd cell) [9:40 (vid.), 540sec (data)] 6.11.22

Flames were seen coming from the cell ends for about 12 seconds while tape from the cells above and below burned until the third cell reacted. The third cell underwent a rapid expansion like the second cell, but in this case, jet-flames were present immediately after the squeaking hiss of the cell casing failure. The first jet-flames from the far end of the battery, lasted just under 3 seconds before jet-flames from the opposing near end of the battery also started, which began with a similar squeaking hiss caused by the failure at the new end. Both versions (digital, IR) of the first moment of the single jet-flame can be seen in Figure 5-36 and Figure 5-37, where both versions of the dual-sided jet action are shown in Figure 5-39 and Figure 5-38

Figure 5-36: 3rd hiss w/ instant jet flames (3rd cell) [10:13 (vid.), 573sec (data)] 6.11.22

Figure 5-37:IR 3rd hiss w/ instant jet flames (3rd cell) [9:52 (IR vid.), 573sec (data)] 6.11.22

Figure 5-38: Jet flames from both ends (3rd cell) [10:16 (vid.), 576sec (data)] 6.11.22

Figure 5-39: IR jet flames from both ends (3rd cell) [9:55 (IR vid.), 576sec (data)] 6.11.22

Upon cessation of the jet flames, the third cell was still engulfed in flames, along with some of the tape above. During this fire, a portion of the flames showed blue for 18 sec, which is believed to be the only test that blue flames occurred in the entire research thus far and indicated a higher temperature of the flames than other tests. At this point charring of the first two cells below had progressed to the outer layers becoming ash, which corresponds to the TC on top of the second cell reading over 900 °C, and the bottom cell TC reading over 600 °C, even without catching fire. A digital and IR still shot, 7 seconds after the jets ended, showing the blue flames can be seen in Figure 5-40 and Figure 5-41 respectively.

Figure 5-40: After jets, partially blue flame (3rd cell) [10:25 (vid.), 585sec (data)] 6.11.22

Figure 5-41: IR after jets, partially blue flame (3rd cell) [10:04 (IR vid.), 585sec (data)] 6.11.22

The third and final ignition, which occurred on the final top cell (fourth), appeared to start 27 seconds after the third cell's jet-flames ended. The beginning of the final fire audible sounded as if jets were about to start, but the battery fell off the stack and hot plate, which may have prevented or muffled the jets. The fourth cell slid down the side of the stack and plate coming to rest on its thin edge leaning on the left side of the hot plate. The falling cell pulled the TC between it and the third cell (Input 13) down with it, leaving the red hot third cell and other two cells still stacked in position. Upon hitting the bed of the test chamber, the largest sustained flames of the test were seen coming up from behind the plate, out of, and around the battery. Some of these flames even appeared to wrap around the corner of the plate, but due to the camera angle, it could not be confirmed if some of these flames were due to debris in the test chamber. Five seconds after the cell fell both of the top TCs and the third level TC that was still attached to the fourth cell, were seen detaching from the cell and coming to rest suspended in air a few inches above the cell, still in contact with flames. Digital and IR still shots of the top-cell fire before and after falling can be seen in Figure 5-42 and Figure 5-43 where the position of the detached TC's is seen in Figure 5-45 and Figure 5-44

Figure 5-42: Start of jet flames before falling (4th cell) [10:44 (vid.), 604sec (data)] 6.11.22

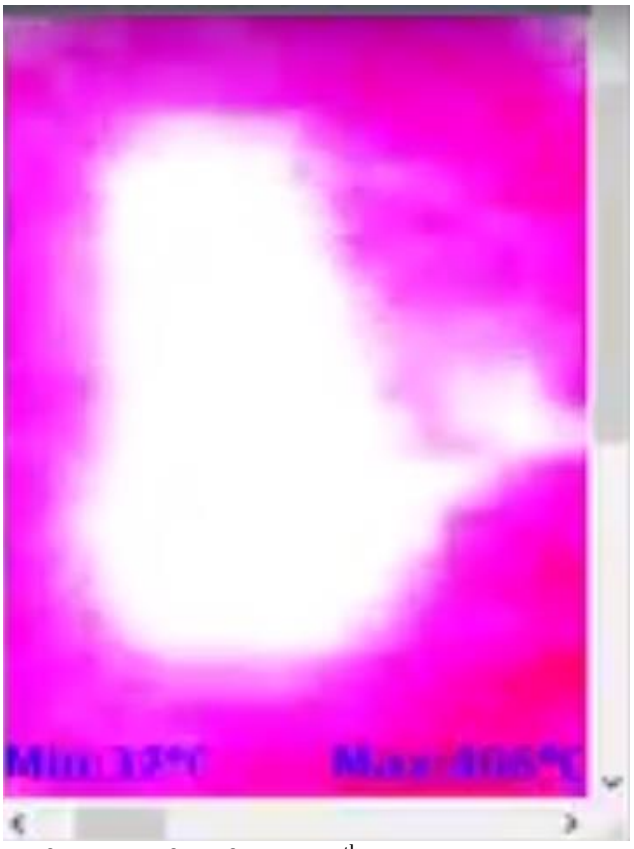

Figure 5-43: IR start of jet flames before falling (4th cell) [10:23 (IR vid.), 604sec (data)] 6.11.22

Figure 5-44: Fallen cell flames, TCs off (4th cell) [10:51 (vid.), 611sec (data)] 6.11.22

Figure 5-45: IR fallen cell flames, TCs off (4th cell) [10:30 (IR vid.), 611sec (data)] 6.11.22

It was quickly realized that the burning fourth cell was in contact with the hot plate power cord, so it was moved with the metal handling rod. This action pulled the TC between the second and third cell out from contact with the cells. The still red hot third cell had now also come in contact with the non-heating surface of the plate, so it was also removed, however the TC between the bottom and second cells remained. While the DAQ system was stopped shortly after, it was still showing real time unrecorded data on the secondary test computer. The two bottom batteries were knocked off the plate 2 minutes after the fourth cell fired and fell. One minute after this, an audible callout was made for the bottom TC that was connected to the bottom cell, still showing a reading of 300 °C (13.45 video).

The cells were safely moved to the top cover of the test chamber for viewing and IR thermometer readings. All of the cells exceeded the 360 °C limit of the handheld FLIR gun, including in between the flipped open, separated layers of the cell shown in the video still shot Figure 5-46 and Figure 5-47, where two of the three intact cells are shown in Figure 5-48.

Figure 5-46: Hot internal cell layers (cell unknown) 6.11.22

Figure 5-47: Hot internal cell layers, flipped open (cell unknown) 6.11.22

Figure 5-48: Hot intact cells (cells unknown) 6.11.22

Four weeks after the test was performed, post-condition photos were taken. An outer foil casing of the layers can be seen along with crystalline formations of residue on the cells. A photo of these cells can be seen in Figure 5-49, with a zoomed in view of the residue shown in Figure 5-50.

Figure 5-49: Approx. 4-week post-test condition 6.11.22

Figure 5-50: Zoomed in view of crystalline buildup, 4-weeks 6.11.22

5.2 Multi-cylinder Tests

For both multi-cell, 18650 tests performed, all cells were INR.

5.2.1 Three-18650 Test (6.4.22)

For this test, the first of two multi-cell 18650 tests, three 18650 cells were extracted from a laptop battery module and were aligned with the similar positive-to-negative end cap format used in the laptop casing but were secured together by tape wrapped around the circuit board strips used as supports along the sides of the cells. The bottom cell contacted the plate at its negative end cap to direct the expected positive end fire event upward into the cell above. The flat negative side also gave more surface area to absorb heat than the positive end. The method used to keep the erected column of batteries vertical on the plate, differs from the method summarized in Chapter 3 for the 6.11.22 18650 propagation test. In this 6.4.22 test, the column of cells was leaned against some of the fire bricks that line the interior walls of the test chamber.

Three bricks were placed on the plate surface closely around the cell columns, exposing the viewport-facing side of the cells so they could be viewed completely by the IR camera at their level. Like the first multi-pouch test (6.8.22), the digital camera was placed on the upper rim of the test chamber giving an overhead view of the test. The column was leaned slightly toward the back brick to help the cells resist tipping over in the gap between the bricks. A snapshot of this arrangement, prior to application of the TCs, can be seen in Figure 5-51.

Figure 5-51: 6.4.22 multi-cell test setup

The TCs were also attached at different locations than the 6.11.22 muli-18650 test. Similar to all of the 18650 single-cell tests, the TCs in this 6.4.22 test, were attached at the mid-height points along the length of the cells. From bottom to top, cells one, two, and three, were attached to the SmartConnect TC, DAQ TC Input 1, and DAQ Input 15, respectively.

The older computer with less RAM, which was discussed in the beginning of this chapter, and used in the 6.11.22 tests, was also used for this test with the SmartConnect and IR systems. While the image quality of this IR video was markedly better and readable, the image froze after less than only 2 minutes. While this was not the first time this issue had been encountered during a test, the time at which it occurred was significantly shorter than any other instance. Note, the audio heard by the IR camera is still being recorded and can be heard when replaying the video during the frozen section. When it was noticed that the video was frozen, about 16 minutes into the test, the program running the camera on the RaspberryPi device was restarted, (which can be seen in the continuous IR video since the recorded video is a screen recording from a remote desktop). The IR video was able to restart with a live image, but the video quality was much worse, similar to the 6.11.22 tests; however, the video was at least functioning minimally for the second key fire event of the test.

Other technical issues arose in this test which were related to both TC systems. Before any significant reaction of the cells, the bottom SmartConnect TC began to display large swings in its temperature reading from one sample cycle to the next (1Hz). The SmartConnect TC wires (one TC consists of two wires) draped down from the center of the bottom cell and contacted the hot plate surface, which melted the wire casings and caused the TC to rapidly switch between reading the plate surface and the battery surface. In the minute leading up to the first fire event, lifting this TC off the plate was attempted with the handling rod but the TC was pulled completely off the bottom cell. Ten seconds after the first fire, the two wires of the DAQ system's middle-cell (Input 1) TC became separated. This separation appeared to be caused by the high heat of the flames from the cell fire below, which altered the input signal to the TC. This separation is indicated by the immediate flatlining of the temperature reading at 2295 ^{o}C, where it remained for the duration of the test. For these reasons, the three TC datasets were not combined like the other tests in this chapter, and the data after Input 1's internal separation was not plotted. The separate plots for the bottom cell SmartConnect TC and the two DAQ TC's on the cells above are shown in Figure 5-52 and Figure 5-53, respectively.

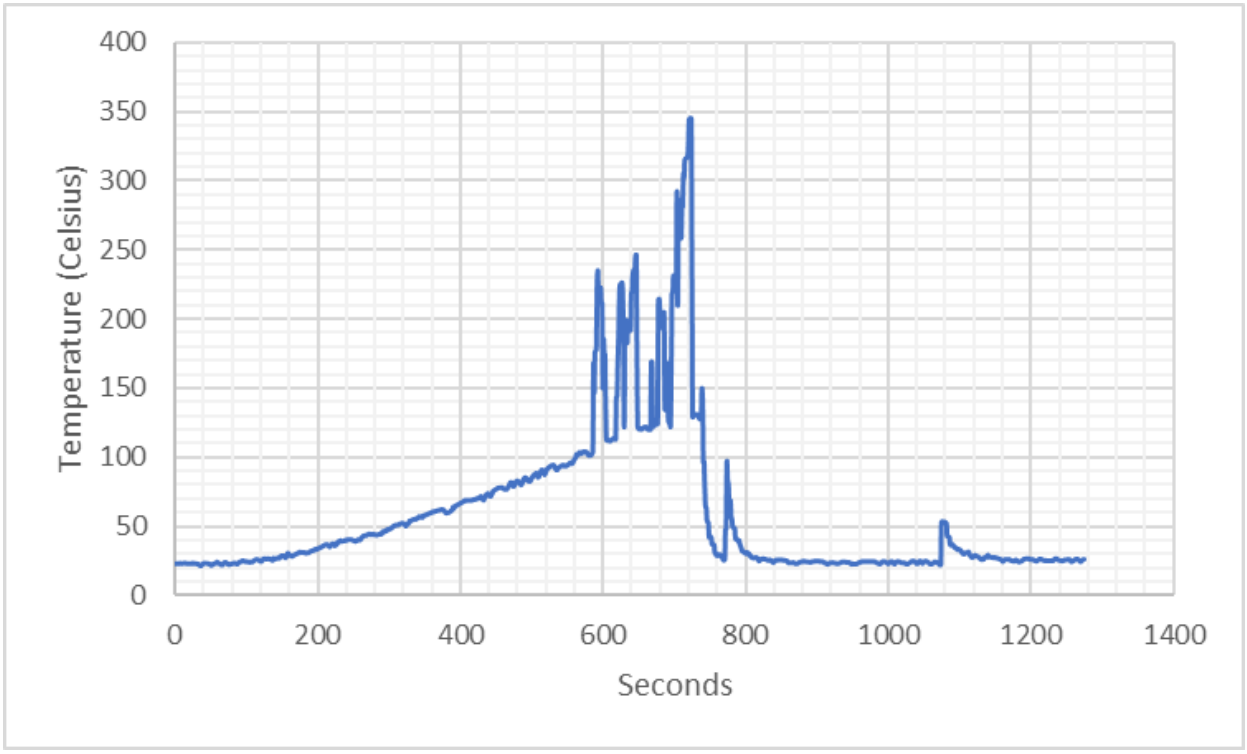

Figure 5-52: SensorConnect TC data plot

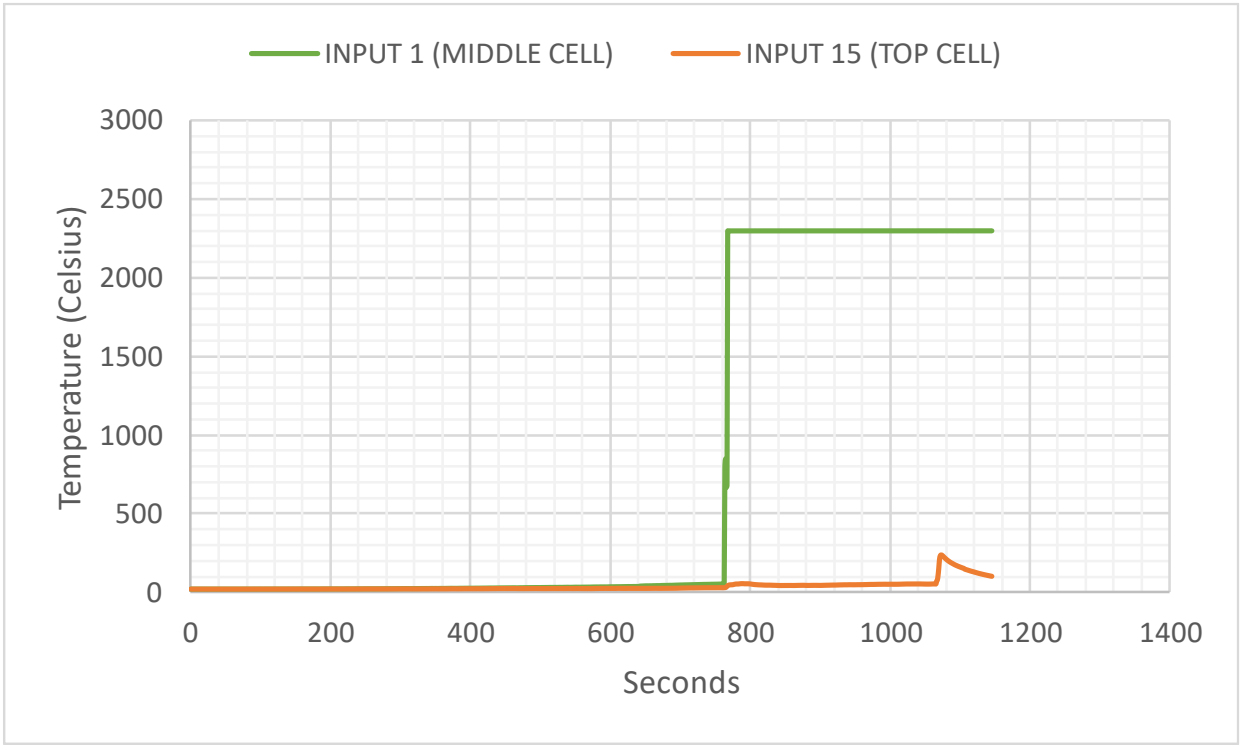

Figure 5-53: DAQ TC data plots 6.4.22

An excerpt of the raw data for the two DAQ TCs across both fire events is shown in Table 5-6; where the data is abridged with a break-row between the events, and the incorrect Input 1 readings are displayed as a hyphen for clarity.

Table 5-6: DAQ raw data excerpts at key times, 6.4.22

Input 1 MIDDLE CELL		Input 15 TOP CELL		Notes
Seconds	°C	Seconds	°C	
757	54	757	31	FIRE 1
758	54	758	31	
759	54	759	31	
760	54	760	31	
761	54	761	31	
762	54	762	31	
763	54	763	31	
764	806	764	31	TAPE FIRE INTO WIRE SEPARATION
765	847	765	32	
766	668	766	35	
767	678	767	39	
768	2294	768	43	
769	2295	769	46	
770	2295	770	48	
771	2295	771	48	
772	2295	772	49	
773	2295	773	49	
774	2295	774	49	
775	2295	775	50	
776	2295	776	50	
…	…	…	…	…
1061	2295	1061	54	FIRE 2
1062	2295	1062	54	
1063	2295	1063	54	
1064	2295	1064	54	
1065	2295	1065	54	
1066	2295	1066	54	
1067	2295	1067	72	
1068	2295	1068	79	HEAT INCREASE DUE TO METAL PLATE TC LANDED ON BEING HEATED
1069	2295	1069	108	
1070	2295	1070	152	
1071	2295	1071	205	
1072	2295	1072	228	
1073	2295	1073	234	
1074	2295	1074	234	
1075	2295	1075	231	
1076	2295	1076	228	

The hot plate was turned on 30 seconds after the digital camera began recording, with the DAQ and SmartConnect systems being turned on 11 seconds and 2 seconds after the plate respectively. The first 12 minutes of the digital video recording was visually uneventful, but very light smoke began to originate from the bottom of the cell column around the 12:25 timestamp. This smoke did not appear to be coming from the battery cells, but more likely the tape and adhesive residue on the cells from the module. Ove the next minute of the video, the smoke transitioned between lightly visible to unseen, while the bottom TC was also detached during this time. Without warning, sparks then violently erupted from the bottom cell upwards into the cell immediately above which forced the sparks out radially in the plane of the first and second battery transition. Initially the brick surrounding only allowed sparks to travel far at the designed gap, but the sparks quickly made their way through the small gaps at the corners between the bricks. In one second the sparks were replaced by audible jet like flames expelling with the same length and trajectory. The progression from the first moment of sparks to the jet-flames can be seen Figure 5-54 and Figure 5-55.

Figure 5-54: Moment of 1st ignition bottom cell, initial sparks [13:22 (vid.), 757sec (data)] 6.4.22

Figure 5-55: Second after 1st ignition bottom cell, jet flames [13:23 (vid.), 758sec (data)]

The bottom cell jets lasted for 2 seconds before subsiding into vertical flames that engulfed the bottom two cells, licking up at the third cell, for about 10 seconds, where the bottom cell tape remained on fire for 40 seconds. These flames produced a significant amount of dark smoke.

Four minutes later, the second fire occurred in the middle cell, which initially behaved like the first fire. In this fire however, the eruption of sparks quickly favored the left side of the video view which shot the column of cells to the right horizontally inside the chamber, projecting it into the wall just below the viewport opening and on top of a raised steel plate area. The video still shots from the digital camera, and the now working IR camera, of the initial in place explosion and the propulsion of the cells into the wall, can be seen in Figure 5-56 through Figure 5-59.

Figure 5-56: Moment of 2nd ignition, 2nd cell, sparks [1:24 (2nd vid.), 1061sec (data)]

Figure 5-57: IR Moment of 2nd ignition, 2nd cell, sparks [18:16 (IR vid.), 1061sec (data)]

Figure 5-58: 2nd ignition, rocket of cells into chamber wall [1:26 (2nd vid.), 1063sec (data)]

Figure 5-59: IR 2nd ignition, rocket of cells into chamber wall [18:18 (IR vid.), 1063sec (data)]

This IR video still in Figure 5-59 shows the moment of impact, but it should be noted that the IR temperature reading reached a maximum temperature of 501 °C, over the cells' entire duration against the wall.

The cells hovered at the wall-plate interface for 2 seconds before an explosion of sparks, flames, and tape consumed the chamber, ending the propulsion and displacing the batteries to their final positions. The second cell, which caused the violent explosion, was red hot with small flames present at each end and had landed on the hotplate just above the temperature dial. This can be seen in Figure 5-60, and the corresponding IR view can be seen in Figure 5-61. A post-condition photo of all three cells can be seen in Figure 5-62, and a close-up photo of the middle cell failure at the negative end can be seen in Figure 5-63.

Figure 5-60: 2nd ignition, after jet, cell red-hot, dual-end flames [1:29 (2nd vid.), 1066sec (data)]

Figure 5-61: IR 2nd ignition, after jet, red-hot, dual-end flames [18:21 (IR vid.), 1066sec (data)]

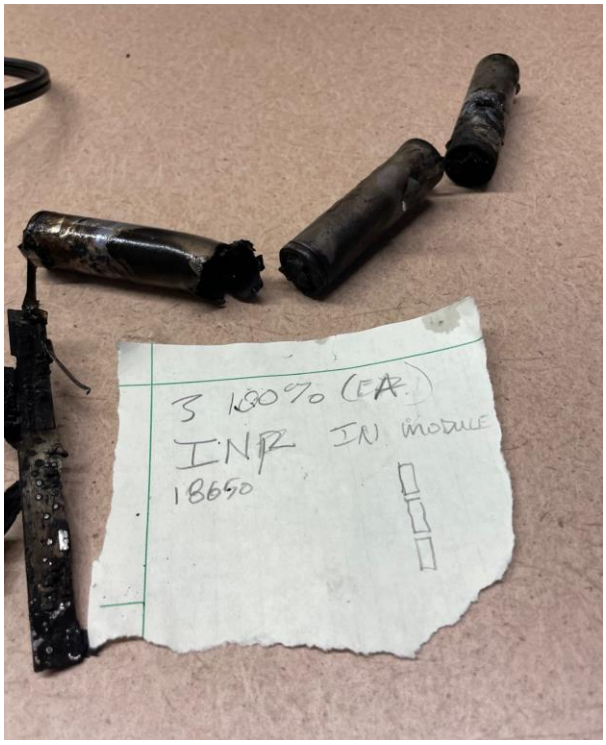

Figure 5-62: Post-condition all, 6.4.22

Figure 5-63: Post-condition middle cell, 6.4.22

5.2.2 Four-18650 Test (6.11.22)

The overall experimental setup for this test was detailed in section 3.4, where in this case, four 18650 cells were attached together, compared to three in the 6.8.22 test. The TC placement utilized in this test was unique to all other cylindrical cell tests. The first DAQ TC was placed on the bottom cell along its long edge, but just above the hot plate surface near the negative end cap. The other three DAQs were placed at the cell-to-cell interface at the end caps, between cells one and two, two and three, and three and four, respectively. The goal of this arrangement was to investigate the temperature transfer at cell-to-cell contact points. The SmartConnect TC was placed on the bottom cell at the typical mid-cell height used in other 18650 tests. Again, the overhead camera angle was used since the tested 18650 cell thus far had shown to displace further with larger projections of flames and effectively showed no expansion visible to the human eye in the videos.

While the hot plate was turned on 16 seconds after the DAQ system, the SmartConnect system was turned on 10 seconds after the plate. The data sets were adjusted to be plotted together and are shown in Figure 5-64.

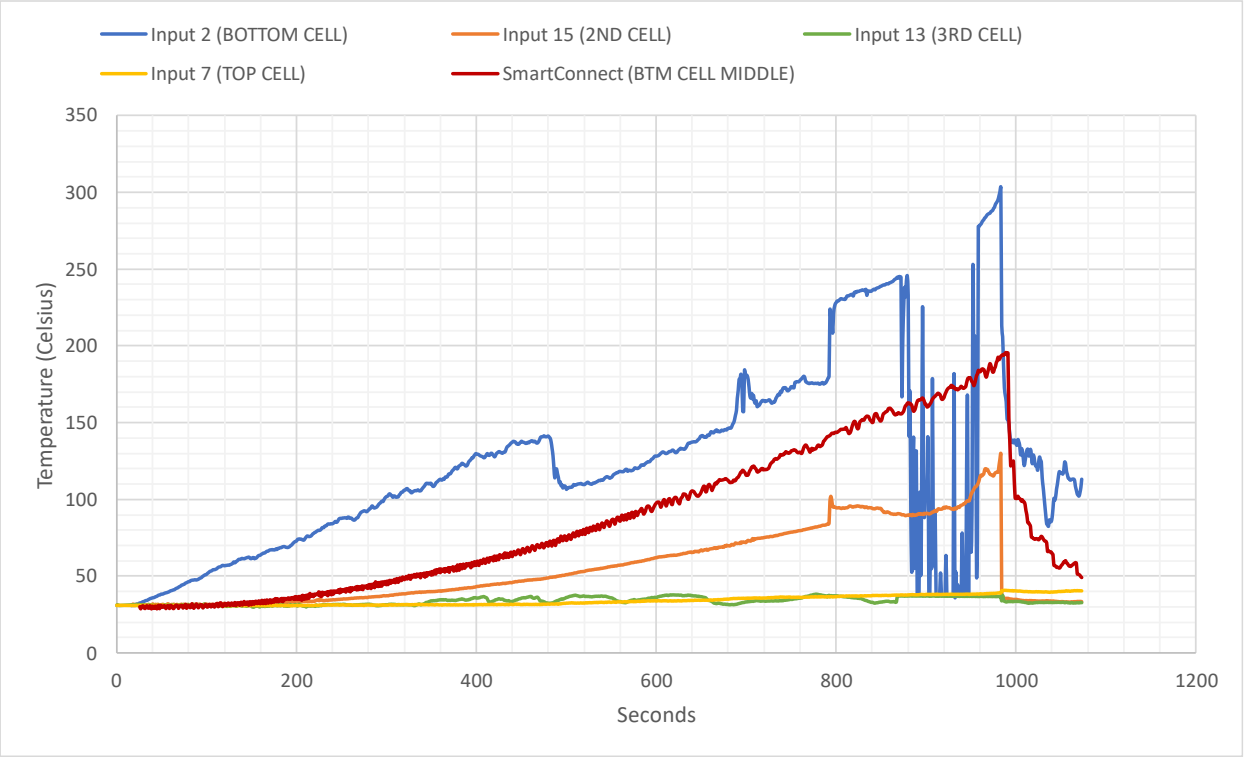

Figure 5-64: Combined TC data plots, 6.11.22(18650)

As seen in previous cases where 18650s were heated through contact of the negative end cap and hotplate (6.4.22, 5.3.22), a significantly longer exposure of heat was required to instigate visible thermal reactions, in comparison to the long-side heating of the individual 18650s. The first pressure release hiss did not occur until 783 seconds after the hotplate was turned on high. It was not until 973 seconds that the only explosion occurred that produced almost no flames.

When analyzing the bottom cell DAQ readings, there a few portions of the data where unexpected temperature drops, and volatility occurred. The first occurrence was around 300 seconds before the first hiss as the data approached 480 seconds of heating, an expected, consistent and gradual rise in temperature was seen, reaching 140 °C; however, at 481 seconds the temperature reading began to gradually decrease toward 130 °C then displayed a rapid decrease to as low as 107 °C, and settled out between 110-144 °C for about 30 seconds, before starting a gradual 100 second climb back to 140 °C. After another minute, a second unexpected data behavior occurred where the gradual increase of temperature made a rapid 30 °C increase

over 8 seconds to 181 °C, took a two-second drop back down to 157 °C, then immediately jumped back to 183 °C. After 15 seconds the data reading reduced to 160 °C and began a gradual climb again.

Up to this point only the bottom cell DAQ exhibited this behavior, and while the SmartConnect TC was connected to the bottom cell about 30mm higher, the SmartConnect TC show gradual heating through up to its removal caused by the explosion; however, 7 seconds before the hiss of the bottom cell, a rapid jump in recorded temperature can be seen in the bottom-cell TC data and in the first-to-second-cell interface TC data. This temperature jump was not seen in the bottom cell's SmartConnect TC. An excerpt of the bottom and second DAQ TC data is shown in Table 5-7, where an over 40 °C and 15 °C respective increase over one second can be seen.

Table 5-7: Combined TC raw data excerpt, at hiss, 6.11.22 (18650)

BOTTOM CELL		2ND CELL		NOTES	SmartConn.	NOTES
Seconds	°C	Seconds	°C		°C	
773	177	773	83		140	
774	178	774	84		141	
775	179	775	84		141	
776	180	776	84	TEMP. JUMP	141	NO TEMP. JUMP
777	223	777	99		142	
778	218	778	102		142	
779	219	779	99		143	
780	208	780	96		143	
781	221	781	95		143	
782	225	782	95		143	
783	227	783	95	HISS	144	HISS
784	228	784	94		144	
785	229	785	94		144	
786	229	786	94		144	
787	229	787	95		145	
788	230	788	94		145	
789	231	789	94		146	
790	230	790	94		146	
791	230	791	94		146	
792	230	792	94		146	
793	230	793	94		146	

This hiss event was relatively quiet compared to some others and gave off little to no smoke or fumes visible in the digital video. A small plume of smoke can briefly be seen in the IR video just after the audible hiss but cannot be effectively shown with a still shot of the video.

Another excerpt of all five TCs' data leading up to and after the lone explosion event was also made and is shown in Table 5-8.

Table 5-8: Combined TC data excerpt, explosion and errors 6.11.22 (18650)

Input 2 (BOTTOM CELL)		Input 15 (2ND CELL)		Input 13 (3RD CELL)		Input 7 (4TH CELL)		NOTES	SmartConn.
Seconds	°C	Seconds	°C	Seconds	°C	Seconds	°C		°C
940	50	940	109	940	37	940	38		181
941	75	941	110	941	37	941	38		182
942	278	942	111	942	37	942	38		184
943	278	943	113	943	37	943	38		184
944	279	944	115	944	37	944	39		183
945	279	945	116	945	37	945	39		184
946	280	946	115	946	37	946	38		185
947	281	947	116	947	37	947	38		185
948	282	948	117	948	37	948	38		185
949	283	949	119	949	37	949	39		183
950	284	950	120	950	37	950	39		181
951	284	951	119	951	37	951	39		180
952	285	952	120	952	37	952	39		182
953	286	953	118	953	37	953	39		184
954	286	954	117	954	37	954	39		187
955	286	955	116	955	37	955	39		189
956	287	956	116	956	37	956	39		187
957	288	957	116	957	37	957	39		185
958	288	958	115	958	37	958	39		183
959	289	959	115	959	37	959	39		183
960	290	960	117	960	37	960	39		185
961	292	961	117	961	37	961	39		186
962	293	962	118	962	37	962	39		189
963	294	963	118	963	37	963	39		190
964	295	964	118	964	37	964	39		193
965	298	965	122	965	37	965	39		191
966	300	966	126	966	37	966	39		192
967	303	967	130	967	37	967	39		193
968	213	968	37	968	34	968	41		194
969	206	969	37	969	38	969	40		194
970	188	970	36	970	34	970	41		194
971	173	971	36	971	34	971	41		195
972	168	972	35	972	34	972	41		195
973	163	973	36	973	33	973	41	EXPLOSION	196
974	152	974	35	974	33	974	41		194
975	152	975	36	975	34	975	41		195
976	148	976	35	976	34	976	41		153
977	142	977	35	977	34	977	41		139
978	138	978	35	978	34	978	41		122
979	137	979	35	979	34	979	41		123
980	138	980	35	980	34	980	41		123
981	137	981	35	981	34	981	40		125
982	139	982	35	982	34	982	41		112

Over thirty seconds before the explosion was shown in the excerpt to further demonstrate the bottom DAQ TC's inconsistencies.

The explosion that occurred was the loudest heard throughout the course of this research, however there were no flames afterwards from or on any of the cells. There was a small flame noted partially in view at the bottom of the video that may have been burning inner layers of the bottom cell, but it could have also been a piece of tape that was ejected from the bottom cell surface, or both. This loudness of this explosion correlated to a rapid displacement of the cell column and the initial part of the explosion before displacement could only be viewed frame-by-frame at quarter speed. The still shot of the moment the explosion occurred can be seen in Figure 5-65, which is followed by Figure 5-66, showing the projectile column of cells and cloud of debris projecting radially upward from around the plate. A corresponding IR video still shot to this explosion is shown in Figure 5-67.

Figure 5-65: Explosion bottom cell, ¼ speed still shot 1 [16:40 (1st vid.), 973sec (data)] 6.11.22

Figure 5-66: Explosion bottom cell, ¼ speed still shot 2 [16:40 (1st vid.), 973sec (data)] 6.11.22

Figure 5-67: IR Explosion bottom cell [16:27 (IR vid.), 973sec (data)] 6.11.22

A still shot showing the position of the cells post explosion and the small flame can be seen in Figure 5-68, with a post-condition photo showing the positive end cap from the bottom cell implanted into the negative end cap of the second cell shown in Figure 5-69.

Figure 5-68: Post-explosion cell position, small flames [16:44 (1st vid.), 977sec (data)] 6.11.22

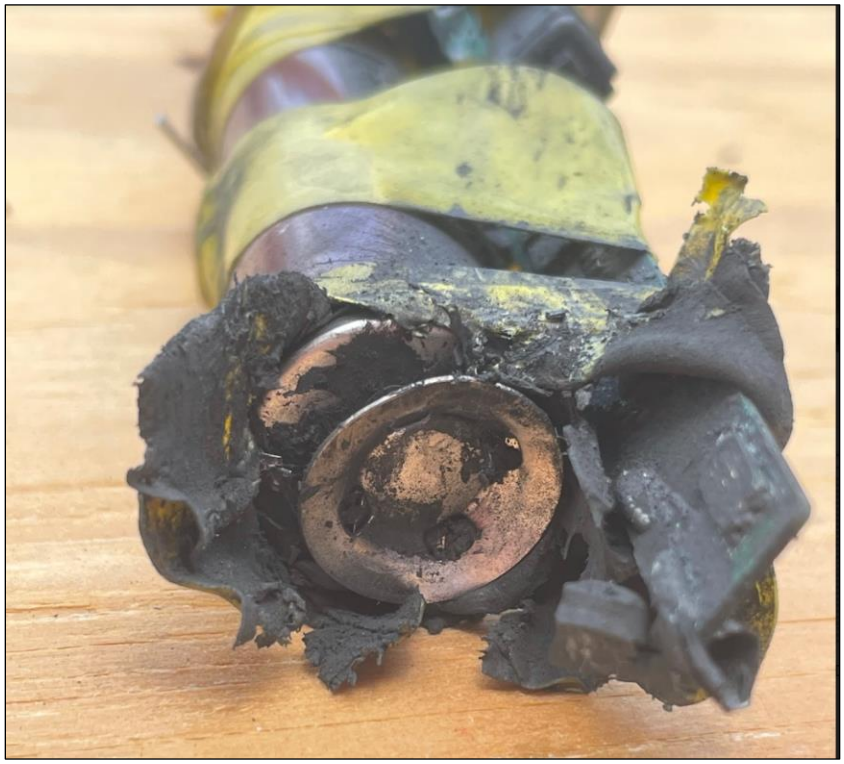

Figure 5-69: Post-condition photo, implanted (+) end cap, 6.11.22(18650)

Upon complete cooling of the tested cells, further post-condition photos Figure 5-70 and Figure 5-71, were taken of the bottom cell, showing its completely emptied casing and some of the recovered inner cell layers.

Figure 5-70: Post-condition photo, emptied bottom cell, 6.11.22(18650)

Figure 5-71: Post-condition photo, bottom cell w/ ejected innards, 6.11.22(18650)

CHAPTER 6: DISCUSSION

6.1 General Test Procedure and Equipment

6.1.1 Digital Recordings

In terms of being able to review the recorded digital video of all tests performed, the digital camera used throughout testing performed well. During the 5.10.22, single-18650 test, the digital cameras SD-card memory ran out of space in the middle of the test, before the hiss or short fire event occurred. After this issue, the memory card was frequently cleared between tests and no other technical difficulties with the camera are of note. While altering the location and zoom level of the camera from test-to-test, certain advantages and disadvantages were determined for each scenario. For the single-cell tests performed in the smaller containment box, the camera was place three to four feet from the battery on the plate and was typically zoomed in slightly to help see some of the smaller visual reactions of the cells. For the prismatic ICR cell that could be seen expanding from thermal abuse, a closer zoom was advantageous. These cells also did not typically move as far during explosion or fire events as their 18650 counterparts; therefore, the reduced total field of vision caused by the increased zoom did not give way to batteries burning out of sight. For the 18650 cells a closer zoom did provide an advantage since these cells do not visibly expand while heated; but did provide a disadvantage for the more mobile 18650s as they would often displace out of the camera's view. In some tests however, the cells were displaced behind the plate or escaped the small test chamber completely, in which the camera was only useful as an audio recording tool until it could safely be moved and pointed to the battery.

As mentioned in Chapter 1, when testing was performed in the large containment box, for both individual and multiple cell tests, two camera angles were used. The overhead view was used for all single and multi-cell propagation tests from 6.4.22 through 6.23.22, except for the 6.11.22 multi-pouch test. The overhead view provided a wider viewing angle which is beneficial for 18650 tests that propelled from the plate surface, for they were often still in view of the camera. Similarly for the multi-18650 tests, the

explosion events saw sparks and flames shooting in random directions radially from the column of cells. The overhead angle allowed for a more complete view of the flames' length and direction. After viewing the first multi-pouch test video (6.8.22), the overhead view made it impossible to see expansion of the lower batteries, and even created difficulty in determining which cell reacted and when. To alleviate these issues the camera was moved down to look through the viewport of the containment box, which showed to be a more optimal position for viewing expansion and origin of flames. The benefits of this view could be seen in the similar view of the single-prismatic tests performed in the small box. At its current location, the hard to move, large box had less time in the shade provided by the nearest building from the sun. While a few of the single-cell 18650 tests were performed in the large box, testing was moved back to the small box to allow for more test time per day, since extended exposure of the test equipment to the hot sun was unwanted. A completely closed containment box with interior lighting and ventilation, combined with multiple interior cameras having varying angles and zooms, would likely decrease the amount of off-camera battery reactions, while also creating a safer test environment.

6.1.2 IR Recordings

The IR camera used throughout all tests presented more challenges than the digital camera. The most important issue this IR device presented was its inaccurate temperature readings. From test-to-test the temperature data of the IR camera was not recorded or compared to the other thermometer devices (TCs, other IR devices) in detail since it was quickly found to be inaccurate; however, throughout testing, the device's readings were found to be between 20 ^{o}C and 90 ^{o}C lower than the other devices. In several tests the IR camera recordings can also be seen showing a split-second increase of hundreds of degrees (Celsius) with and equally fast return to its consistent temperature display. For instance, a smoldering battery on the hot plate would be reading 300 ^{o}C and suddenly show a reading of 900 ^{o}C before dropping back to 300 ^{o}C, with no correlating event to explain this increase. This is believed to be caused by a momentary lapse in the device's image processing performance and is not occurring. This ADAFRUIT IR camera consists of a

24x32 array of thermal sensors, capable of 2 °C degree of accuracy from -40 to 300 °C, according to the manufacturer [40]. It is believed that a higher resolution (more arrays) camera with a higher temperature range would lead to more accurate results.

Another issue encountered with the IR camera was occasional poor image quality and "freezing" of the video, which required the camera be rebooted mid-test. This is believed to be a system level issue that would occur on any IR camera operating with the current RaspberryPi-to-main computer connection. As stated in Chapter 3, this connection requires both the main test computer, and the RaspberryPi device, to be connected to the same Wi-Fi network. While the video froze in some of the longer tests performed in the small containment box, issues were more prevalent in tests performed in the large containment box (multi-cell tests), which included unreadable temperature display due to poor image quality and in one test the image froze within the first 2 minutes of starting. This is assumed to have occurred since the large-box tests were performed further away from the closest building that contained the Wi-Fi network being used. When considering use of a similar system in trains, it's clear that Wi-Fi connectivity cannot be used, and a different method of communication between instruments and monitors must be used. While the SmartConnect TC node does not require Wi-Fi connectivity, the gateway-connected does. At minimum an internal hotspot would be required for the current system travelling far distances, and with travelling through low cellular network areas likely, a satellite supported network would be needed. Wireless capability is not a must-have requirement however, for a similar system to be used on a train or any passenger vehicle; a long, wired connection, designed to withstand damage, and prevent human hazards could deliver similar results, both in research and real-world application.

6.1.3 Thermocouples and DAQ

A fully wired connection that was used during the multi-cell tests, was that of the DAQ system. This system was able to give the same final product of data as the SmartConnect system, but with more than one TC. One issue did arise from the DAQ system though, due to the default sampling rate being set to 5Hz.

For the two 6.11.22 propagation tests, this setting was not changed to 1Hz in error. The intended 1Hz sampling rate both matches the SmartConnect TC rate and provides a reasonable number of data points to examine when exported into excel. In the 6.11.22 18650 test, this mistake led to 5367 different temperature readings across the course of the test, for all four TCs on the system. While this large number of data points can be easily graphed, navigating the data, and pulling excerpts of certain portions of the test is inefficient. Most importantly, comparing and plotting these datapoints side-by-side with the SmartConnect data is virtually impossible without removing thousands of rows in excel. Finding an effective method to remove these unwanted rows in both 6.11.22 tests was not straight forward, but an arithmetic formula was eventually developed and combined with excel filter settings applied to the DAQ data.

The physical properties of the TCs, regardless of their operating system, and the methods used to attach them to the cells, proved to be an important factor in the quality of test results. Early in the experiment design process high-capacity, surface (flat) TCs were determined to be the best option for the scope of this research. While type-k TCs were used throughout testing, supply-chain issues led to the use of two different brand TCs that were validated to have equivalent accuracy but had physical size differences. Of the two surface TC brands used, Omega and Evolution, where two Evolution sizes were used, the second model Evolution used had significantly thinner wires and insulation. The thinner components displayed connectivity issues, as they have a weaker shear capacity, and can slip out from the adhesive tape used to attach them to the cells easier. The thin TCs were removed from the battery prematurely, separated at their welded point of temperature measuring, or were even observed to be pulled from the clamps of the signal-conditioner due to their size, more often than the first Evolution model. The thin TCs also displayed a smaller heat capacity as contact with either the hot plate surface, or flames from testing, melted and removed the insulation on a few occasions. The failure of the insulation would cause the wires to touch at the wrong location giving the temperature at that undesired location, usually rendering the data useless from that point on. Both the temperature and shear failure modes of the thin TCs can be seen in the 6.4.22 propagation test. The first Evolution TCs were all around larger, having higher gauge wires, thicker insulation, and a larger

weld at its measuring end. While these TCs never melted from hot plate contact, wear and tear from multiple test use would eventually cause shear failures separating either the weld, or the entire wire, completely, however, these failures happened considerably less. Due to the tape used to apply them, neither TC was able to stay on the batteries for long during extended fires or large displacements of the battery. While the tape used to secure the TCs was heat resistant up to 80 °C, temperatures reached much higher in most test. Often the tape was observed melting from the hot plate temperature alone, and TCs would peel away with the melting tape. In most tests where fire occurred the tape on the outside of the battery would catch fire and would typically burn longer than parts of the battery, meaning sometimes the only visible flames were that of the burning tape. It's believed that these tape fires interfered with the TC readings intended for the cells' surfaces, and the various IR thermometer readings of the cells and their flames. A tape-free connection of multiple TCs, attached integrally within and on the cells, which would not alter the behavior of the cells or the thermal properties in the test environment would be ideal.

6.1.4 Batteries

In terms of the batteries themselves, there were two main challenges they presented for the scope of this research. The first was the supply limitations of similar brands, chemistries, and sizes. The second issue was chargeability. With variation in the amount of use by the cells prior to being acquired for this research as the predicted cause, some cells were not able to be charged or even display their SOC. With the prismatic "universal" charger, often only cells with three charging prongs could be charged, compared to most of the more prevalent, 4-pronged cells, which would not charge. With the "universal" cylindrical cell charger, some batteries that were labelled to be lithium-ion, would be identified as a different type of battery by the charger, while other cell's SOC would change back and forth between 20 and 80 %. Any cell that experienced charging issues that was intended for individual testing was not used. In the products that use prismatic and pouch cells, the use ICR chemistry dominates the industry, so only this chemistry of prismatic cells was found. The IMR cathode chemical makeup design is considered a precursor to the now more

common INR cells, so finding chargeable IMR cells was less common. The combination of these limitations led to a statistical imbalance in the number of each chemistry tested, and in the number of different states of charge tested within each chemistry. There were significantly more INR cells tested, where multiple tests of each SOC level were able to be performed. Ideally there would have been more SOC variability in a higher number of total tests performed for both the IMR and ICR cell-types. For both multi-cell battery types, SOC was not able to be determined and charging was not able to be performed, but this parameter was not deemed to be necessary to investigate the group behavior of the cells. Note, plans for using a resistor to discharge the batteries was developed but ultimately did not have to be used.

6.1.5 Hot Plate

In general, the hot plate was an effective tool for repeatable heating of the cells with consistent temperature application from test-to-test. The Oster hot plate's designed intent was for typical kitchen use, which likely means occasional-to once-daily use where the highest heat level is not always used. While the testing schedule of this research was not daily, many test days required multiple heating sessions from the plate at full-heat capacity. Combining this heavy usage, with the physical abuse applied to it from high temperature at its wiring components, and large impact forces, depreciation in the plate's heating capacity likely occurred sooner than in consumer kitchen use. Integrating a scientific-grade hot plate into the fully enclosed test chamber (proposed above) floor, where the heating surface of the plate is flush with the chamber, would likely help prevent damage to the non-heating elements of the hot plate device, thus extending its usable life. With all cell types tested, the hot plate surface was significantly larger than required for full coverage of the cells. A smaller total plate surface with a heating element of equal size below it, would help to alleviate temperature variability across the plate's surface.

6.2 General Prismatic and Selected 5.4.22 Discussion

Contrary to the 18650 cells, expansion of the softer, hard-plastic encased, ICR cells was able to be seen, often before smoke, failure of the cell casing, or fire occurred. Unlike the 18650 cells, there were no designed safety vents in the cells, so the first point of failure in the cells was less predictable, but mostly occurred at the shortest thin edge of the cells, where the whole edge would flip open or be removed entirely. Overall, a release of pressure hiss occurred sooner in the prism cells than the other battery types, and at a lower temperature, while more pressure appeared to be able to escape out of the larger end edge failures. These observations are believed to have led to the overall less violent explosions compared to the cylinder cells. Of the five prismatic tests reported the zero and 50% SOC cells did not produce flames, where the two 100% and 75% cells did, however, explosions did occur in every test, again believed to be due to the weaker casing material. The prismatic cells showed to displace much less during explosions than the 18650s.

In the Chapter 4 detailed prismatic test (5.4.22), expansion was the only visible warning sign before the explosion event, where the release of pressure, explosion, and fire occurred almost simultaneously. This even happened in this 100% SOC cell sooner than any other cell tested and burned longer. The post-condition photos from this test show a spiral arrangement of the cell layers similar to the 18650 cells, where the pouch cells showed a flat layering system when their innards were exposed.

While the 5.4.22 reaction from the 100% SOC cell was expected, the 4.13.22 100% test went against these expectations, which took longer to explode and at a higher temperature.

The only jet like flames seen amongst the prismatic cells, which was more common among the cylindrical cells, occurred during the test performed on a cell that had already experienced some expansion. While this cell was still able to be charged, this prior damage may have contributed to the projectile flames.

6.3 General 18650 and Selected 4.27.22(3) Discussion

The safety vents at the positive end of the 18650 cells were the initial point of failure in every test performed on these cells, in turn, validating the proper function of these vents. Occasionally, boiling, liquid electrolyte was also seen spilling out from the activated safety vents onto the plate, where it continued to bubble and evaporate. In most of the post-condition photos of the 18650 tests, dried electrolyte was seen encrusting the vents and rim of the positive end cap. Prior to failing of these vents, there were no visible signs of thermal runaway in any 18650 tests. Typically, when these vents activated and pressure was released from the cell, the battery remained in place or moved minimally, however, in a few cases the cell immediately shot off the plate surface. In these instances, thermal runaway did not continue to the point of fire or further pressure release. In the 4.26.22, 60%-IMR's instance of immediate cell removal from plate, the cell was placed back on the plate once it was able to be handled safely. It took over 140 seconds for smoke to appear in both heating sessions, but it took longer for off gassing to occur in the second heating (140 vs 180 seconds). While no explosion occurred in the second heating, the restarting of pressure release after cooling may point to reasons EV battery fires have been reported to restart several days after the first fire event, like the various fire incidents reported in Chapter 2 [12], [21].

A descriptive quality of fire events that was mostly unique to the 18650 cells (similar, less powerful molten droplets seen in 6.11.22 pouch propagation test), was the initial expulsion of sparks before progressing into flames. In research by Kahn, its noted that some observers believed these sparks to be molten fragments of lithium, but Kahn states this is highly unlike due to the very small amount of lithium that can plate onto electrodes, even during charging; instead, Kahn points to these sparks most likely being molten aluminum ejecting from the vents [41]. Sometimes sparks and flames would shoot through the safety vents, but the positive end cap would remain intact. In more violent explosions the end cap would be separated entirely from the rest of the cell, and in the most powerful fire events the cell casing would fail

at both ends and/or shred open down its full length. In all cases where the end cap was fully removed the inner layers of the cell either partially or fully exited the cell casing.

For the 4.27.22(3) test, from first-hand account and review of the digital test video, the battery explosion appeared to have an ample amount of force that may have caused the battery to dangerously displace many feet, however, the battery became lodged between the containment box and the side of the hot plate. The positive end cap was contacting the containment wall which prevented the high-pressure gas, sparks, and flames from exiting the vents and removing the end cap. The built-up pressure quickly found a way out of the cell through the wall of the casing. An approximately one-inch gash was cut through cell, which was the only case of this occurring. Note that this was a Molicel brand INR, indicated by the grey plastic wrapping.

As stated, failure of the positive end only was typical, and always initiated at this location. For a select set of 18650s however, the damage to the casing was more pronounced. In four 18650 INR tests [4.27.22(1) and (2), 5.5.22(1), and 6.25.22(3)], and one 18650 IMR [5.14.22(1)], after vent activation occurred first at the positive end, the proceeding explosion event either caused removal or puncture of both end caps, or the casing was shredded down the length, and in one case [5.14.22(1)] split into two, mangled pieces. All of these cells were 100% SOC except for the 6.25.22(3) cell which was 60% SOC. Notably, all of these cells were Samsung brand 18650s denoted by their green plastic wrapping. The only individual 100% SOC cells tested that were not this brand was the 4.27.22(3) cell, and the 5.3.22 end-cap heated test. In both of these tests, and all other single-cell tests of different 18650 brands with less than 0% SOC, this extensive case damage did not occur. To determine if this level of failure was due more to the Samsung cell design or full SOC (100%), more tests of lesser SOC similar Samsung cells and 100% SOC other-brand cells would be required. If supply issues could be resolved, a more extensive investigation of specific brand LIB fire safety could be performed, though this was not part of the scope of this research; however, brand-specific data could be used to make recommendations towards LIB selection in general and locomotive use. Note that a

similar, dual-end cap failure occurred in the 6.4.22 multi-18650 test; and while the brand of these cells was different (LG), the cause of this failure is theorized to be a different reason, as discussed in section 6.5.

For the detailed 4.27.22(3) 18650 test, the use of slow-motion video (SMV) was employed to capture a detailed progression of the LIB's explosion and fire if they occurred. This, and the second test performed on 4.27.22, were the only tests SMV was recorded, but the first SMV video quality was not as good. The SMV function of a newer personal iPhone was used through a gap in the steel curtain with the operator of the recording device safely behind the curtain. With safety prioritized, it was difficult to get a clear shot of the test chamber due to the standard test equipment (IR camera, digital camera) set up in between the SMV device. In general, one-minute of filming a SMV at a ten percent of normal speed, would produce a ten-minute video. In the case of this test, the iPhone was recording at 240 frames per second, or quarter-speed. Based on previous tests, SMV recording was started about 2 minutes before the eventual fire event, which in real time was a relatively accurate estimation of when to start filming; however, this created over 9 minutes of video before the fire occurred and over 7 more minutes to see the flames extinguish. With the unpredictability of the LIB fire events, the inefficiency of its large file sizes, and test proximity safety concerns, the use of this SMV was not continued; however, a high-speed camera, or high-speed IR camera, properly integrated into the experimental design, would seem to provide benefits in understanding the physical behaviors before in during thermal runaway.

6.4 Inter-chemistry Comparison

By using simulated thermal abuse as the method to manually create ISC, and in turn TR, differences in the physical shape and component material makeup, the ability to make confident comparisons between the test cell chemistries was hindered. As detailed in Chapter 1, the geometric shape and size of the prismatic cells tested is different than the two 18650 cell types tested, which leads to a difference in their respective layer arrangement design. There was also notable size difference within the prismatic cells tested. While both the prismatic and cylinder cells showed a spiraling of their inner layers, the length of one pass around

the spiral for the 18650 cells is considerably less than the prismatic cells, meaning the diameter across all layers of the spiral in the prismatic cells at its thinnest axis was smaller; this is believed to play a role in how the batteries react differently to thermal abuse. A bigger factor in the cell types' differing reactions to thermal abuse is believed to be the different material used for their protective casings. The hard-plastic case of the prismatic cells was more susceptible to damage from heat, and internal and external force. Equal size and casing material across all cell chemistries would be required to compare their external thermal abuse behavior. If further investigation into the ISC and TR reactions of each cell chemistry was desired, and similar supply challenges persisted giving different casing types amongst the chemistries, a different method of manual short-circuiting would likely give more comparable data. For instance, a controllable method of electrical abuse would be ideal; but a simple puncture test that could be inserted through the same number of layers regardless of cell structure, would likely produce more comparable data than the current hot plate method. The average temperatures and times of parameters standard to this research, for each chemistry evaluated, are shown in Table 6-1.

Table 6-1: Comparison of chemistry averages

ALL TEMPS (C°) *ALL TIME (sec)*		ICR	IMR	INR
EXPANSION	*FIRST SIGN TIME*	137	-	-
	TIME-TO-MAX	326	-	-
SMOKE/SMELL	*PLATE TEMP*	262	324	313
	BATTERY TEMP	114	145	144
	TIME	255	367	329
PRESSURE RELEASE (HISS)	*PLATE TEMP*	264	341	326
	BATTERY TEMP	127	162	154
	TIME	298	402	353
EXPLOSION	*PLATE TEMP*	292	341	357
	BATTERY TEMP	144	184	192
	TIME	356	404	409

For the two types of 18650 cells, virtually the same average battery temperatures can be seen for each applicable parameter, however, the time to reach the similar temperatures showed more variability. This difference in time can be seen, but similar temperature of reaction, can be seen when looking at individual tests as well. For example, the last reported test performed on the second hotplate was a 20% SOC INR [6.18.22(2)], while the next test that was reported [6.23.22(1)] was also a 20% INR of the same brand (Molicel), however; the brand new, third hot plate was now being used. In the old-plate test it took 489 seconds for the battery to reach 186 ^{o}C at its time of explosion, where the new-plate test only took 388 seconds to reach 182 ^{o}C. This scenario can be seen in other parts of the data set as well, which led to the theory that the magnitude of temperature reached in the cell has more effectual capacity on a LIB thermal failure than the time the cell is exposed to heat. At the same time this observation of difference in time required to reach certain temperatures from test to test also highlights imperfections in the controlled environment aspect of the current experiment design. While the overall heating of the plate is consistent, some depreciation occurred; while the variability of temperature across the plates surface likely effected the consistency of heat applied from cell-to-cell due to slightly different positioning of the batteries in each test.

For the ICR tests, all tests on the plate used for the bulk of test events saw an explosion and fire (4.12, 4.13, 5.4.22). In the 50% SOC test, performed on the first plate which showed less heating, the explosion created so much smoke that confirmation of a fire could not be confirmed or denied. The first partially reported test on the matrix was the 3.2.22, 0% ICR, for this test instruments were still being validated and the experiment procedure was early in development. In this test the hot plate was turned to medium for a few minutes before eventually being turned to high, which is believed to cause the over 16-minute time to explosion. The cell expanded close to two inches without visible or audible failure of its casing, and sustained this shape for around 5 minutes, before an extremely loud explosion with minimal smoke occurred. This gradual buildup of pressure, demonstrated by the three phases in Figure 6-1 through Figure

6-3, is believed to have allowed the plastic case to become more malleable, instead of being ruptured by a more rapid expansion.

Figure 6-1: Phase 1, no expansion, ICR 3.2.22

Figure 6-2: Phase 2, medium expansion, ICR 3.2.22

Figure 6-3: Phase 3, full expansion, ICR 3.2.22

6.5 SOC Comparison

For both ICR and IMR cell types, it was determined that the overall number of each test type performed, combined with an uneven distribution of SOC instances in each chemistry, a comparison of the SOC levels within each type could not be performed.

With a more statistically balanced and relevant field of INR tests, a more detailed comparison between the tested SOC levels within this chemistry was able to be conducted. All the performed, single-cell INR tests were split into six groups, identified by their similar SOC, except the 5.3.22 end cap test and the 5.10.22 0% SOC test. Multiple technical difficulties were encountered in the 5.10.22 test, including loss of the digital video due to SD storage at capacity, no audio recorded in the IR video, and the removal of the TC before the short fire event. It should be noted that the TC fell off 442 seconds into the TC data, where the hot plate was activated 2 seconds before the TC network, at a temperature of 209 ^{o}C; which can be inferred by the immediate drop in temperature in the TC data at this time. The temperature, and time to reach said temperature, was greater than the average time and temperature of explosion for every other SOC level, except for the average time to explosion of 446 seconds for 20% SOC. While there was no audio in the IR video, the explosion event can be clearly seen at the 8-minute mark. Comparing this IR timestamp with the first part of the digital video, before the SD capacity was reached, where the IR camera was voiced starting roughly 8 seconds before the TC network, it can be estimated that the explosion of the cell occurred 30 seconds after the TC fell off. It can be assumed that in these 30 seconds, the battery temperature increased beyond the 20% average of 208 ^{o}C at the time of explosion. Note that this is the only individual, 0%-SOC 18650 to experience an explosion or fire. The average time, top of cell temperature, and hot plate temperature for the initial pressure-release hiss at the vents and any explosions experienced across each SOC level's cells is denoted in Table 6-2.

Table 6-2: INR SOC averages

ALL TEMPS (C°) ALL TIME (sec)	S.O.C.	mAh	PRESSURE RELEASE (HISS)			EXPLOSION			FIRE %	
			PLATE TEMP	BATTERY TEMP	TIME	PLATE TEMP	BATTERY TEMP	TIME		
100% Averages			304	130	330	335	170	386	100	% YES
80% Averages			324	176	321	-	-	-	0	% YES
60% Averages			346	151	356	375	170	409	100	% YES
40% Averages			313	148	326	357	216	394	75	% YES
20% Averages			348	165	394	375	208	446	0	% YES
0% Averages			327	177	367	-	-	-	0	% YES

To demonstrate the prevalence of fires in each SOC level, a percentage of the tests that experienced fire for each level is shown. Note that no fires occurred in the 20% SOC tests, and no fire or explosions occurred in the 0 and 80% tests. The lack of explosions and fire amongst the 80% tests is considered an outlier to the expected behavior of these higher SOC cells. An unreported 80% test in the single-cell matrix, which occurred on 6.22.22, also experienced no explosion or fire; however, during this test the hotplate was noticed to be heating significantly less than other tests, which prompted the use of the newer (third) Oster hot plate for the remaining tests performed. The three 80%, INR tests were Molicel brand (grey wrap). As a note, the lone 80%, IMR cell (brand not recorded, pink wrap) tested did explode but no fire occurred. The relatively higher thermal stability seen in all 80% cell is not believed to be a product of this SOC level, but a possible combination of manufacturing differences and the statistical probability issues caused by the smaller number of 80% cells tested.

The average SOC data was prepared graphically, to visually demonstrate the recorded behavior of the cells tested for each SOC level. The plot in Figure 6-4, shows the average time and corresponding temperature of the first hiss and explosion, if applicable, for each SOC grouping.

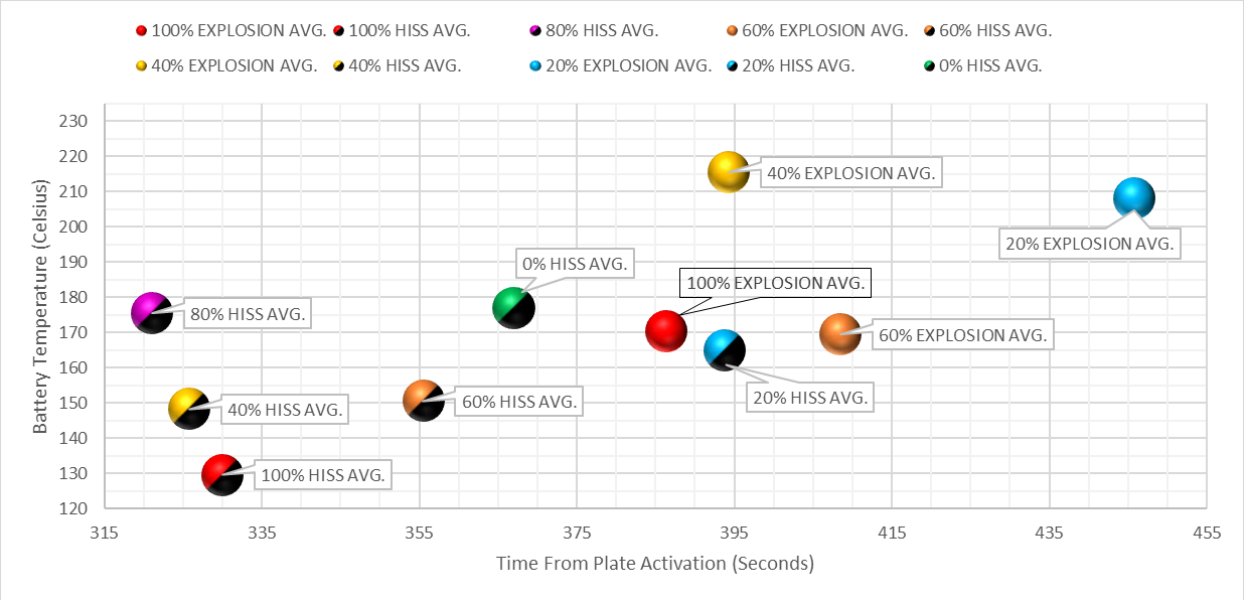

Figure 6-4: INR pressure and explosion average temperature and time

Based on the literature review findings, starting at the 100% SOC averages, a gradual increase in time and temperature was expected to be seen from each SOC decrease increment, when moving across the groupings in descending order, both the hissing and explosion parameter. When focusing on the hiss parameter only, the 100% average temperature is the lowest, as expected, but both the 40% and 80% average hiss time was sooner, with the average temperature of the 80% cells being the second highest, just below the 0% cells. Where the 0 and 20% hiss events took longer and were at a relatively higher temperature than the other levels (excluding 80% temp), the 20% group's hiss was not expected to take longer than the 0%. Since there were not always explosions in some of the tests, while hissing always occurred, these averages may be less accurate statistically; however, an expected trend in the higher SOC cell groups (100, 60) was seen, in that they on average both exploded at 170 ^{o}C, which is 38 ^{o}C and 46 ^{o}C less than the 20% and 40% averages, respectively. Another outlying characteristic can be seen in the 40% SOC cell though, they exploded at a highest temperature, but the second fastest of all SOC groups where explosion occurred.

The following box and whisker plots and their corresponding zoomed-in sections, seen in Figure 6-5 and Figure 6-6, provide a visual aid to investigate the statistical dispersion of the data points in each SOC

group for the parameters of hiss temperature and hiss time, respectively. Note that the median of each dataset was included in calculating the quartiles of the data, which is typical of smaller datasets.

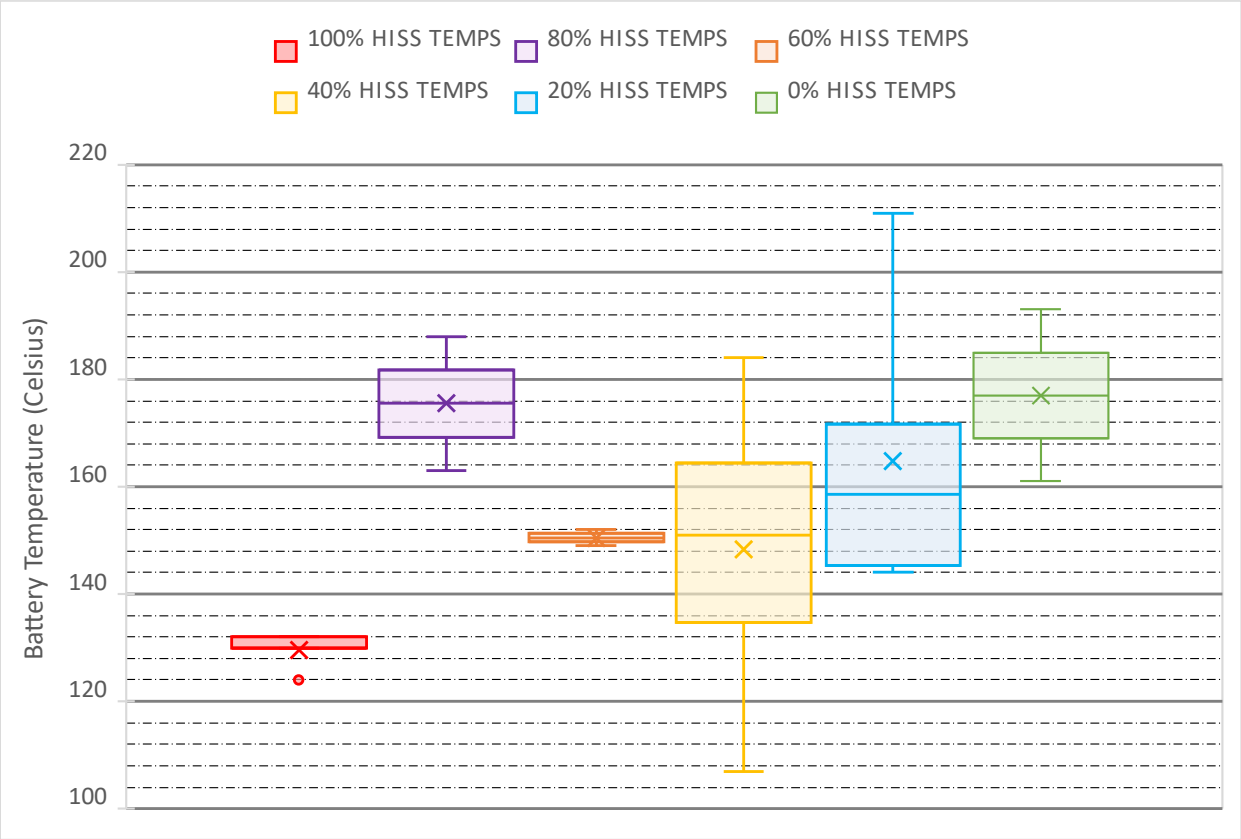

Figure 6-5: INR pressure release (hiss) temps, box and whisker (inclusive)

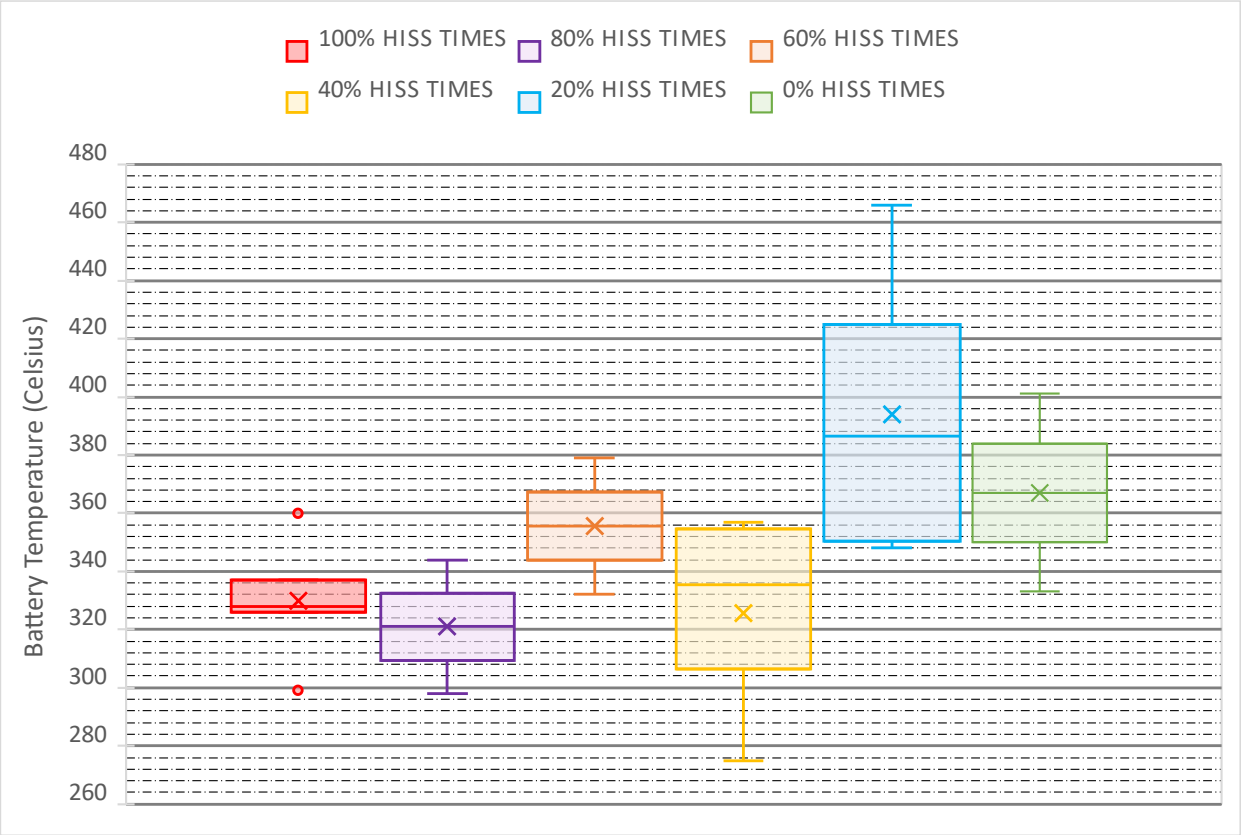

Figure 6-6: INR pressure release (hiss) times, box and whisker (inclusive)

For the 0%, 60%, and 80% SOC groups, only two reportable tests were performed with the INR chemistry, so the amount of variation in their hiss-failure datapoint values cannot be determined at this time. For the 20, 40, and 100% groups however, six, four, and five tests were performed for each group, respectively, giving a more statistically relevant set of values. In the 100% SOC cells, a smaller inner-quartile range can be seen for both the temperature and time of hiss failure, when compared to the 20 and 40% SOC data. From these findings, it is believed that the initial activation of vents is controlled by the SOC in 100% cells, while in other cells with lower SOC, the charge level is not the controlling factor in making the cells react. To state differently, while the same vent failure occurs in the lesser SOC cells, other physical properties in the cell besides the SOC may dictate how long the battery can resist TR before vent activation. For instance, a brand new 20% SOC cell may hiss later and at a higher temperature than a similar 20% cell that has seen 100 charge and discharge cycles, whereas the same two cells at 100% SOC may

react closer to the same time and temperature. More cell tests amongst each SOC level, that also evaluate additional parameters, would need to be tested to build confidence in this theory.

In the similar box and whisker plots, now dedicated to explosion temperature, and explosion time, seen in Figure 6-7 and Figure 6-8, smaller margins of variation from the mean was observed across the 100% SOC dataset, when compared to the 20% and 40% sets.

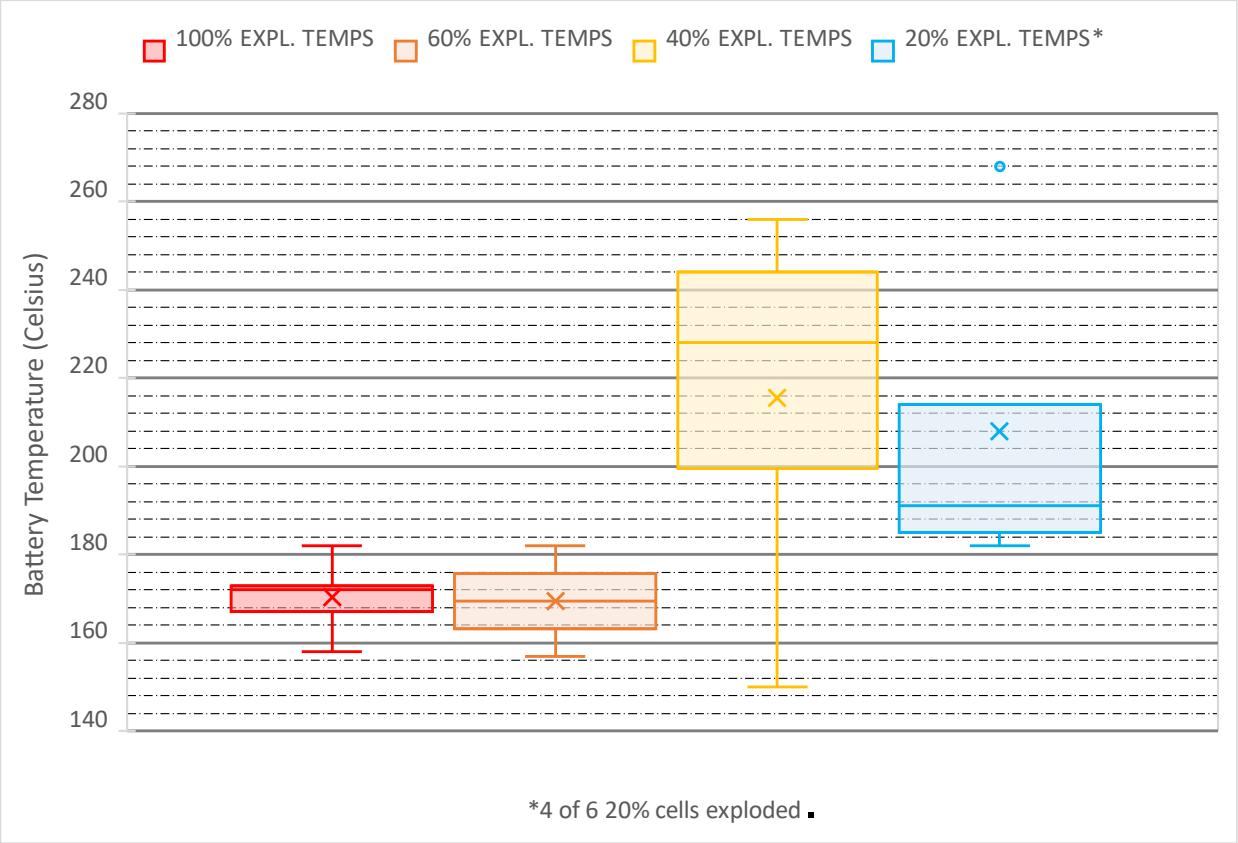

Figure 6-7: INR explosion temps, box and whisker (inclusive)

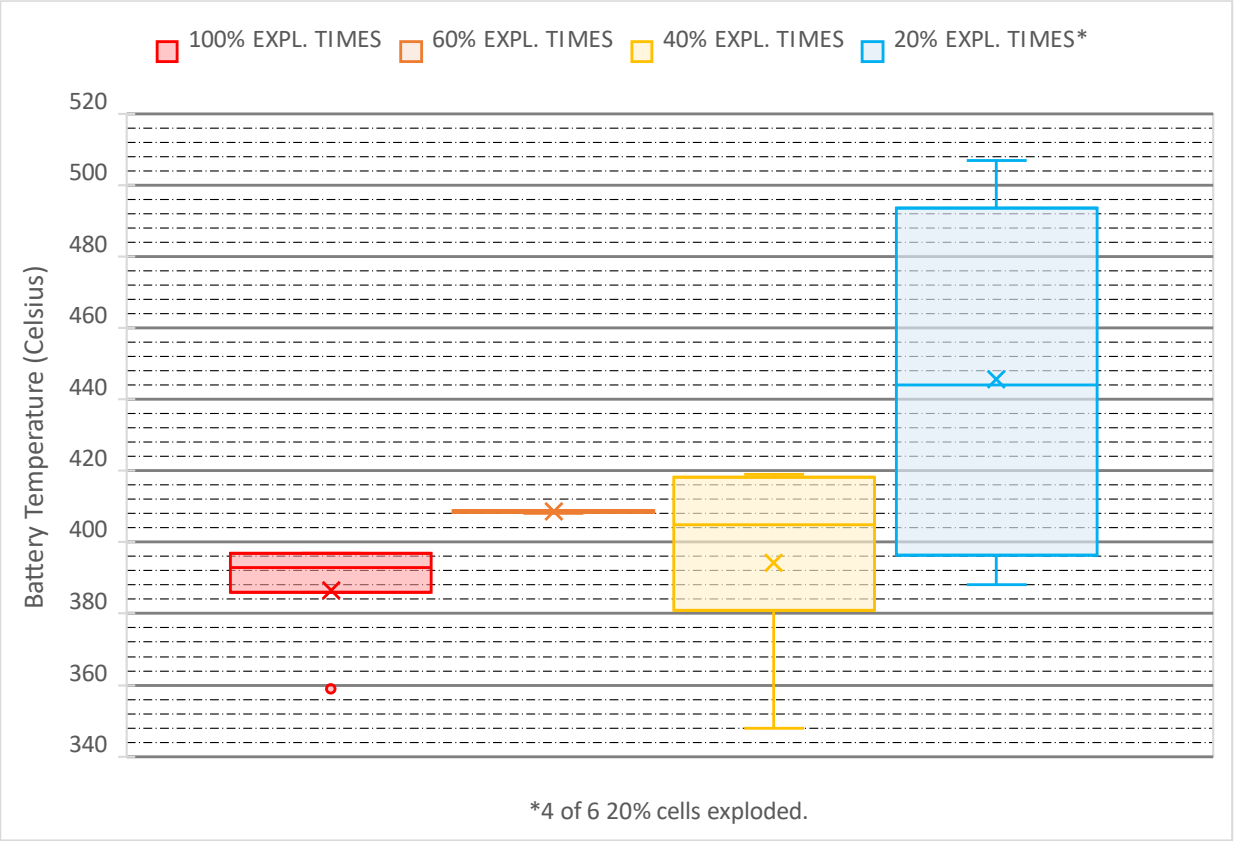

Figure 6-8: INR explosion times, box and whisker (inclusive)

6.5 Multi-cell Propagation Discussion

The inability to charge the multi-cell modules tested in this research added an unknown variable to the test that ideally would be known. Through the analysis of the single-cell tests however, certain behavioral trends were identified for different SOC levels. These SOC findings can be applied to the observations seen in the multi-cell tests, to predict how SOC might contribute to thermal propagation in battery packs and be used to make recommendations to module and pack design. In both the 6.11.22 multi-cell tests, where one was a multi-pouch test and one was a multi-18650 test, the bottom cell required longer exposure to heat before a failure reaction was seen, and in both cases, there was no fire event with the bottom cells. The 6.11.22 18650 cell did experience an explosion, but it took over 16 minutes of heating to occur. In both 18650 propagation tests, and the one test performed on a single 18650 cell on its negative end cap (5.3.22), the explosion reaction took between 10-16 minutes to occur. In all cases the explosion event was potent,

with the 6.11.22 test producing the loudest explosion of any test, and the side-tested 5.3.22 cell rocketing out of the test chamber travelling approximately 35 ft, which is assumed to have been longer if the battery did not skip along the façade of the nearby building. This extreme reaction prompted the use of the larger test box for the 18650 tests and was decided too dangerous to be performed again at the single-cell level. The weight of the combined 18650s prevented equally dangerous displacements. The weight of the combined pouch cells prevents their displacement as well; where the expansion of the bottom cell was limited by the cells above, and once pressure was released the upper cells partially compressed the bottom cell back down.

Based on the behavior of both multi-cell test types, the chosen arrangement for each is believed to have contributed to the high level of activity in the tests. With the pouch cells stacked on top of each other by their wide flat surface, the contact surface area from cell-to-cell contributed to a faster propagation of heat through the cells, especially once the first fire event occurred. The center pouch cells that experienced a fire event and were also between two cells that had also reacted, reached the highest temperature recorded through all tests. Temperature in these cells grew after they had completed burning as well, with the heat from each additional fire event building and being trapped if cells were undisturbed.

As seen throughout all 18650 tests, consistent failure from the positive end cap, made the end-to-end column arrangement of the multi-18650 tests the most hazardous arrangement, as any heat or fire projecting from the battery below would be aimed directly at the cell above, also causing sparks and flames to project radially from the interface point of the cells in all directions. In the 6.4.22 test the cell directly above the bottom cell, which erupted with heavy sparks and flames, the battery was found to have failed at both end caps. It is believed that the battery fire from the positive end cap below, being directed at this cell's negative end cap, caused this side of the battery to be weakened before failure occurred internally. Leading to the atypical dual-sided failure of the cell.

The temperature transfer at the 18650 cell interfaces was attempted to be investigated with TC placed in between the cells along with the bottom cell's DAQ TC being placed near its plate contacting end. This

bottom TC showed that its connection to the battery surface was not solid, likely due to the tape securing it being near the plate. The first cell's explosion was so violent, that the cells above were separated, and no further propagation occurred, giving virtually no data on the cells' interfaces.

A technical issue related to the DAQ system, was encountered in the 6.11.22 test. When the DAQ system's raw data was exported to an excel file, there was an issue where the timestamp listed at the start of the data was not correct. This issue created difficulty in lining up the data with the videos (digital, IR) and SmartConnect data. Since the DAQ system was wired, the operating computer did not require an internet connection during testing, and it's believed that the computer was not connected to internet during this time which led to an error in the time displayed on the data. Again, technical issues like this, demonstrated the importance of clear voice callouts when specific data recordings began, with a to-the-second degree of accuracy, and not relying solely on software timestamps.

CHAPTER 7: CONCLUSION

Overall, the hot plate method employed in this research to instigate ISC and TR, in various types of LIBs, proved to be effective. To investigate the behavior characteristics of the LIBs exposed to this manual thermal abuse, a multi-point, LIB fire monitoring system (FEDS) was developed. The initial proposal for developing this system included gas and smoke measuring devices, IR video thermography, and on-cell(s) TC readings, which could operate concurrently to provide real-time and logged data wirelessly, to a monitoring device a safe distance away. While this system provided the ability to efficiently perform the LIB behavior research, it was also intended to be a prototypical monitoring system for trains powered by LIBs. While modern LIB powered car or bus-scale cell modules/packs already contain BMSs, this proposed system would be able to check more parameters that are indicative of LIB TR hazards, which may be found in the LIB testing performed. As expected, some initial equipment issues were encountered in the earliest versions of the monitoring system's development. Challenges with the gas and smoke detectors caused their use to be tabled until sufficient equipment was acquired so they could be integrated into the design to provide functional results. Based on the observation that smoke was one of the first sign of thermal runaway in the heated batteries, use of some version these detectors is recommended in both the final experimental and train system design.

Another key monitoring system issued was caused by the low-resolution IR video camera used for this first phase of the system. While this camera gave less detailed images than expected, and consistently lower than expected temperature readings, its thermal images were still shown to be useful in understanding the performed battery tests. Its use also showed some best practices for general IR camera functions. While other equipment difficulties encountered during this research were considered minor, recommendations toward preventing and improving all aspects of the system are provided in Chapter 8.

The supply and charging limitations faced during this research caused deficiencies in the number of some LIB types tested. While an extensive comparison cannot be made on the ICR and IMR, general trends that are expected from the literature review can be seen.

For the IMR cells, only two of the five cells tested exhibited explosions indicating TR – these two cells were the 80% and 100% SOC cells. Only the 100% SOC cell produced flames after TR. While it's unable to be determined if the 60% SOC IMR that was reheated after being knocked off the plate would have exploded, it's believed that this initial release of pressure, followed by cooling, helped prevent TR, or reduced the severity of TR, since some materials likely escaped during the first failure.

Over 20 INR cells were tested, where at least two cells at each increment of SOC investigated, gave viable data. While more tests are required to reduce the percentage of perceived outliers in the INR datasets, and other cell types, a general trend in higher thermal stability of lower SOC INR sells was seen. Where on average, the activation of 18650 safety vents, and occurrences of smoke/off gassing, explosions, and fires for 100% SOC cells, happened sooner and at a lower cell temperature than that of the less charged cells. The fire events across the 100% cells were typically more violent and produced more flames that burned longer. In general, the time and temperature of key TR reactions increased inversely with SOC decrease, however, more variability in the lower SOC tests were seen.

Overall, the plastic (and pouch) cells are much weaker structurally, making them more susceptible to damage with the hot plate method.

For the propagation tests, the cell arrangement, and separation between the cells, or lack thereof, showed the greatest influences on the severity of thermal propagation between cells, as was also seen in literature review. In general, the tape arrangement for the 18650 cells, and the unsecured stacking of the pouch cells, allowed for propagation between the cells. However, the 18650 cells in both propagation tests eventually separated and full TR failure was not able to propagate to every cell. Similarly, in the 6.11.22 pouch test, the top cell fell off just after TR ignition, due to expansion and movement of the lower cells. Restraining the cells mechanically, similar to the FAA study [38], would be more representative of a closed

module design. The end-to-end 18650 cells (laptop module arrangement) present more challenges in keeping them connected and static, with their high energy reactions that are directed toward each other, opposed to the side-by-side FAA method.

Similarities can be seen in the behavior of the 6.11.22 18650 test and the 3.2.22 0% ICR hard-cased prismatic cell (tested on original plate). The bottom 18650 took a significant amount of time to react, and when it did the explosion was the loudest of the entire research, while little smoke and no fire was seen in the cell afterwards. When also compared to the 5.3.22 100% SOC side-tested 18650, it is believed that the bottom cell in the 6.11.22 test was at or near 0% SOC. Likewise, for the 6.11.22 pouch test, its longer time to uneventful reaction is also believed to be caused by low to no SOC.

CHAPTER 8: RECOMMENDATIONS FOR FUTURE STUDIES

The inspiration for this current study, though not explicit, is the concept of battery locomotives. Battery locomotives are electric trains that run on LIBs, instead of relying on overhead catenaries or underground third rail electrification technologies. Research of LIB trains found three designs for battery locomotive systems: 1) below-car 2); engine room replaced; and 3) battery trailer car. A general diagram for the engine room replacement can be seen in Figure 8-1.

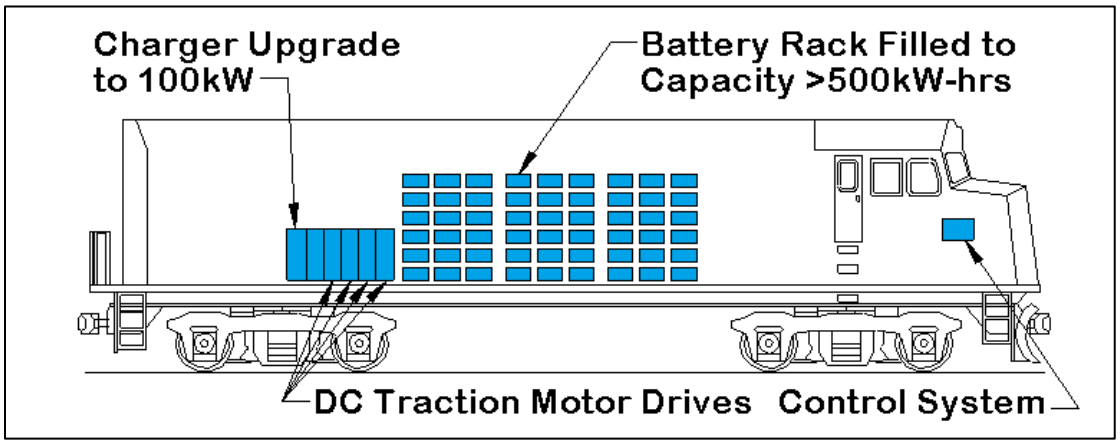

Figure 8-1: Engine room replaced, LIB powered train schematic

Sample designs for options 1 and 2 were discussed in detail in Chapter 2. The third arrangement has been employed for the town of Belmont, NC's installation of a new public-transit trolley. This prototypical, two-member-consist design includes a single trolley car for the operator and passengers, and a small, steel trailer that was custom fabricated for battery storage for this system. The separate trailer houses the LIB pack(s) that will externally power the electric motor in the trolley through inter-car wiring. Figure 8-2 shows the fully functional trailer car at Belmont, NC, where the trailer is holding a Nissan LEAF battery module that powers the historical trolley car (Car # 1).

Figure 8-2: Belmont battery trailer car

While currently fitted with one LEAF battery module, plans for an additional second LEAF battery module are in development, including programming logic that will allow a BMS to communicate with both modules concurrently, which will be required for charging and SOC monitoring. The trailer car will eventually be protected from rain and other types of damaging exposure.

A similarity between the trailer car and engine replaced locomotive designs is that the LIBs are separated from the freight or passenger cars, such that if the batteries catch on fire, it will likely not impact occupied (persons, goods) cars. For the Belmont trolley a safety release mechanism has been proposed, where the trailer car could detach and separate from the main cab to a safe distance; but this has merely been discussed at this point and presents its own set of challenges and risks. Despite the apparent safety

advantages in the separated battery-trailer design, it is still essential to take all actions toward preventing fire, and other LIB hazards.

The FEDS design has been developed for future integration into rail applications, including the battery trailer car, where the external and independent battery monitoring system targets the capture of early-initiation signs of fire causing failure failures.

The current study sets the foundation for future development of the FEDS system. To ensure a viable FEDS, the following equipment and research recommendations should be considered or performed:

- FEDS equipment:
    - The current FEDS requires four, separate power supplies for operation [signal conditioner, node, IR camera (RaspberryPi), computer (battery/charger)] all of which use standard wall outlets. The number of power supplies should be consolidated for real-world FEDS application. All FEDS equipment should be adaptable to different power sources, including the option to be powered by the batteries they are monitoring (excluding insufficient-capacity batteries and fire experiment cells), while also containing a durable, back-up power supply.
    - Research IR video camera technology to determine the specifications required to, most importantly, increase the accuracy of reported temperature readings by the camera, but also improve the live and recorded image quality. While the IR camera's main functional intent is to monitor active LIBs for the FEDS, a durably designed integration of the device into a train car (or BESS), could aid emergency responders in determining battery temperatures after fire events (see Tesla Model S emergency response guide [30]). This design consideration should include making the IR camera fireproof, heat resistant, waterproof, and shock-proof.

- Multiple TCs should be added to the FEDS (eliminating DAQ), who's current node-capacity allows for the addition of seven more instruments on top of the current, single TC in use. Additional TCs would require to be passed through a signal conditioner similar to the current Omega conditioner. The current conditioner only translates one TC at a time, therefore, a multi-signal conditioner should be researched and employed if available. While many modern battery modules and packs have internal TCs already integrated into the cells monitored by the BMS, like the LEAF batteries used in the current Belmont Trolley design, the FEDS TC(s) can provide independent, corroborating, back-up data at the same or different locations. While surface TCs are thinner in comparison to many other TC application types, a thicker wire gauge and insulation thickness is recommended for the chosen FEDS TC, especially for future cell fire-by-hot plate (or other method) testing. Again, the larger Evolution TCs showed significant durability advantages over the thinner Evolution option also used in this study. Regardless of TC size, considerable challenges were met when attempting to keep the TCs in contact with the cell surface. It is recommended to use a different method, other than the tape method used in current experiment, for attaching the TCs to all cell types. The wire-wrapping technique used in the FAA research may be more effective, but this method was used with a thicker non-surface probe, and only for cylindrical cells [38]. Additional TC-specific adhesives should be investigated as well, which could be separately applied, compared to the self-adhesive type surface gages used.
- While originally an existing component in the first phase of the FEDS, the initial gas detector was removed due to errors in its readings. It is recommended that proper gas detectors be re-installed into the FEDS. Prior to selecting a new sensor, a gas-bag collection system should be designed into future fire testing. Effective collection of gas during future fire tests could be analyzed soon after the test, on-site, in one of UNC Charlotte's labs (or

similar lab); where the contents and quantities of the bags could be used to determine the appropriate type of gas sensor(s) for specific cell types. The current FEDS allows for different sensors to be quickly switched to align with what is appropriate for each cell/module/pack. Relatedly, the proposed smoke detector in the original FEDS conception should also be further researched but based on smoke being one of the earlier signs of battery failure in this current research, it is likely beneficial to be used in testing and field application.

- In terms of the FEDS' monitoring software, computer, and network the following recommendations are provided: combine the IR camera and SmartConnect systems into one, where all instruments record and display data in one software on one device, this includes eliminating the current intermediate RaspberryPi device, ideally the main "hub-device" would be mobile (tablet), dependable, and capable of remote access by other devices (satellite, back-up hub) in case of hub damage; for testing specifically, at minimum the IR and TC systems should activate with one command at the same time; eliminate the need for Wi-Fi network while maintaining function across safe distances and in remote areas, while a fully wireless and mobile communication to a person-monitored hub-device should be the goal for real-world application, a long-wired connection for experiments may be more dependable than Wi-Fi, especially for large tests where extended distances from occupied buildings is required for safety; program audible and visible alarm activation into the monitoring software at specific indicator-points for all sensors' data types; the operation of the system should be turn-key and require little prior LIB/LIB-fire knowledge.

This study also aimed to contribute to the community of LIB fire research. Areas of improvement, general tips, and recommendations for the experiments performed in this research, not-directly part of the FEDS, are as follows:

- In the occurrence of TC removal before/during/after TR, the use of handheld IR thermometer devices (gun, tablet) proved to be an effective tool in determining surface temperatures of the cell, cell-shrapnel, or plate; however, many times during their use, the cell temperature was greater than the capacities of the devices (only one hand-held device was able to fully capture temperatures with a maximum capacity of 2000 ^{o}C). An additional handheld IR thermometer should be upgraded immediately to a higher capacity option. Having two high-capacity options, where one is calibrated for short-distance readings and the other for long-distance, may be even more effective.
- The digital video recordings of the tests were important in determining the time of key occurrences during all the tests, especially since TC data does not always visually correlate to the failures occurring. For many of the tests however, the cells would displace out of the camera's view; therefore, the use of multiple cameras at different locations and zoom levels is recommended. The use of a high-speed camera that can be started remotely is also recommended to capture slow-motion videos, especially during fires and explosions. With the current functionality of the FEDS and other data collection devices, the camera is often needed to line up the different datasets, which may start several seconds apart, with each other, key events, and the plate activation time. It is recommended to make a loud and clear voice-callout of any action or event seen or heard during the test, even calling out recorded TC data in real time as reference points.
- In the prismatic cells (pouch, hard-cased) the change in expansion was minimal most of the time, thus, hard to visually identify live or in recorded test video. However, by incrementally moving through the videos while keeping them paused, even the slightest of expansions is noticed by staring at edge of the cell. This technique could be improved through ad-hoc image correlation if a camera was angled directly perpendicular to the edge of the cell facing it. With a uniform, checkered background applied to the test-chamber wall behind the cell, in view of the camera, the dimensions of the squares in the checker pattern could be adjusted for the camera's perspective distance and be used to determine the distance of expansion with a considerable degree of accuracy. The same

practice could be performed by multiple camera angles at once and/or with high-speed cameras to determine length of smoke/flame-jets and cell/fragment projectile speeds.

- For 18650 (any cylinder) tests, the positive end cap, containing the safety vents, should be angled toward the camera(s) so that their activation and any electrolyte leakage can be seen. Noting that failure always occurred here first and preparations for this failure (and all possible failures) should be made accordingly.
- Ideally the test chamber could be upgraded into a closeable container that is see-through and/or contains internal lighting where the entire container is fully viewable by live and recording camera feed. Until a structurally sound, inescapable container is available, cylindrical cells should never be tested by placing their endcap directly on heating surface. This can cause massive projectile forces, creating a large radius of danger around the test site.
- To increase the statistical confidence in the current data, more cells of each of the three chemistry-shape combinations tested should be performed for each SOC increment. Ideally this new batch of test cells would include new and used cells to investigate any thermal stability and fire performance difference in magnitude and consistency that use history may have. Additional parameters to investigate, such as brand, and anode chemistry, amongst the cells may help answer outlier events and data.
- An alternate test method, where the batteries are safely removed at different times before the different failure reactions (expansion, hiss, smoke) seen throughout the heat application seen in this study, should be developed and performed. This test could include reheating of the cells like the 4.26.22 IMR test, and/or be used to find a “TR trigger temperature”, that even when the battery is removed from the heat source, fire or explosion still occurs. This may help to determine effective alert landmarks for the FEDS.

- Additionally, devising a way to heat the cells while they are actively discharging (powering lightbulb) may be more representative of LIB fires in systems that are operating during and leading up to failure.
- For the propagation tests the capability of gaining SOC information for the in-series modules should be attained. Different arrangements of both cell types should be tested and like the TC, an alternative method to constrain the cells and keep them connected should be determined. This would better represent the cell-confinement conditions of actual module and pack designs. Researching common industry propagation barrier materials which are used in some module designs at cell-to-cell interfaces, and testing their performance, would also be a valuable parameter to add to these tests.

The current industry standard amongst most EVs is the use of 18650 INR cells for their battery packs. Similar INR use is expected in the emerging LIB train industry, for the cell type's energy density advantages. The effectual capacity of SOC on the INR cells thermal-abuse behavior, was one of the main focuses of this research. If proper charge/discharging practices coupled with keeping INR cells (and LIBs in general) at certain SOC levels can help prevent TR and LIB fires, these would be the easiest parameters to control in the battery at the consumer level.

Where electric cars have limited space and users charge cells to capacity, trains provide a greater amount of space for battery storage. If this space is taken advantage of, it could be used to hold extra battery cells so that all cells could be kept in a safer range of SOC. While limiting the SOC on any cell decreases its operating time, the extra cells on the train could be charging, while the remaining cells are being used to power the train. Certain percentages of the cells could be rotated between charging and use so that the optimal SOC window could in theory always be used. While further research is recommended to increase the statistical relevance of all cell data collected, it is recommended that in general cells be kept between 30% and 50% SOC to reduce TR probability in INR cells. If the charging frequency required to maintain

this window is not possible, the window should be increased incrementally until charging requirements become reasonable.

Based on the multi-cell tests performed, general and cell-shape-specific, recommendations can be made towards module design, which will apply to train and general LIB travel. Preventing or limiting cell-to-cell contact should be a priority in module and pack designs for all LIBs. For cylindrical INR modules, the design should prevent any positive end caps of the cells pointing toward other cells or hazardous areas near the module. Combining these arrangement considerations with conservative charging practices will promote safer general LIB use and safer LIB powered trains.

REFERENCES

[1] R. Matulaka, "The History of the Electric Car," 15 September 2014. [Online]. Available: https://www.energy.gov/articles/history-electric-car. [Accessed May 2022].

[2] J. Rowlatt, "Why electric cars will take over sooner than you think," BBC, 1 June 2021. [Online]. Available: https://www.bbc.com/news/business-57253947. [Accessed May 2022].

[3] B. Smith, "Chevrolet Volt Battery Incident Summary Report," NTIS, Washington DC, 2012.

[4] M. Brand, S. Gläser, J. Geder, S. Menacher, S. Obpacher, A. Jossen and D. Quinger, "Electrical safety of commercial Li-ion cells based on NMC and NCA technology compared to LFP technology," *2013 World Electric Vehicle Symposium and Exhibition (EVS27),* pp. 1-9, 2013.

[5] M. Sheikh, M. Elmarakbi, S. Rehman and A. Elmarakbi, "Internal Short Circuit Analysis of Cylindrical Lithium-Ion Cells Due to Structural Failure," *Journal of the Electrochemical Society,* vol. 168, no. 3, 2021.

[6] Underwriters Laboratories, "What is Thermal Runaway?," UL Research Institutes, 24 August 2021. [Online]. Available: https://ul.org/research/electrochemical-safety/getting-started-electrochemical-safety/what-thermal-runaway. [Accessed May 2022].

[7] Tarascon, J. Tarascon and M. Armand, "Issues and challenges facing rechargeable lithium batteries.," *Nature,* vol. 414, pp. 359-367, 2001.

[8] M. Eberhard, "A Bit About Batteries," TESLA, 30 November 2006. [Online]. Available: https://www.tesla.com/pt_PT/blog/bit-about-batteries. [Accessed May 2022].

[9] S. Nadimpalli, V. Sethuraman, D. Abraham, A. Bower and P. Guduru, "Stress Evolution in Lithium-Ion Composite Electrodes during Electrochemical Cycling and Resulting Internal Pressures on the Cell Casing," *Journal of The Electrochemical Society*, vol. 162, no. 14, 2015.

[10] P. Taheri, A. Mansouri, M. Yazdanpour and M. Bahrami, "Theoretical Analysis of Potential and Current Distributions in Planar Electrodes of Lithium-ion Batteries," *Electrochimica Acta*, vol. 133, pp. 197-208, 2014.

[11] Tesla Fire, "Tesla Fire," 6 August 2022. [Online]. Available: https://www.tesla-fire.com/. [Accessed 2022 August 2022].

[12] S. Blanco, "Chevy Volt battery catches fire at NHTSA [UPDATE]," Autoblog, 11 November 2011. [Online]. Available: https://www.autoblog.com/2011/11/11/chevy-volt-battery-catches-fire-in-nhtsa-lab/. [Accessed September 2021].

[13] Knowledge at Wharton Staff, "Is This the Year Electric Cars Become Exciting?," Wharton School of the University of Pennsylvania, 19 January 2018. [Online]. Available: https://knowledge.wharton.upenn.edu/article/2018-auto-industry-outlook/. [Accessed September 2021].

[14] V. Lara-Cinisomo, "Tesla Model S catches fire on Kent highway, stock dips," Silicon Valley Business Journal, 3 October 2013. [Online]. Available:

https://www.bizjournals.com/seattle/blog/techflash/2013/10/tesla-model-s-catches-fire-on-kent.html. [Accessed September 2021].

[15] Reuters Staff, "UPDATE 1-Tesla says cause of Toronto garage fire not yet known," Reuters, 14 February 2014. [Online]. Available: https://www.reuters.com/article/tesla-fire/update-1-tesla-says-cause-of-toronto-garage-fire-not-yet-known-idUSL2N0LJ1EI20140214. [Accessed September 2021].

[16] C. Thompson, "A Tesla Model S burst into flames during a test drive in France," Insider, 15 August 2016. [Online]. Available: https://www.businessinsider.com/tesla-model-s-fire-test-drive-in-france-2016-8. [Accessed September 2021].

[17] S. Beausoleil, "Lithium batteries causes train car explosion in NE Houston," Click2Houston.com, 23 April 2017. [Online]. Available: https://www.click2houston.com/news/2017/04/24/lithium-batteries-causes-train-car-explosion-in-ne-houston/. [Accessed September 2021].

[18] E. Sutcliffe, "Electric vehicle fires on ships," Gulf Fire, 4 June 2022. [Online]. Available: https://gulffire.mdmpublishing.com/electric-vehicle-fires-on-ships/. [Accessed 1 August 2022].

[19] S. Kyoung-Son and K. Jung-Seok, "Battery system blamed as Kona EVs start bursting into flames," Korea JoongAng Daily, 4 October 2020. [Online]. Available: https://koreajoongangdaily.joins.com/2020/10/04/business/industry/Hyundai-Motor-Kona-EV/20201004180400408.html. [Accessed September 2021].

[20] M. Huffman, "Tesla investigating Model S fire in Los Angeles," ConsumerAffairs, 19 June 2018. [Online]. Available: https://www.consumeraffairs.com/news/tesla-investigating-model-s-fire-in-los-angeles-061918.html. [Accessed September 2021].

[21] CBS Pittsburgh - KDKA, "Tesla Vehicle Bursts Into Flames, Burns For Hours In Monroeville," CBS Pittsburgh - KDKA, 17 April 2019. [Online]. Available: https://www.cbsnews.com/pittsburgh/news/monroeville-tesla-fire/. [Accessed September 2021].

[22] F. Lambert, "Tesla Model S caught on video bursting into flames seemingly on its own when parked," electrek, 21 April 2019. [Online]. Available: https://electrek.co/2019/04/21/tesla-bursting-into-flames-video/. [Accessed September 2021].

[23] D. Hill, "McMicken Battery Energy," DNV, 2020.

[24] P. Crompton, "Report on lithium-ion battery explosion that killed two China firemen proves inconclusive," 9 July 2021. [Online]. Available: https://www.bestmag.co.uk/report-lithium-ion-battery-explosion-killed-two-china-firemen-proves-inconclusive/. [Accessed September 2021].

[25] P. Eisenstein, "Chevy Bolt, Hyundai Kona EV Fires Put Battery Maker LG Under the Microscope," The Detroit Bureau, 8 September 2021. [Online]. Available: https://www.thedetroitbureau.com/2021/09/chevy-bolt-hyundai-kona-ev-fires-put-battery-maker-lg-under-the-microscope/. [Accessed 1 August 2022].

[26] F. Lambert, "Hyundai to recall 77,000 Kona electric cars over risk of battery fire, fights LG Chem over cause," electrek, 12 October 2020. [Online]. Available:

https://electrek.co/2020/10/12/hyundai-recall-77000-kona-electric-cars-risk-battery-fire-lg-chem/. [Accessed 1 August 2022].

[27] G. H. Ruffo, "LG Energy Solution Reveals Suspected Cause For Kona Electric Fires," InsideEVs, 26 February 2021. [Online]. Available: https://insideevs.com/news/490950/lg-energy-solution-suspected-cause-kona-fires/. [Accessed September 2021].

[28] J. Szczesny, "GM Broadens Battery Replacement to Cover All Recalled Bolts," The Detroit Bureau, 17 August 2021. [Online]. Available: https://www.thedetroitbureau.com/2021/08/gm-broadens-battery-replacement-to-cover-all-recalled-bolts/. [Accessed 1 August 2022].

[29] M. Wayland, "LG to pay up to $1.9 billion to General Motors over Bolt EV battery fires," CNBC, 12 October 2021. [Online]. Available: https://www.cnbc.com/2021/10/12/lg-chem-to-pay-up-to-1point9-billion-to-gm-over-bolt-ev-battery-fires.html. [Accessed 1 August 2022].

[30] Tesla, Inc., "Information for First and Second Responders Emergency Response Guide Tesla Model S Electric," 2022. [Online]. Available: https://www.tesla.com/firstresponders. [Accessed 29 July 2022].

[31] Siemens Mobility, "Siemens Mobility receives first order for battery-powered trains," Siemens, 17 March 2020. [Online]. Available: https://press.siemens.com/global/en/pressrelease/siemens-mobility-receives-first-order-battery-powered-trains. [Accessed 25 July 2022].

[32] Wabtec, "BHP Group Orders Wabtec's FLXdrive Battery Locomotives," Wabtec Corporation, 17 January 2022. [Online]. Available:

https://www.wabteccorp.com/newsroom/press-releases/bhp-group-orders-wabtec-s-flxdrive-battery-locomotives. [Accessed 25 July 2022].

[33] Wabtec, "FLXdrive battery electric locomotive," Wabtec Corporation, 2022. [Online]. Available: https://www.wabteccorp.com/locomotive/alternative-fuel-locomotives/flxdrive. [Accessed 25 July 2022].

[34] R. Bisschop, O. Willstrand, F. Amon and M. Rosengren, "Fire Safety of Lithium-Ion Batteries in Road," RISE, 2019.

[35] D. Ouyang, J. Weng, M. Chen and J. Wang, "What a role does the safety vent play in the safety of 18650-size lithium-ion batteries?," *Process Safety and Environmental Protection,* vol. 159, pp. 433-441, 2022.

[36] C. Orendorff, J. Lamb, G. Nagasubramanian, K. Fenton and J. L. Langendorf, "Quantifying Thermal Runaway and Improvements Through Materials Development.," Sandia National Lab, Albuquerque, 2015.

[37] R. Xiong, S. Ma, H. Li, F. Sun and J. Li, "Toward a Safer Battery Management System: A Critical Review on Diagnosis and Prognosis of Battery Short Circuit," *iScience,* vol. 23, no. 4, 2020.

[38] S. Summer and T. Maloney, "FIRE HAZARD ANALYSIS FOR VARIOUS LITHIUM BATTERIES," U.S. Department of Transportation, Atlantic City International Airport, 2017.

[39] SAMSUNG SDI Co., Ltd, *Safety Data Sheet,* Yongin-si, 2018.

[40] Adafruit Industries LLC, *Adafruit MLX90640 24x32 IR Thermal Camera Breakout,* 2022.

[41] C. Mikolajczak, M. Kahn, K. White and R. T. Long, "Lithium-Ion Batteries Hazard," The Fire Protection Research Foundation, Quincy, 2011.

APPENDIX: SMARTCONNECT INSTRUCTION GUIDE

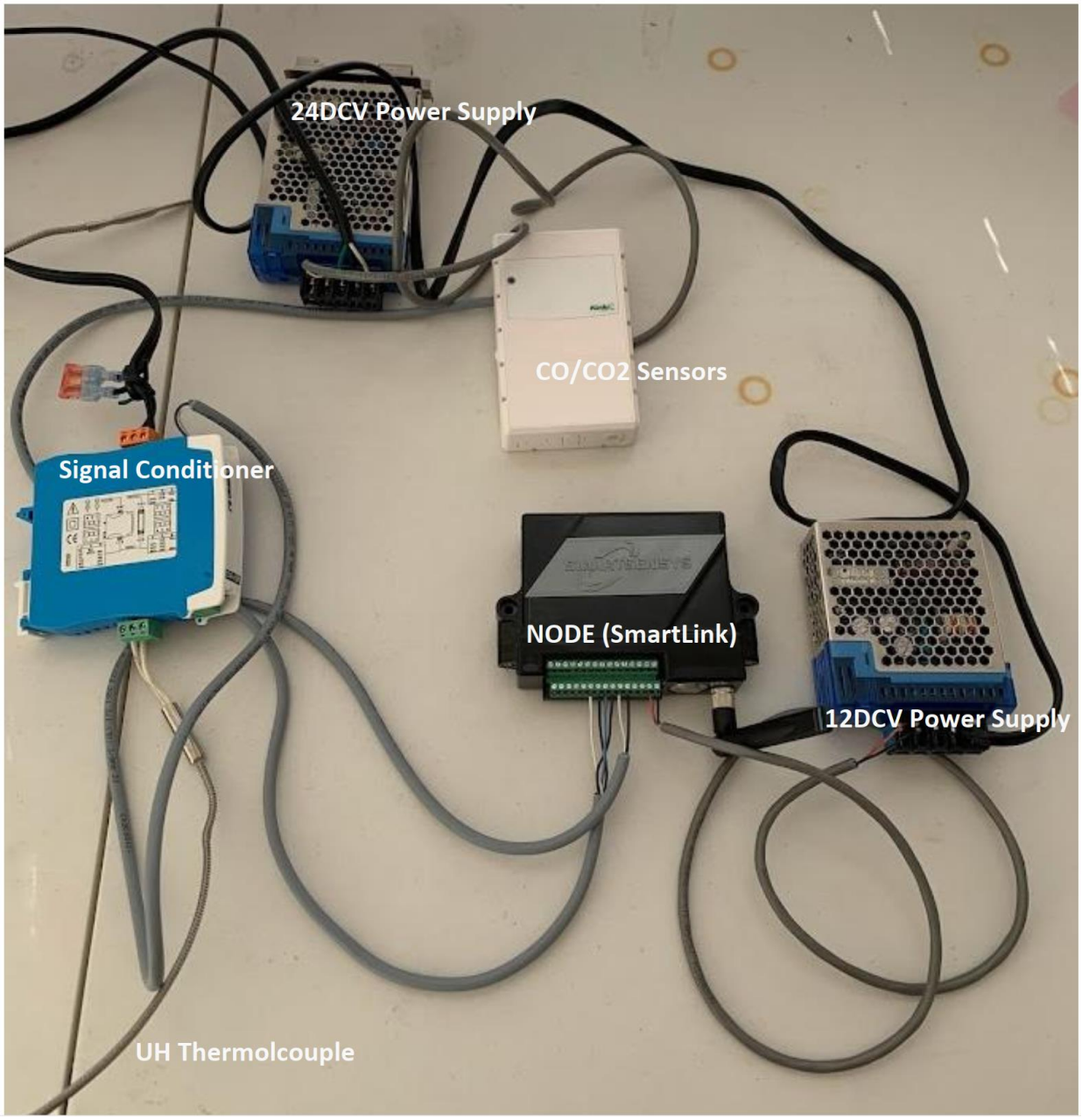

Figure 0- Analog System Connection Guide

- Simply plug in 12V and 24V power supplies to power the sensor and Node. (A detailed wiring configuration is provided in IPT Team Drive>>SmartLink/IR Camera guide>>Analog system connection guide.pdf)

Smart Link/Sensor Connect Setup

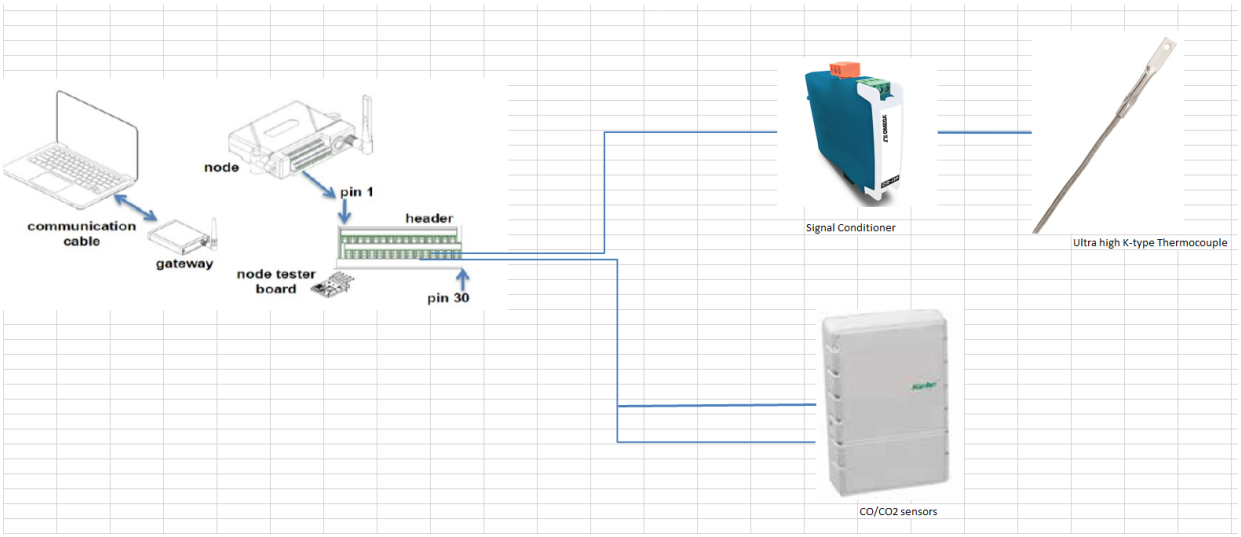

Figure 1- System schematic

- Download SensorConnect software (Sensorconnect_14.2.4_x64.msi) w/ default settings.
- Found in IPT Team Drive>>SmartLink/IR Camera guide>>
- First step is to connect Gateway (Base Station 69874) [Fig. 2] and make sure it is recognized. Under the “DEVICES” tab the base station should automatically appear. [Fig. 3] (If the node is not turned on for the first connection it will not appear like in Fig. 3 yet.)

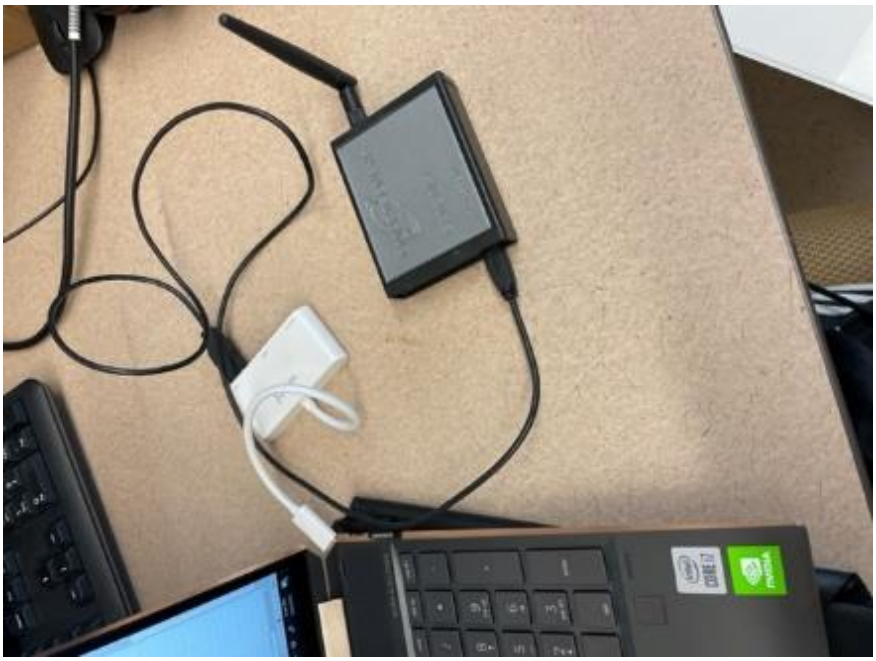

Figure 2- Base station to computer connx. (white USB-C adapter not required)

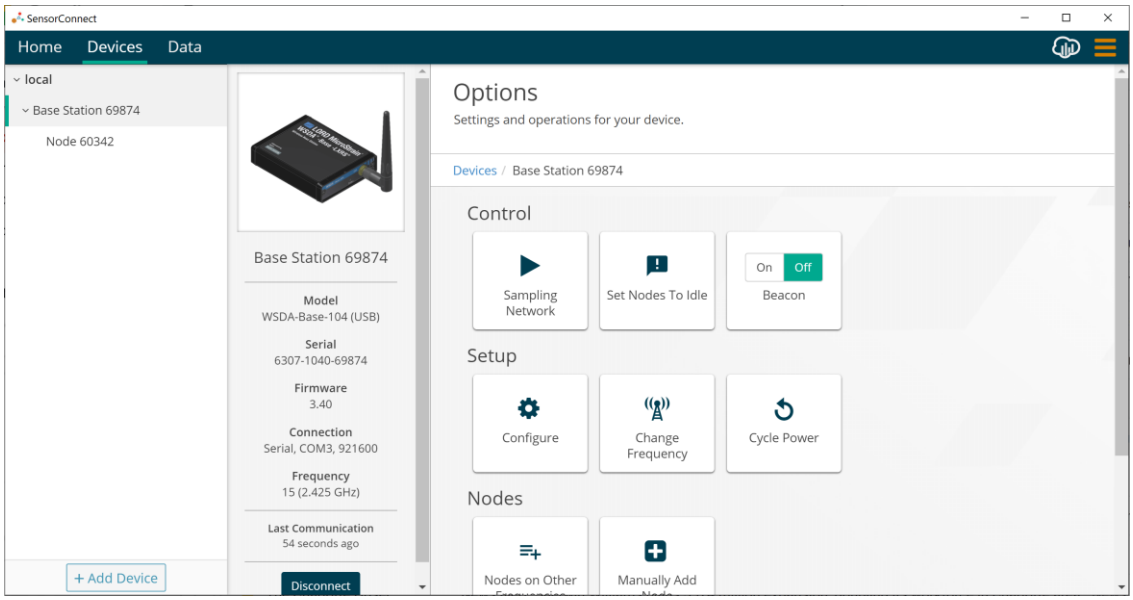

Figure 3- Successful base station connection

- If base station not immediately connected perform the following checks!
- Determine that USB port is working and identifying the gateway device. In computer's device manager page scroll down to "PORTS (COM and LPT)" (if no ports section is found the computer is not connecting to the device) if silicon labs device is shown then computer is connected. Determine com# (likely 3) as seen in [fig. 4].

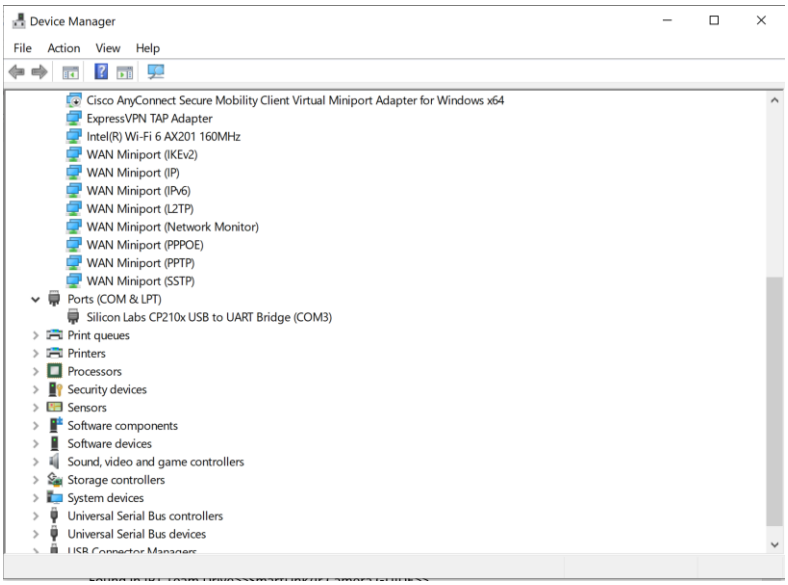

Figure 4- Windows device manager screen

- Upon confirmation of hardware connection, the issue is likely in the Baud Rate limits of the USB port connected to. If a port does not have 921,600 bits/sec capability the device will not work in that port. This has only occurred so far on a computer that has both USB and USB-C connections.

It appears the Baud Rate capacity is focused on the newer USB-C connection. Switching to a USB-C port will be the likely remedy [Fig. 2] but not the only step.

- Once you have switched to USB-C connection, in SensorConnect under “DEVICES” tab click the “+ Add Device” button in the lower left [fig. 3]. This will pull up [Fig. 5] screen which defaults to a wireless TCP/IP device.

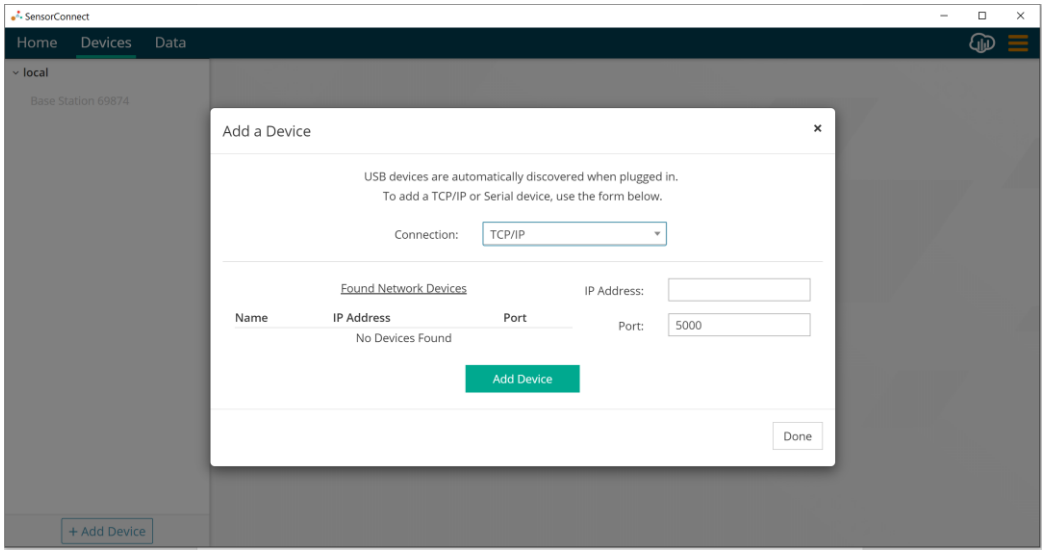

Figure 5- Add device default screen (wireless device)

- While our system is wireless to the gateway, it is plugged into the computer, so we want to change to add device by “SERIAL” in the drop-down menu. This will bring up [Fig. 6] screen where we want to input our COM# (COM3), and our Baud Rate of 921,600 in the drop-down menus. Note! This step may not happen instantly. You may need to restart the software and unplug/re-plug in the USB-C before 921,600 becomes an option. From here simply click “Add Device”. (If this procedure doesn’t work there is likely a hardware issue)

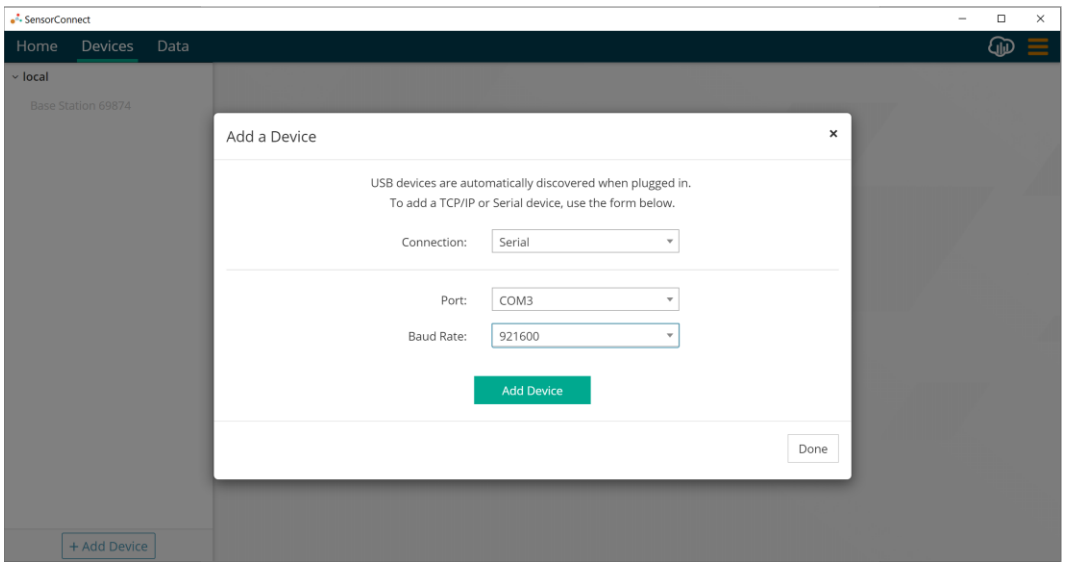

Figure 6- Serial device addition menu

- After successfully adding base station, turn on the Node (Node 60342) with one push of the silver button. [Fig. 8] (Node light will flash green once per second when on and idle)

Figure 8- Node powered on

- The node should be automatically added by the base station. [Fig. 3]

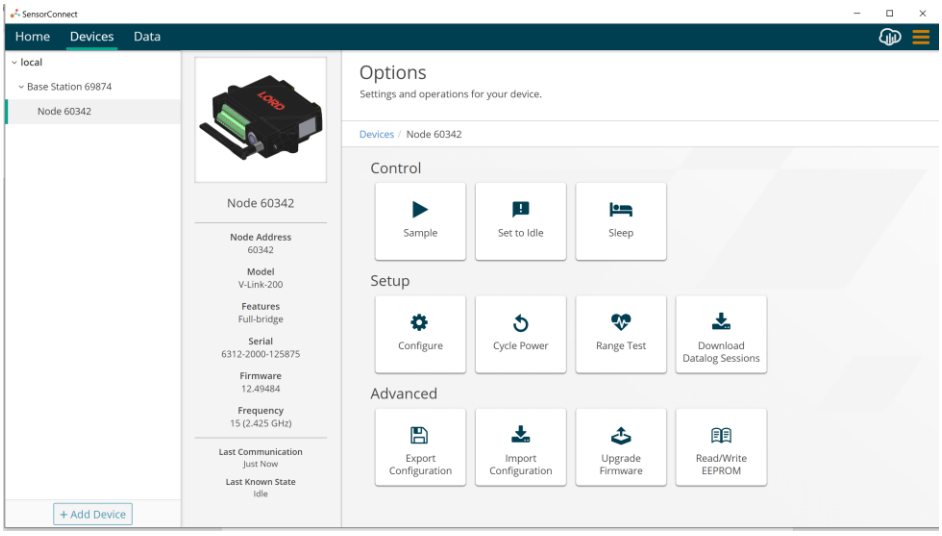

Figure 9- Node control options

- Upon clicking on the identified node in SensorConnect, the menu in [Fig. 9] will appear. The “Set to Idle” button will be used before and between all data collections. While the node is idle when first powered on it is good practice to confirm this by clicking it and then re-click it to end continuous data collection and/or before starting up a new round of data collection.
- The system should already be configured so that it is ready to sample and interpret data correctly. When you hit the “Sample” button the screen in [Fig. 10] appears. The “Channels” tab shows the current 3 active sensors (CO2, CO, TC.), besides the sampling rate menu, all other default options should be unchanged. We do not need to log our data this way as we will manually export our data as an excel.

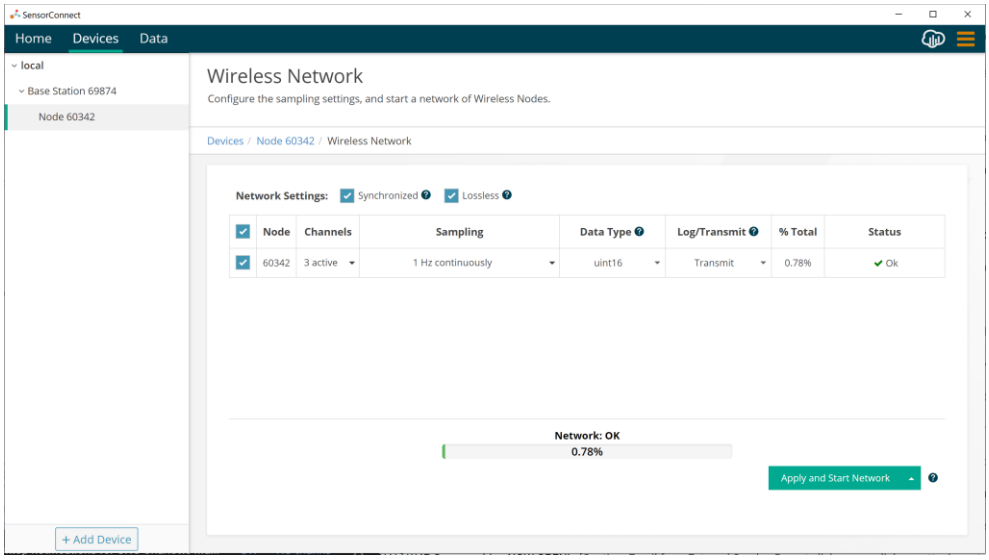

Figure 10- Sampling start menu

- [Fig. 11] shows the sampling rate options. Here you can change the samples per second (Hz) and whether there is a time limit for sampling or if it is continuous. (While it has not been used yet, the bursting effect sends out a single data collection cycle at the desired time. It also appears that the on events option can be programmed for the data collection to happen only when a certain event criterion has been met (voltage drop?, temperature level?)) To begin sampling hit the green “apply and start network” button.

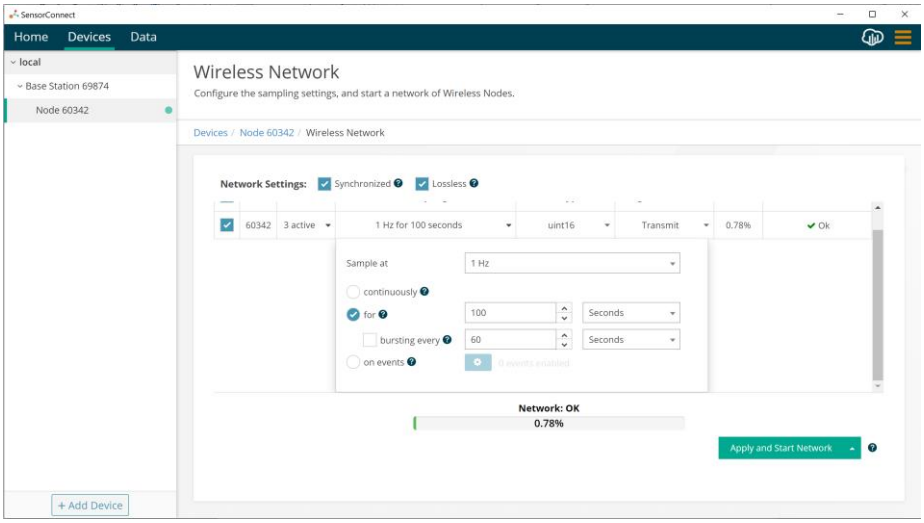

Figure 11- Sampling rate options

- Either before or right after sampling starts. “Widgets” should be setup to view the data being collected. As seen in [Fig. 12], after entering the “Data” tab, click the “+ Add Widget” button and select the “Time Series” option.

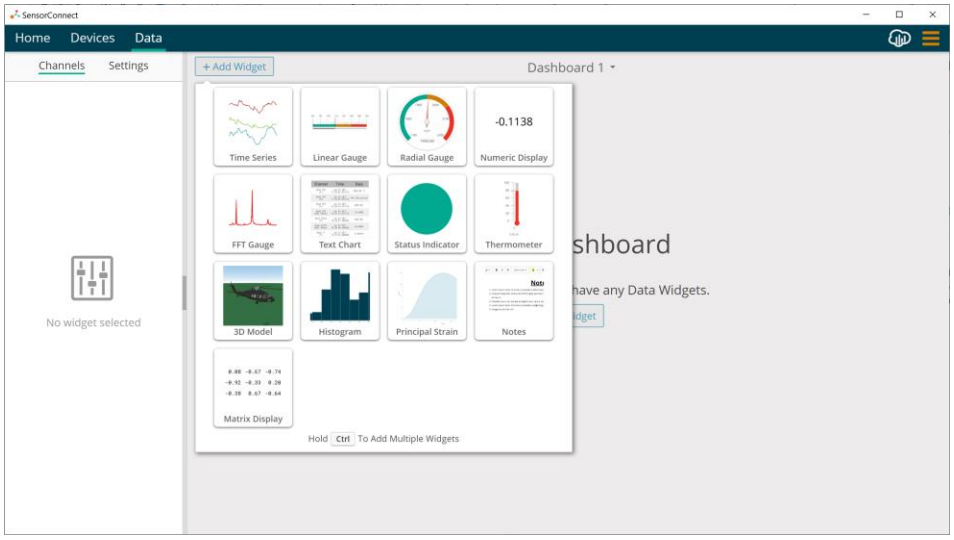

Figure 12- Adding widgets

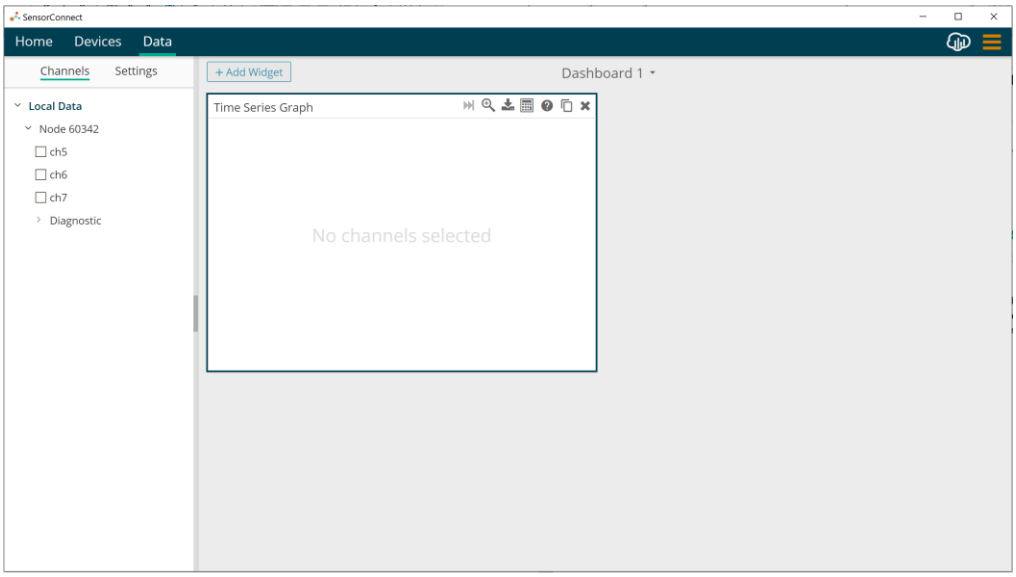

Figure 13- Widget channel selection

- A channel(s) must be assigned to the time series graph. [Fig. 13]
- CHANNEL 5= CO2 SENSOR
- CHANNEL 6= CO SENSOR
- CHANNEL 7= THERMOCOUPLE
- Multiple widgets can be added at one time and multiple channels can be added to a single widget. Example results are shown in [Fig. 14]

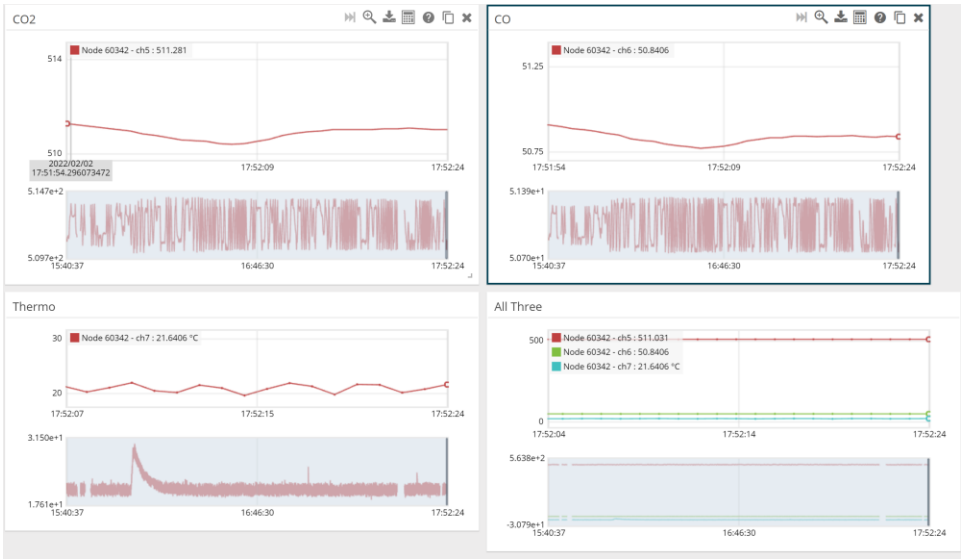

Figure 14- Sample data (single channel and combined)

- Graph titles and visibility settings can be changed in the settings tab next to the channels tab for the selected graph (blue box).

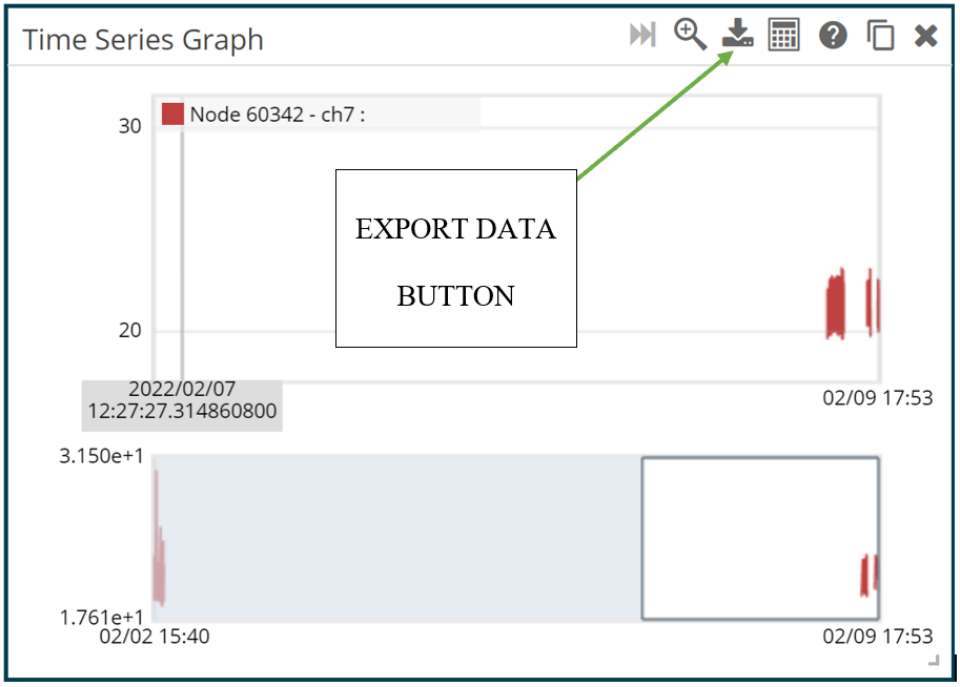

Figure 15- Zoomed out data window

- You can zoom in and out on the main graph to decrease or increase the length of the viewed data points in time. [Fig. 15] You can also grab the box in the blue shaded portion below and move it back to a paused point of interest in time while the data is still being collected. Previous collection periods are stored even after idling. (Notice the weeklong gap in data) To start with a fresh slate of data, begin a new data repository folder in the "Home" tab of SensorConnect.
- To export the data to excel, click the indicated button in [Fig. 15] and the menu in [Fig. 16] will appear. A time range for exportation can be selected. Use "standard" time format.

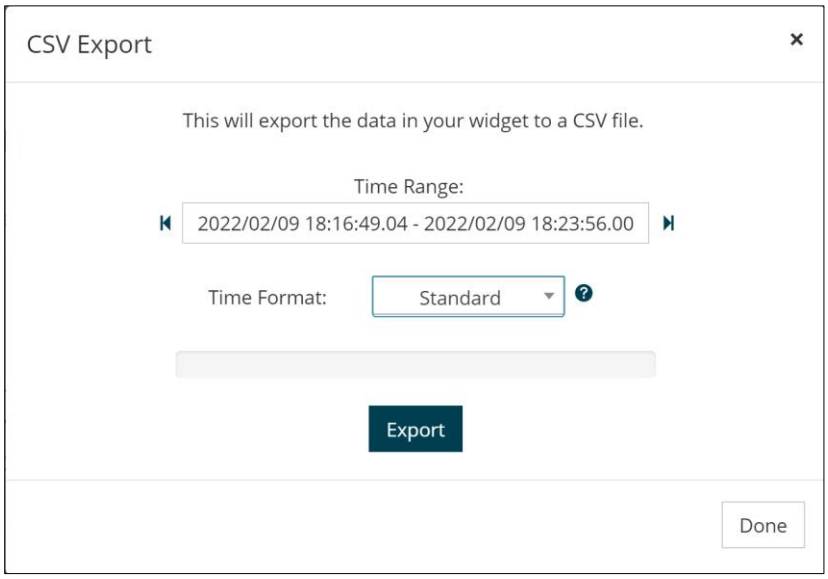

Figure 16- Export data to .csv

14									
15	CHANNEL_INFO								
16	Channel	Type	SampleRat	Equation	Coefficient	Unit	UnitSymbo	WhereApp	WhenApplied
17	60342:ch5	Timeseries	1Hz						
18	60342:ch6	Timeseries	1Hz						
19	60342:ch7	Timeseries	1Hz						
20									
21	DATA_START								
22	Time	60342:ch5	60342:ch6	60342:ch7					
23	52:05.0	510.5313	50.7875	20.28125					
24	52:06.0	510.4375	50.78125	21.4375					
25	52:07.0	510.4063	50.77188	21.3125					
26	52:08.0	510.4375	50.77813	20.28125					
27	52:09.0	510.5313	50.78438	21.0625					
28	52:10.0	510.625	50.79688	21.96875					
29	52:11.0	510.7813	50.81563	20.5					
30	52:12.0	510.875	50.825	20.17188					
31	52:13.0	510.9375	50.83438	21.53125					
32	52:14.0	510.9688	50.83438	21					
33	52:15.0	511.0313	50.84375	19.64063					
34	52:16.0	511.0313	50.84375	20.84375					
35	52:17.0	511.0313	50.84063	21.90625					
36	52:18.0	511.0313	50.84375	21.3125					
37	52:19.0	511.0625	50.84375	19.8125					
38	52:20.0	511.0625	50.84688	21.67188					
39	52:21.0	511.0938	50.84063	21.59375					
40	52:22.0	511.0625	50.8375	20.15625					
41	52:23.0	511.0313	50.84375	20.79688					
42	52:24.0	511.0313	50.84063	21.64063					
43									

Figure 17- Screenshot example of exported data from 3-channel widget